HEAT TRANSFER DURING RUN-OUT TABLE BOTTOM JET COOLING OF STEEL

by

Debanga Kashyap

B.Tech.(Hons.), Indian Institute of Technology Bhubaneswar, 2014

A THESIS SUBMITTED IN PARTIAL FULFILLMENT OF

THE REQUIREMENTS FOR THE DEGREE OF

MASTER OF APPLIED SCIENCE

in

THE FACULTY OF GRADUATE AND POSTDOCTORAL STUDIES

(Materials Engineering)

THE UNIVERSITY OF BRITISH COLUMBIA

(Vancouver)

April 2018

Abstract

Accelerated cooling on a run-out table in a hot mill governs the final microstructure and mechanical properties of thermo-mechanically controlled processed (TMCP) steels. Thus, it is crucial to delineate the heat transfer mechanisms and develop models adept to predict the temperature history of a steel strip or plate on a run-out table. In this work, controlled accelerated cooling experiments under transient conditions were performed on stationary steel specimens using an impinging bottom planar jet of water. Spatial sub-surface temperature history was recorded from 700 °C to below the saturation point of water. A two-dimensional inverse heat conduction algorithm was employed to quantify the heat fluxes and surface temperatures in order to obtain representative boiling curves. A range of water flow rates (160-300 l/min), water temperatures (10-40 °C) and jet inclinations (0-20 degrees) were investigated to examine the influence of process parameters on heat extraction rates.

The obtained boiling curves show the presence of different heat transfer regimes with varying surface temperatures, i.e. nucleate boiling and transition boiling. Heat extraction rates increase with increasing water flow rates and decreasing water temperatures, particularly in the transition boiling region. Heat flux values show a strong dependence with respect to distance from the stagnation line, demarcating an impingement zone and a parallel flow zone. Characteristic boiling curves represent the two zones. A shoulder in the transition boiling region is observed to be an important feature in the boiling curves of the impingement zone.

Based on the experimental data, empirical correlations have been proposed for the heat fluxes, considering the amalgamated effect of process parameters and distance from the stagnation line. Boiling curves for transient cooling have been constructed in the impingement zone and the parallel flow zone for a range of cooling temperatures relevant to the production of TMCP steels.

Lay Summary

Steel strips and plates are industrially produced using the hot rolling process, which gives us the final dimensions and properties of the material. Advanced grades of steel with tailored mechanical properties are needed for sustainable growth and increased efficiency in different applications like transportation, constructions, energy sector etc. In as rolled steel, the constituent iron atoms are arranged in a particular crystalline structure at high temperatures. An accelerated cooling process in the run-out table of a hot mill alters the crystal arrangement at low temperatures, which determines the mechanical properties of the steel. To obtain high-quality products, heat transfer models are used as a tool to predict and control the patterns of accelerated cooling.

This thesis describes the findings of an experimental study on the accelerated cooling of steel plates. Based on the experimental results, a preliminary model has been proposed to describe the heat transfer characteristics.

Preface

All experimental methodologies, sample instrumentation, data processing, experimental analysis and mathematical modelling presented in this thesis were performed by the author in the Department of Materials Engineering, The University of British Columbia. Test samples described in Chapter 4 were fabricated by the machine shop in the Department of Materials Engineering. The test procedure required the assistance of a second individual, and each experiment was conducted with the cooperation of Mr. Gary Lockhart. The source code for the IHC algorithm was developed by Mr. Peng Zhang at UBC.

This study was conducted under the supervision of Dr. Matthias Militzer, Materials Engineering, UBC.

The methodology described in Chapter 4 and some of the results described in Chapters 5 and 6 were presented in the Materials Science & Technology 2017 Conference (Pittsburgh, PA, 2017) [*D. Kashyap, M. Militzer, and V. Prodanovic, "Heat transfer during bottom jet impingement cooling of a stationary steel plate", MS&T17 Conference, Pittsburgh, PA, USA, October 2017*].

Some of the figures shown in Chapters 4 and 5 were presented in the 10th International Conference on Boiling and Condensation Heat Transfer (Nagasaki, Japan, 2018) [*G.G. Guedia, D. Kashyap, V. Prodanovic and M. Militzer, "Experimental investigation and jet impingement boiling model development for quenching of steel plates using an upward directed water jet: the spatial*

distribution of heat flux", 10th International Conference on Boiling and Condensation Heat Transfer, Nagasaki, Japan, March 2018].

Table of Contents

List of Tables

List of Figures

List of Symbols

a	Empirical parameter in maximum heat flux correlation at $x = 0$
a'	Empirical parameter in shoulder termination temperature correlation
A	Empirical parameter dependent on water temperature in maximum heat flux correlation for $x > 0$
A_n	Cross-sectional area of nozzle (m^2)
b	Empirical parameter in maximum heat flux correlation at $x = 0$
b'	Empirical parameter in shoulder termination temperature correlation
B	Empirical parameter dependent on water temperature in maximum heat flux correlation for $x > 0$
c	Empirical parameter in maximum heat flux correlation at $x = 0$
c'	Empirical parameter in shoulder termination temperature correlation
C	Empirical parameter for nucleate boiling
C_1	Empirical constant in nucleate boiling correlation
C_2	Empirical constant in initial cooling correlation
C_p	Specific heat capacity (J/kg.°C)
d	Diameter of circular nozzle/jet (mm or m)
F	Fraction of surface area in contact with water
FR	Flow rate (l/min)
g	Acceleration due to gravity (m/s^2)
h_r	Radiation heat transfer coefficient ($W/m^2.°C$)
H_n	Nozzle stand-off distance (mm or m)

k	Thermal conductivity (W/m.°C)
n	Empirical parameter for nucleate boiling
n_1	Empirical constant in nucleate boiling correlation
n_2	Empirical constant in initial cooling correlation
N	Ratio of maximum heat flux value to shoulder heat flux value
q''	Heat flux (W/m^2 or MW/m^2)
$\dot{Q}$	Volumetric flow rate (m^3/s)
r	Radial distance from the stagnation point of a circular jet (mm or m)
r, z	Cylindrical co-ordinate axes
t	Time (s)
T	Temperature (°C)
u_i	Streamwise velocity (m/s)
v	Velocity (m/s)
w	Width of planar nozzle/jet (mm or m)
x	Distance from the stagnation line of a planar jet (mm or m)
x, y, z	Cartesian co-ordinate axes

Greek symbols

Δ	Change in quantity
Θ	Nozzle inclination angle (in degrees)
ρ	Density (kg/m^3)

Subscripts

air-water	Transition from air cooling to water cooling
i	Impingement jet
j	Jet/water jet
l	Liquid
initial	Start of cooling
max	Maximum
n	Nozzle
pool	Pool boiling
sh	Shoulder
sh_end	Termination point of shoulder
sat	Saturation
sub	Sub-cooling
sup	Superheat
surface	Cooled (bottom) surface of test plate
v	Vapor
water	Water from planar nozzle

List of Abbreviations

2D	Two-dimensional
AMPEL	Advanced Materials and Process Engineering Laboratory
AISI	American Iron and Steel Institute
CFD	Computational Fluid Dynamics
CHF	Critical Heat Flux
DNB	Deviation from Nucleate Boiling
FEM	Finite Element Method
HSLA	High Strength Low Alloy
HSMM	Hot Strip Mill Model
IC	Initial Cooling
IHC	Inverse Heat Conduction
MHF	Minimum Heat Flux
NB	Nucleate Boiling
ONB	Onset of Nucleate Boiling
PNB	Partial Nucleate Boiling
SPC	Single Phase Convection
TB	Transition Boiling
TC	Thermocouple
TD	Thermocouple Hole Depth
TR	Thermocouple Radius
TMCP	Thermo-Mechanical Control Process

UBC The University of British Columbia

Acknowledgements

First of all, I would like to express my gratitude to my supervisor Dr. Matthias Militzer for giving me the opportunity to conduct this research. His continuous supervision, guidance, support and expertise were invaluable and pivotal to the success of this project. Special thanks are extended to Dr. Vladan Prodanovic for all the valuable advice and suggestions throughout the project.

I would like to sincerely thank Mr. Gary Lockhart for all the training and help, without whom none of the experiments would have been possible. I would like to thank Dr. Gilles Guedia for his inputs and suggestions. I would like to extend my gratitude to Mr. Ross McLeod, Mr. David Torok, and Mr. Carl Ng for preparation of samples, and the Department of Materials Engineering, UBC for making this experience a memorable one.

Thanks to my colleagues, for all the good times spent both at and outside work. My late parents, whom I always look up to for inspiration. My extended family, particularly my aunt Ms. Pronita Deka, and all my friends, who have always been a constant source of support and encouragement, especially in times of distress.

Finally, I would like to thank the Natural Sciences and Engineering Research Council of Canada and ArcelorMittal Dofasco Inc. for funding this research.

Dedication

This thesis is dedicated to my parents, Dr. Banti Deka Medhi (1959-2017) and Dr. Debendra Nath Medhi (1956-2003), who devoted their lives to academia.

Chapter 1: Introduction

Global steel production has seen a steady upward trend in the last few decades, and is expected to continue to do so in the future. With the constantly improving lifestyle standards across the planet, there is an ever-increasing need for advanced grades of steel with high strength, durability and versatility of application. To meet the demands of high-quality steel products, the last few decades have seen an increase in the production of hot rolled thermo-mechanical controlled processed (TMCP) steel strip(s) and plate(s) with customized microstructure and mechanical properties [1–4]. The use of TMCP steels is widespread across a number of sectors such as ship building, constructions, pipelines, transportation and energy. These advanced grades of steel facilitate to reduce the amount of material needed to meet the same strength requirements, and hence contribute towards sustainable growth. For example, the use of high strength TMCP steel plates in ship building has made it possible to cut costs and save energy by a significant reduction of the ship weight [4]. Another example of TMCP steel plate application are the offshore wind farms, which play a major role in the supply of energy by renewable sources [3]. One of the main advantages of using low carbon TMCP steels is their improved weldability. Products with the same mechanical properties can be produced with lowered alloying additions by utilizing the thermo-mechanically controlled process, hence improving cost effectiveness [4].

The desired mechanical properties and microstructure are obtained by the thermo-mechanically controlled process (TMCP) in two steps. First, the austenite evolution is controlled in the hot rolling process. Thereafter, the phase transformation(s) during austenite decomposition is controlled on the run-out table by a combination of cooling rates and cooling stop temperatures (for plates) or coiling temperatures (for strips). Careful design and control of the cooling rates and

cooling stop or coiling temperatures in the run-out table is being used to tailor the final microstructure and mechanical properties in TMCP steels. Hence, it is pivotal to study and quantify the heat transfer during the cooling process on a run-out table.

On an industrial run-out table, accelerated cooling of the steel strip or plate is achieved by arrays of top and bottom water jets, and a typical run-out table can be as long as 150 m [5]. Study of the process is not feasible and affordable on a full scale industrial run-out table. Therefore, experimental research is generally performed in a small-scale laboratory setup with one or an array of water jets impinging stationary or moving test samples.

At the University of British Columbia (UBC), a pilot scale run-out table facility is situated, which is capable of simulating industrial cooling conditions. The in-house facility is equipped to study the effect of different process parameters such as nozzle configuration, nozzle orientation, plate speed, water flow rate and water temperature during the accelerated cooling process. In the past decade and a half, a number of experimental studies have been conducted in the facility [6–11]. Results of such experimental studies form a database for the development of robust heat transfer models for better control of the industrial run-out table cooling process.

This thesis describes the boiling heat transfer during impingement cooling of a stationary low carbon steel plate by a bottom water jet of planar geometry. This work is part of a much larger project with the goal to develop fundamental physical models capable of accurately predicting the cooling behaviour on an industrial run-out table.

Chapter 2: Background and Literature

2.1 Industrial Run-out Table

In a conventional hot strip mill, the run-out table is situated between the finishing mill and the down coiler (Figure 2.1). However, in a plate mill the run-out table is not followed by a down coiler [3]. The steel strip or plate temperature is typically 800-900 °C at the exit of the finishing mill. Thereafter, the strip or plate is moved to the run-out table for cooling by means of water jets. The strip or plate is cooled to the respective coiling temperature or cooling stop temperature in the run-out table. A typical industrial run-out table consists of a series of top and bottom cooling banks to achieve symmetrical cooling [12]. Each bank comprises of headers containing nozzle(s) of different configurations. Three different types of nozzles are conventionally used to cool the moving steel strip or plate: planar nozzles (slot) for curtain jets, circular nozzles for laminar jets and spray nozzles for spray jets (Figure 2.2).

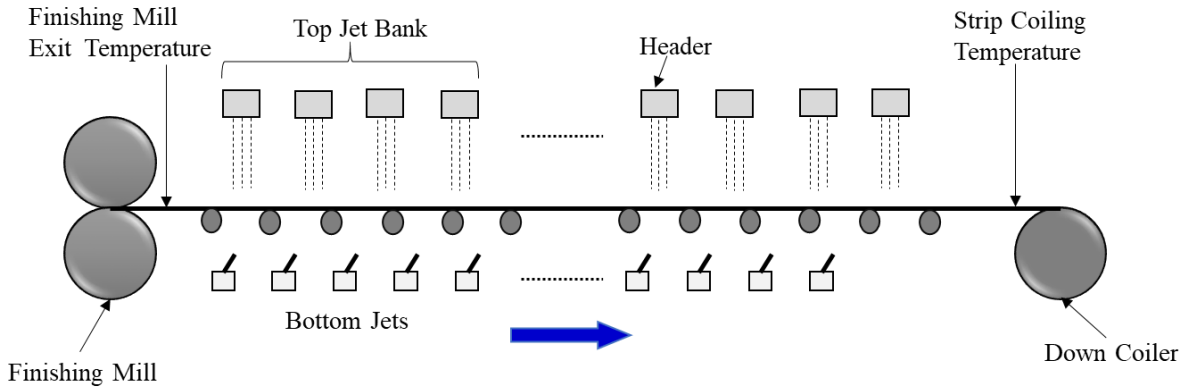

Figure 2.1 Schematic of an industrial run-out table in a hot strip mill (modified from [10]).

In the curtain jets, water exits the slot of a long planar nozzle and provides uniform cooling across the width of the steel strip. Generally, an array of circular nozzles is used for cooling purposes in the laminar cooling system. In the spray cooling system, water is sprayed over the surface of the steel strip, which typically covers a large area of the strip surface. Heat transfer rates during cooling can also be affected by the interaction of water flowing from adjacent jets in the run-out table [13].

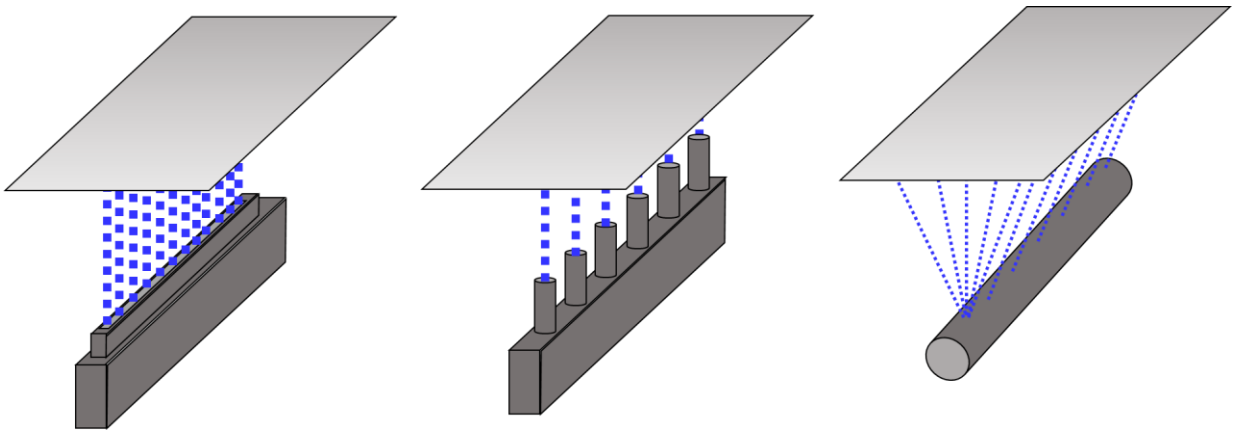

(a) **(b)** **(c)**

Figure 2.2 Schematic of (a) curtain jet system (b) multiple laminar jets system (c) spray jet system for bottom cooling.

2.2 Boiling Curve

An industrial run-out table utilizes water to cool down hot steel strip/plates from high temperatures. Due to high surface temperatures of the plate/strip, the prime mechanism of heat transfer is the boiling of water. The high latent heat of the phase change (vaporization) and specific heat capacity of water makes it an efficient coolant. The fundamentals of the classical case of pool boiling provides a good background to grasp the mechanisms of heat transfer during boiling. Pool

boiling is defined as the mode of boiling when a pool of water covers a hot surface. Although cooling is achieved on a run-out table by an impinging water jet, the fundamental mechanisms of pool boiling heat transfer can be extended to run-out table cooling. Boiling heat transfer is generally represented by a boiling curve, which depicts the heat flux values as a function of surface temperatures. Figure 2.3 shows the schematic of a qualitative pool boiling curve.

Numerous studies of pool boiling experiments have established the existence of four distinct heat transfer regimes i.e. natural convection, nucleate boiling, transition boiling and film boiling [14–16]. The existence of these boiling regimes depends on the temperature of the surface (Figure 2.3). At temperatures below the saturation point of water, heat transfer occurs in single phase (no boiling) by natural convection. No vapor formation occurs in this range of temperatures, and heat transfer is due to conduction from the heated surface and movement of the cooling medium (water). At temperatures slightly above the saturation point of water, vapor bubbles start to form at preferential isolated locations on the hot surface. This point marks the beginning of nucleate boiling and is termed as the onset of nucleate boiling (ONB). The initial stage of nucleate boiling is characterized as partial nucleate boiling. Heat transfer is enhanced by the latent heat of vaporization and enhanced fluid motion as the bubbles rise into the bulk of the fluid (water). Upon further increase of surface temperature, bubble nucleation sites increase, causing the increasing number of vapor bubbles to coalesce and form columns of vapor which escape from the top surface of the pool of water. This region at higher surface temperatures is characterized as the fully developed nucleate boiling regime. Heat transfer rates increase substantially due to increased vapor formation and enhanced fluid motion, and the boiling curve shows a sharp rise in the heat flux values. Nucleate boiling is considered as the most efficient mode of boiling heat transfer [16]. Eventually, the dynamics of increasing vapor bubbles interfere with the movement of liquid near

the heated surface, impeding efficient heat transfer, and a local maximum in the boiling curve is reached known as the critical heat flux (CHF). The CHF marks the termination of the nucleate boiling regime.

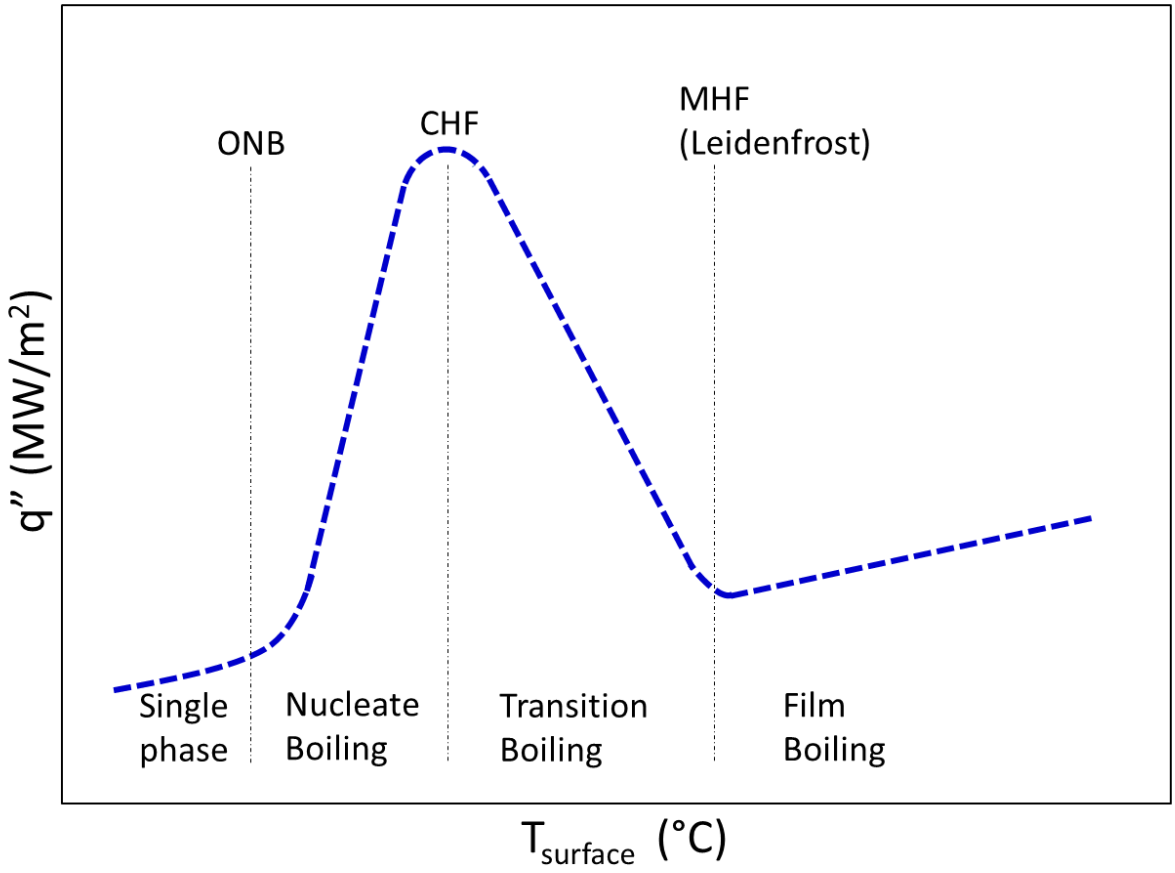

Figure 2.3 Schematic of a classical pool boiling curve showing different boiling regimes.

Beyond the CHF, transition boiling is observed, which is associated with the formation of vapor patches on the hot surface due to high rates of bubble formation. The conductivity of vapor is much lower than that of water [14], and the vapor patches effectively insulate the surface from the liquid and thus heat flux values decrease. At any point during transition boiling, the hot surface

is in dynamic contact with both liquid and vapor. With increasing surface temperature, vapor begins to cover larger areas of the surface, further decreasing the heat flux values till a minimum heat flux (MHF) value is reached, known as the 'Leidenfrost' point. The Leidenfrost point marks the entry into the film boiling regime. During film boiling, the heated surface is completely isolated from the liquid medium by a stable vapor film. Heat extracted from the surface must traverse through the insulating vapor film, before reaching the liquid medium, which results in comparatively low heat flux values. Eventually, at high surface temperatures, radiation through the vapor film becomes the dominant mode of heat transfer and heat transfer rates increase gradually.

2.3 Jet Impingement Hydrodynamics

In contrast to pool boiling, water impinges the surface of a hot strip/plate on an industrial run-out table by means of different conventional jet systems, i.e. planar jets, circular jets and/or spray jets. Water jets with continuous cross-sections (planar and circular) impinging on a surface can be classified into five different configurations, i.e. free-surface, plunging, submerged, confined, and wall jets [16]. During industrial run-out table cooling, free-surface jets and plunging jets are generally observed. In free-surface jet impingement, water travels and hits a solid surface without any hindrances or obstructions. Whereas, in plunging jet configuration, the jet impinges on to an already existing pool of water on the surface.

Both top and bottom jet systems are used in a run-out table for homogeneous cooling of strip(s)/plate(s) moving in the horizontal direction. The fundamental difference between top and bottom jets is the effect of gravity. For top jets, gravity accelerates the water jet exiting the nozzle, whereas the opposite is true for bottom jets (Figure 2.4). Moreover, for top jets, water is

accumulated on the impinging surface with time, which is not the case for bottom jets as the water tends to fall off the surface due to gravity.

The average impingement velocity (v_i) and impingement jet width (w_j) are correlated to the nozzle exit velocity (v_n) and nozzle width (w_n) of a planar nozzle by the following equations [16, 17]:

$$v_i = \sqrt{(v_n^2 + 2gH_n)} \qquad \text{(for top jets)} \tag{2.1}$$

$$v_i = \sqrt{(v_n^2 - 2gH_n)} \qquad \text{(for bottom jets)} \tag{2.2}$$

$$w_j = \left(\frac{v_n}{v_i}\right) w_n \tag{2.3}$$

$$v_n = \frac{\dot{Q}}{A_n} \tag{2.4}$$

where $\dot{Q}$ is the water flow rate and A_n is the cross-sectional area of nozzle exit. H_n is the vertical stand-off distance between the nozzle exit and impingement surface. For top planar jets, due to acceleration by gravity, the jet impingement velocity (v_i) is higher than the nozzle exit (v_n) velocity (equation 2.1), and consequently the width of the impinging jet (w_j) is smaller than that of the nozzle exit (w_n). On the contrary for bottom planar jets, due to deceleration by gravity, the jet impingement velocity (v_i) is lower than the nozzle exit velocity (v_n), and the width of the impinging jet (w_j) is larger than the nozzle (w_n). Figures 2.4 (a) and (b) show the schematics of an impinging planar jet on a stationary surface for top and bottom nozzles, respectively. Equations 2.1-2.4 can be used for a circular nozzle by replacing the widths of a planar nozzle (w_n) and water jet (w_j) in equation 2.3 with the squares of the diameters of a circular nozzle (d_n^2) and water jet (d_j^2), respectively.

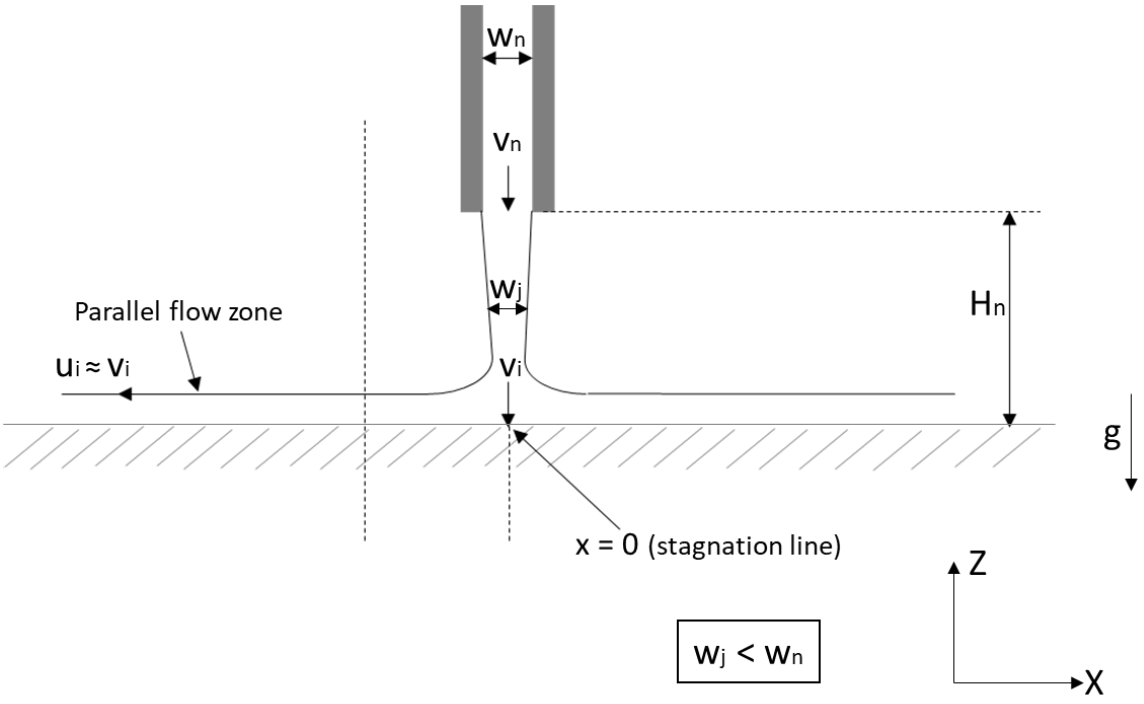

(a)

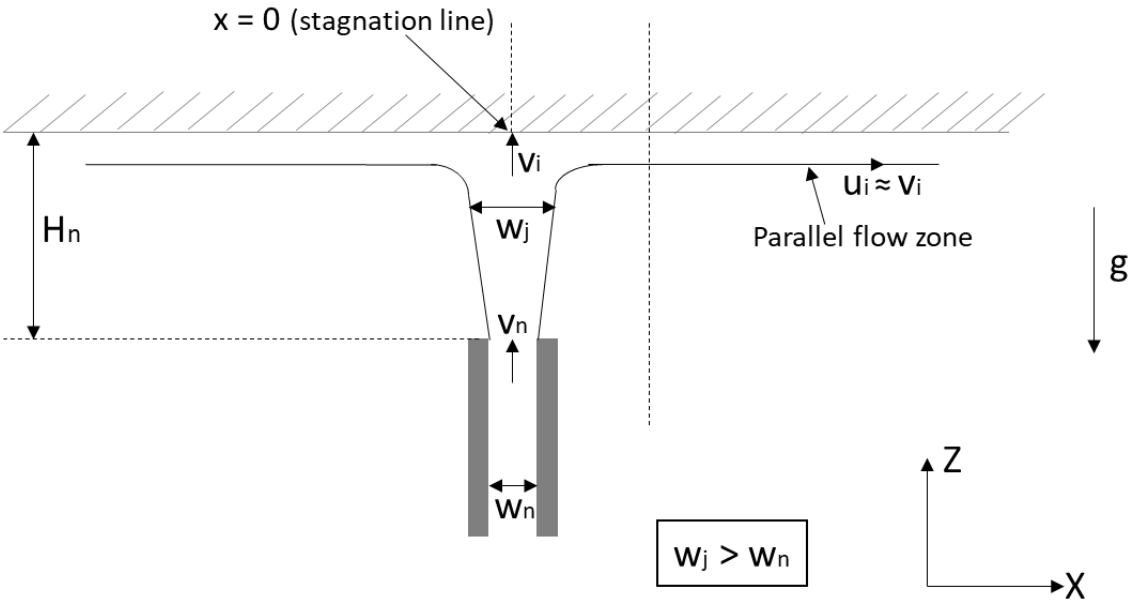

(b)

Figure 2.4 Schematic showing an impinging water jet on a stationary surface by a (a) top planar nozzle (adapted from [18]) (b) bottom planar nozzle.

As the impinging jet hits the surface, it changes direction to traverse in the horizontal direction along the surface of the plate. At the stagnation line (planar jet)/point (circular jet), the streamwise velocity (u_i) is zero. As the jet starts travelling in the horizontal direction, the liquid accelerates till it reaches the speed of the impinging jet [16]. Thereafter, the streamwise velocity remains constant with increasing distance from the stagnation line of a planar jet (Figure 2.5(a)), whereas it gradually decreases with increasing radial distance from the stagnation point of a circular jet (Figure 2.5(b)) [19].

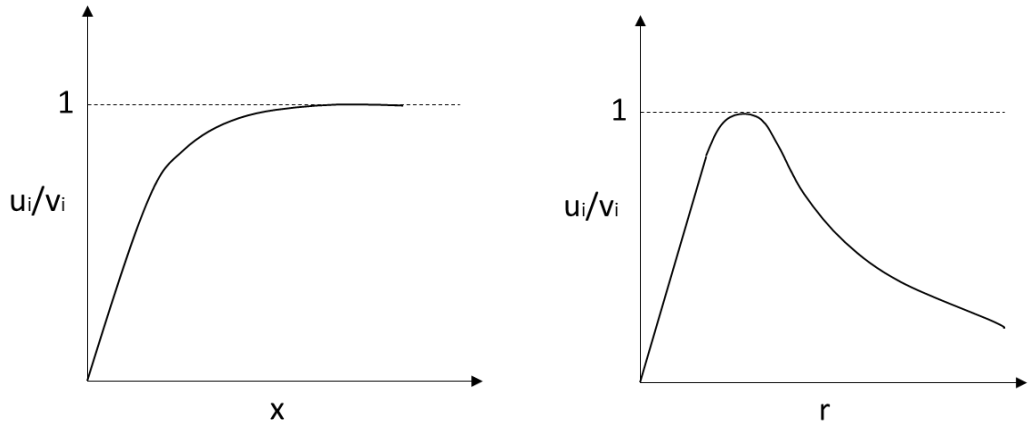

(a) **(b)**

Figure 2.5 Schematic showing the velocity profile of an impinging (a) planar jet (b) circular jet (adapted from [19]).

The water flow can be divided into two different zones: the 'impingement zone' at and near the stagnation line/point and the 'parallel flow zone' at a certain distance from the water jet [20]. Liu et al. [21] video recorded an impinging circular top jet on a hot steel surface, and observed an effect of water temperature on the size of the instantaneous 'impingement zone' as the water jet hits the surface. With lowering the water temperature from 30 °C to 13 °C, the impingement zone became larger, and the impinging jet travelled faster in the radially outward direction.

2.4 Jet Impingement Heat Transfer

2.4.1 Experimental Research

2.4.1.1 Overview

Jet impingement heat transfer is characterized as forced flow boiling [16]. As opposed to classical pool boiling, liquid is in motion relative to the hot surface and flows over it. Although differences lie in the liquid flow hydrodynamics, all four boiling regimes i.e. natural convection, nucleate boiling, transition boiling, and film boiling are observed in jet impingement cooling [18, 22]. The different boiling regimes are affected by process parameters and can coexist at different locations from the water jet [23]. Correlations for the different boiling regimes during jet impingement cooling are discussed in the subsequent sections. Numerous experimental studies have been conducted to understand the mechanisms of jet impingement boiling heat transfer. Table 2.1 summarizes the different experimental conditions such as jet type, nozzle dimensions, water temperature, jet velocity and stand-off distance for the studies discussed in this section. This comprehensive literature review is focused on experiments with stationary samples. Jet impingement experiments are conducted in two different methods: steady state and transient. During steady state experiments, either the surface temperature or the heat flux is controlled, and steady state is obtained. In transient experiments, the test sample is first heated to a desired temperature, and then it is cooled using a water jet. The heat flux extracted during transient cooling is determined using mathematical methods such as inverse heat conduction [12, 24–26]. Also, an additional portion of the boiling curve termed as ‘initial cooling’ is observed in transient experiments corresponding to the initial interaction of the surface with water [19, 26]. This region is characterized by a rapid increase in heat flux values with decreasing surface temperature coincident with the impact of the jet on the hot surface. The slope of the heat flux rise during initial

cooling is unaffected by the initial surface temperatures ranging from of 400-1000 °C [26]. Run-out table cooling is best represented by experiments under transient cooling conditions.

Table 2.1 reveals that the majority of jet impingement studies have been conducted for top cooling, and experimental studies on bottom cooling are limited and mainly focused on laminar jets (circular nozzle). Also, most of the studies on planar jets are based on experiments under steady state conditions. There is no instance of an experimental study conducted for a bottom planar jet under transient conditions in the available literature.

Table 2.1 Experimental conditions of stationary tests for studies cited in section 2.4 (values that have not been reported are shown by "-")

Authors	Steady state/transient	Nozzle type	Top /bottom cooling	Nozzle width/diameter	Nozzle stand-off distance	Test material	Water temperature	Jet velocity or flow rate	Measurement positions
Bogdanic et al. (2009)	Steady state	Planar	Top	1 mm	8 mm	Copper	80 °C	0.4 m/s	Stagnation
Chester et al. (2012)	Transient	Circular	Bottom	18 mm	400 mm	DQSK steel	30 °C	35-55 l/min	Radial
Gradeck et al. (2009)	Transient	Planar	Top	4 mm	-	Nickel	17-90 °C	0.8-1.2 m/s	Circumferential (cylindrical block)
Hall et al. (2001)	Transient	Circular	Top	5.1 mm	56.1 mm	Copper	25 °C	2-4 m/s	Radial
Hamed et al. (2015)	Steady state	Planar	Top	1 mm	6 mm	Copper	85 °C	0.6-0.75 m/s	Stagnation
Hauksson et al. (2004)	Transient	Circular	Top	19 mm	1500 mm	DQSK steel	30-50 °C	15-45 l/min	Radial
Ishigai (1978)	Steady state/transient	Planar	Top	6.2 mm	15 mm	Stainless steel	45-95 °C	1-3.2 m/s	Stagnation
Islam et al. (2008)	Transient	Circular	Bottom	2 mm	45 mm	Steel, brass	20-95 °C	3-15	Radial
Leocadio et al. (2009)	Transient	Circular	Top	10 mm	300 mm	AISI 304	22 °C	2.7 m/s	Radial
Liu et al. (2002)	Transient	Circular	Top	18.92-30 mm	1500mm	DQSK and stainless steel	13-30 °C	5.6-6.53 m/s	Radial
Miyasaka et al. (1980)	Steady state	Planar	Bottom	10 mm	-	Platinum	15 °C	1.1-15 m/s	Stagnation
Mozumder et al. (2005)	Transient	Circular	Bottom	2 mm	44 mm	Copper, brass, steel	20-95 °C	3-15 m/s	Radial

Table 2.2 Experimental conditions of stationary tests for studies cited in section 2.4 (continued…) (values that have not been reported are shown by "-")

Authors	Steady state/transient	Jet type	Top /bottom cooling	Nozzle width/diameter	Nozzle stand-off distance	Test material	Water temperature	Jet velocity or flow rate	Measurement positions
Mozumder et al. (2007)	Transient	Circular	Bottom	2 mm	44 mm	Copper, brass, steel	20-95 °C	3-15 m/s	Radial
Nobari et al. (2016)	Transient	Planar/ circular	Top	3 mm/ 19 mm	100 mm	Low carbon steel	10-40 °C	2.3-4.8 m/s	Longitudinal /radial
Ochi et al. (1984)	Transient	Circular	Top	5-20 mm	25 mm	Stainless steel	20-95 °C	2-7 m/s	Radial
Robidou et al. (2002)	Steady state	Planar	Top	1 mm	3-10 mm	Copper with nickel layer	83-93 °C	0.6-0.8 m/s	Longitudinal
Robidou et al. (2003)	Steady state	Planar	Top	1 mm	3-10 mm	Copper with nickel layer	83-93 °C	0.6-0.8 m/s	Longitudinal
Wang et al. (2016)	Transient	Circular	Top/bottom	4 mm	0-400 mm	AISI steel	10 °C	1.5-25 l/min	Radial
Wolf et al. (1996)	Steady State	Planar	Top	10.2 mm	102 mm	Ni-Cr-W-Mo alloy	50 °C	2-5 m/s	Longitudinal
Xu et al. (2006)	Transient	Circular	Top	19 mm	1500 mm	DQSK and stainless steel	30-80 °C	0.88-2.64 m/s	Stagnation

2.4.1.2 Film Boiling and Wetting

Although film boiling is not favorable for high heat extraction rates, film boiling may be observed during jet impingement cooling due to high initial surface temperatures of steel strips/plates on a run-out table. A stable vapor layer separating the hot surface from contact with water characterizes film boiling. The beginning of wetting coincides with the Leidenfrost point in the boiling curve [27] and is characterized by boiling noise and a sharp increase in the heat flux values with decreasing surface temperature. Experimental observations have shown that heat extraction rates of film boiling depend on parameters such as cooling water temperature, jet velocity, sample material [28] and distance from the water jet.

Filipovic et al. [29] conducted transient experiments on a pre-heated sample quenched by a parallel wall jet on the top surface to obtain local heat transfer coefficient values during film boiling. Results showed an increase in local heat transfer coefficients and decrease in the vapor layer thickness with decreasing water temperature and increasing jet velocity. Bogdanic et al. [30] used a miniature optical probe of 1.5 μm tip diameter as a tool to measure the vapor height in the stagnation line under a top curtain jet in steady state. The measured vapor film thickness was reported to be approximately 8 ± 2 μm for a jet velocity and water temperature of 0.4 m/s and 80 °C, respectively.

Ishigai [31] observed the transient quenching by a top planar nozzle in the stagnation zone of stainless steel samples pre-heated to 1000 °C. A stable vapor film was visible from the beginning of cooling till the point where the heat flux values dropped to a minimum in the obtained boiling curves (Leidenfrost), which was coincident with the collapse of the vapor film and wetting of the surface. Film boiling heat flux values increased with increasing jet velocity and film boiling ceased to exist when the water temperature was lowered to 45 °C. The minimum heat flux value at the

Leidenfrost point (MHF) was found to increase with increasing jet velocity and decreasing water temperature. They proposed a correlation for the MHF heat flux on the stagnation line as a function of jet velocity and water sub-cooling, i.e.:

$$q^{"}_{MHF} = 5.40\ X\ 10^{4}\ (1 + 0.527\ \Delta T_{sub}) v_i^{0.607} \ldots\ldots \text{(W/m}^2\text{)} \ldots \text{[Planar Nozzle]} \quad (2.5)$$

Similarly, Ochi et al. [32] reported that water temperatures less than 35 °C prevents the formation of a vapor film during quenching transient top cooling by a laminar jet even for surface temperatures as high as 1000 °C. A similar correlation for MHF heat flux was proposed, i.e.:

$$q^{"}_{MHF} = 3.18\ X\ 10^{5}(1 + 0.383\ \Delta T_{sub}) \left(\frac{v_i}{d}\right)^{0.828} \ldots \text{(W/m}^2\text{)} \ldots \text{[Circular Nozzle]} \quad (2.6)$$

where *d* is the diameter of the circular nozzle. For equations 2.5 and 2.6, v_i is the jet impingement velocity in m/s and $\Delta T_{sub} = T_{sat} - T_{water}$ is the sub-cooling of quenching water. Visual recordings made by Liu et al. [21] and Leocadio et al. [33] confirmed the absence of film boiling during transient cooling for initial surface temperatures as high as 900 °C in the jet impact zone of a top circular nozzle (water temperature 22 °C).

Filipovic et al. [29] observed a decrease in local heat transfer coefficient values with increasing distance from the wetted region. It was inferred to be the combined effect of liquid-vapor boundary layer development and decrease in the local liquid sub-cooling. Robidou et al. [18, 22] obtained the local boiling curves up to a distance of x/w_n = 55 from the stagnation line for cooling by a top planar jet in steady state. Film boiling was observed in the boiling curves for all

locations. However, the Leidenfrost temperature shifted from a higher temperature (~450 °C) in the stagnation line to a lower temperature (~180 °C) in the parallel flow region. A linear dependence of the Leidenfrost temperature on the water sub-cooling was proposed for the stagnation zone of a top circular nozzle by Liu [34]. Film boiling heat fluxes increase steadily with increasing surface temperature [18, 29]. Local boiling curves obtained by Nobari et al. [19] show film boiling following the 'initial cooling' region at a distance from the stagnation line/point for transient top cooling by planar/circular nozzles. However, film boiling was found to be absent in the boiling curve at the stagnation line/point for a cooling start temperature of ~720 °C. This may be due to the local sub-cooling of quenching water, which is highest in the stagnation line/point and decreases with increasing distance from the water jet, as the water absorbs heat as it travels along the hot surface with time.

Several experimental studies were conducted to observe the wetting propagation for a bottom circular nozzle impinging on a pre-heated block of copper/steel/brass [28, 35–37]. Mozumder et al. [35] observed a delay in wetting front propagation after the jet hits the surface. A resident time was defined as the time from when the jet strikes the hot surface until the wetting front starts moving and is synonymous to delay in wetting [38]. The resident time varied from less than a second to over 15 minutes and was found to be strongly dependent on sample material and jet sub-cooling but only weakly dependent on jet velocity and initial sample temperature. The delay time in wetting decreased with increasing sub-cooling. Islam et al. [28] observed the flow pattern on steel and brass blocks pre-heated to 500-600 °C. Different types of flow patterns were observed (splashed droplets, liquid sheet, conical liquid etc.) depending on surface conditions, sample material and initial temperature. Film boiling upon impingement was observed in the liquid sheet type of flow whereas flow patterns such as splashed droplets hinted against a stable vapor

film. The complexity of the problem is compounded due to two mutually coincident phenomena i.e. boiling mechanisms and jet impingement hydrodynamics [6].

2.4.1.3 Transition Boiling

During transition boiling, liquid is in intermittent contact with the heated surface. Unstable vapor patches prevent complete wetting of the surface [39]. The transition boiling regime is bounded by the CHF (maximum) and Leidenfrost (minimum) heat flux points in the boiling curve and is described as a mixture of unstable film boiling and unstable nucleate boiling [40]. Based on the proposed mechanism by Berenson [40], the transition boiling regime has been described mathematically as a combination of nucleate boiling (liquid contact) and film boiling (vapor contact) by many researchers [41–43]:

$$q_{TB}^{"} = q_{l}^{"} F + q_{v}^{"} (1 - F) \tag{2.7}$$

where F is the fraction of surface area in contact with the liquid and $q_{l}^{"}$ and $q_{v}^{"}$ are heat fluxes during contact with liquid and vapor, respectively. Nishio and Auracher [44] as well as Ragheb and Chan [45] replaced the two heat flux terms $q_{l}^{"}$ and $q_{v}^{"}$ with the heat flux values of the critical heat flux (CHF) and at the Leidenfrost point (MHF), respectively. In a log-log plot of heat flux vs surface superheat (boiling curve), a linear relationship in the transition boiling regime is established by interpolating these boundary values.

An atypical trend in the transition boiling regime during jet impingement cooling termed as the ‘shoulder’ has been observed by a number of researchers [18, 22, 31, 46, 47] . The ‘shoulder’ is characterized as a region with nearly constant heat flux values in the transition boiling regime

of the boiling curve. The 'shoulder' was first seen in the experiments conducted by Ishigai [31] when the water temperature was lower than 75 °C. A stronger influence of water temperature was observed on the shoulder region as compared to jet velocity for the range of experimental conditions. The width of the shoulder region, and the heat flux values increased with decreasing water temperatures (45-95 °C).

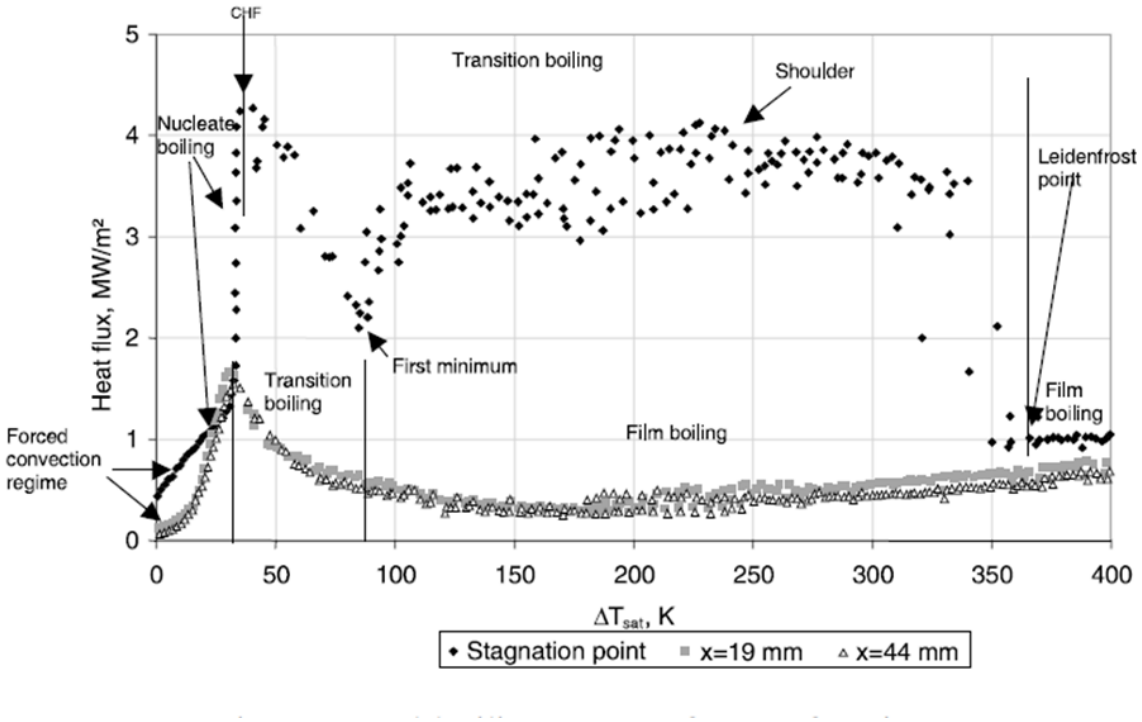

Figure 2.6 Local boiling curves; experimental condition: steady state, ΔT_{sub}=16 °C, V_j = 0.8 m/s, H_n = 6mm (Reprinted from [18], with permission from Elsevier).

Robidou et al. [18, 22] observed a shoulder in the steady state boiling curves for distances less than $^{x}/_{w_n} = 6$ from the stagnation line even for water temperatures as high as 93 °C using a top planar nozzle (Figure 2.6). In the characteristic boiling curves with a shoulder in Figure 2.6, the heat flux values are seen to decrease in the transition boiling region for surface temperatures

greater than the CHF point. The heat flux values eventually reach a 'first minimum' in the boiling curves. Thereafter, with increasing surface temperatures, the heat flux values are seen to increase sharply and becomes nearly independent of surface temperatures (with some fluctuations) in the 'shoulder' of the transition boiling region. With increasing surface temperatures, the transition boiling region terminates as the film boiling regime is reached at the corresponding Leidenfrost point (MHF). However, the first minimum point observed by Robidou et al. [18, 22] has not been observed in other experimental results [31, 46, 48]. The characteristic boiling curve obtained by Robidou et al. [18] in the stagnation line with the 'shoulder' was reproduced in the steady state experiments conducted by Bogdanic et al. [30] and Hamed et al. [47].

The shoulder heat flux values decrease with increasing distance from the stagnation line and decreasing water sub-cooling in the local boiling curves obtained by Robidou et al. [18]. The influence of jet velocity was not found to be substantial for the shoulder heat flux values. Seiler-Marie et al. [49] and Hamed et al. [47] have attempted to develop physical models for the shoulder heat flux in the stagnation line for top cooling using two different approaches. Based on the experimental results of Robidou et al. [18], Seiler-Marie et al. [49] modelled the shoulder heat flux at the stagnation line. The correlation for the shoulder was based on the assumption that periodic bubble oscillations occurred on the superheated surface due to the hydrodynamic instability at the liquid-vapor interface. The instability at the liquid-vapor interface was determined to be due to the contribution of two sources: the pressure of the heavier liquid phase on top of the lighter vapor phase and the pressure of water jet impingement. The Rayleigh-Taylor instability criterion was applied to determine a critical wavelength for the liquid-vapor interface. It was hypothesized that when the vapor patch diameter is greater than the critical wavelength, it breaks up into smaller patches and is eventually displaced into the bulk flow of liquid by growth of bubbles, hence

enhancing the liquid contact with the surface. Comparison of the calculated and measured shoulder heat flux values showed a relative error of 24 %. Nobari et al. [19] extended this model to determine shoulder heat flux values during transient top cooling by circular/planar nozzles at varying distances from the water jet, considering the decrease of pressure due to jet impingement and decrease in local sub-cooling of water with increasing distance from the stagnation zone. The developed mechanistic model is capable of mapping boiling curves at varying distances from the stagnation point for top cooling of stationary plates.

Bogdanic et al. [30] developed a method to measure the contact frequency of liquid throughout the shoulder using a miniature optical probe of 1.5 μm tip diameter. The contact frequency was observed to be 900 Hz at the first minimum, increased to 2 kHz at the beginning of the shoulder, and further increased to 20 kHz at the end of the shoulder. Hamed et al. [47] proposed a wall heat flux partition model based on these observations. It was assumed that at lower surface temperatures, liquid reaches the surface and covers relatively large patches of surface during the unstable vapor break up cycle. At higher surface temperatures, the ability of the liquid to reach the surface decreases and the liquid penetrates the vapor layer in the form of intruding jets, hence increasing the contact frequency on the surface. Mathematically, the wall heat flux model was proposed as a combination of the liquid intrusion heat flux and liquid wetting heat flux. Comparison of calculated heat fluxes with measured values by Robidou et al. [18] and Bogdanic et al. [30] show a relative error of 30%. The calculated heat flux values do not show good agreement for higher surface temperatures in the shoulder region.

2.4.1.4 Critical Heat Flux

The critical heat flux (CHF) is the maximum heat flux value in the pool boiling curve and is the transitioning point between the nucleate boiling and transition boiling regimes. Several experimental studies have been performed to derive correlations for the CHF during jet impingement cooling in relation to process parameters such as jet velocity and water sub-cooling etc. [16]. In general, the critical heat flux value is seen to increase with increasing jet velocity and increased water sub-cooling (decreasing water temperature). The review of Wolf et al. [16] shows that the CHF varies approximately with $v_i^{1/3}$ at the stagnation point for most experimental data. Miyasaka et al. [48] termed the critical heat flux as the deviation from nucleate boiling (DNB) and described it as the heat flux where the values deviate from the nucleate boiling correlation. A correlation was proposed for the steady state critical heat flux in the stagnation line for a bottom planar jet with respect to jet impingement velocity as:

$$q''_{DNB} = q''_{CHF,pool,sub.}(1 + 0.86v_i^{0.38}) \tag{2.8}$$

where v_i is the jet impingement velocity in m/s, $q''_{CHF,pool,sub.}$ is the critical heat flux value for boiling of a stationary sub-cooled pool of water. Ishigai and Mizuno [50] proposed a correlation for the CHF with respect to jet velocity ($1.3 < v_i < 9$ m/s) and water sub-cooling ($45°C < \Delta T_{sub} < 80°C$) for a bottom circular nozzle as:

$$q''_{CHF} = 0.0142\ X\ 10^6 \left(\frac{v_i}{d}\right)^{0.34} \Delta T_{sub}^{1.15} \tag{2.9}$$

where v_i is the jet impingement velocity (m/s), d is the nozzle diameter (m), and $\Delta T_{sub} = T_{sat} - T_{water}$ is the amount of sub-cooling (°C). The correlation provides a good fit for the range of experimental conditions it was developed for (jet velocity: $1.3 < v_i < 9$ m/s and water sub-cooling: 45°C $< \Delta T_{sub} <$ 80°C). However, the dependence of CHF with the inverse of the jet diameter in inconsistent with most of the CHF literature [16].

The maximum heat flux in the boiling curve for transient cooling may not be equivalent to the critical heat flux obtained in steady state experiments and is dependent on the thermo-physical properties of the material [36]. Hall et al. [51] examined the local maximum heat flux values at radial positions from the stagnation point for a top circular nozzle. A sharp drop of the heat flux values was seen with increasing distance clearly demarcating the impingement zone and the parallel flow zone. Nobari et al. [19] observed a similar trend in the local maximum heat flux values for transient jet impingement cooling for top planar/circular nozzles. Close to the water jet, the maximum heat flux values remained almost constant or dropped slightly. Thereafter, a rapid drop in the local maximum heat flux values are seen, which becomes nearly independent of distance at farther locations (Figure 2.7). Robidou et al. [18] observed a drop in the CHF values for steady state boiling curves during impingement by a top planar nozzle up to a distance of $x/w_n = 10$. Thereafter, the CHF values become nearly constant (Figure 2.6).

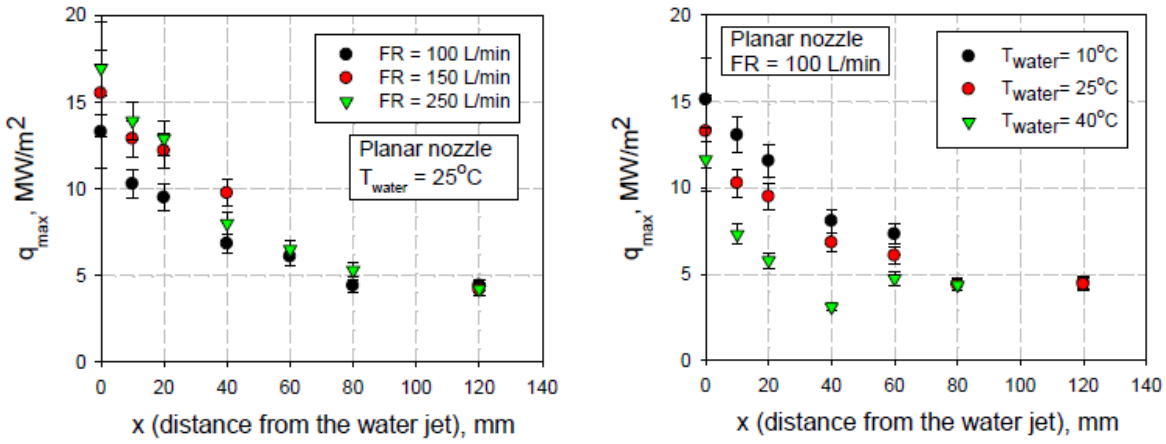

(a) **(b)**

Figure 2.7 Experimental maximum heat flux for a top planar jet for: (a) different water flow rates (b) different water temperatures (Reprinted from [6], with permission from the copyright holder).

2.4.1.5 Nucleate Boiling

Literature shows that the most thoroughly studied mode of boiling heat transfer is nucleate boiling. Due to its high heat transfer efficiency, nucleate boiling has seen a considerable number of experimental studies. It is mostly agreed that heat flux in the nucleate boiling region is dependent solely on the surface temperature, and is independent of other process parameters such as jet velocity, water sub-cooling etc. [16]. The steady state local boiling curves for different distances from a planar jet obtained by Robidou et al. [18] showed that the boiling curves in the fully developed nucleate boiling regime merge into a single boiling curve which is independent of distance from the water jet as well as jet velocity and sub-cooling. Transient experiments have reproduced the same trend in the nucleate boiling regime [19, 20]. However, the results obtained by Hall et al. [51] disagree with this trend. The nucleate boiling heat flux values in transient cooling were found to vary with jet velocity for a circular nozzle.

In general, the heat fluxes in the fully developed nucleate boiling regime are described by the following equation [16]:

$$q''_{NB} = C\left(\Delta T_{sup}\right)^{n} \tag{2.10}$$

where *C* and *n* are process related constants and ΔT_{sup} is the amount of surface superheat.

2.4.1.6 Effect of Nozzle Inclination

In common industrial practice, the bottom jet nozzles in the run-out table are often inclined at an angle with respect to the horizontal. In most experimental studies, orientation between the jet and the heated surface has been considered as a secondary factor during heat transfer and its effects on heat extraction rates have not been considered even in the most detailed studies [10]. The effects of orientation between the jet and surface have been mostly investigated for pool boiling, or in the case of jet impingement, air is used as a coolant and the surface is usually rotated around a fixed jet [52–55]. The pilot scale run-out table facility at UBC is equipped to study the effect of varying nozzle inclinations for a bottom circular or planar nozzle. Previously, Chester et al. [56] studied the heat transfer on a hot steel plate cooled by an inclined bottom circular water jet. The same has not yet been investigated for a bottom planar water jet.

Changing the nozzle inclination causes asymmetry in the flow pattern during jet impingement cooling [10]. Figure 2.8 shows a schematic of an inclined water jet impinging on the bottom surface of a sample. The jet travels in a projectile path and the impact on the surface occurs at an angle with respect to the vertical [57]. The vertical impingement velocity is a fraction ($v_i =$

$v_j cos\Theta$) of the overall jet velocity and decreases with increasing nozzle inclination, however the overall impact velocity (v_j) of the jet remains constant for same vertical spacing between nozzle exit and impinged surface. A small component of velocity ($v_x = v_j sin\Theta$) parallel to the surface exists in the direction of jet inclination (+x direction in this case), causing the wetting front to travel faster in this direction. For the opposite direction (-x direction in this case), the impingement hydrodynamics would follow a pattern similar to a vertical jet (Section 2.3).

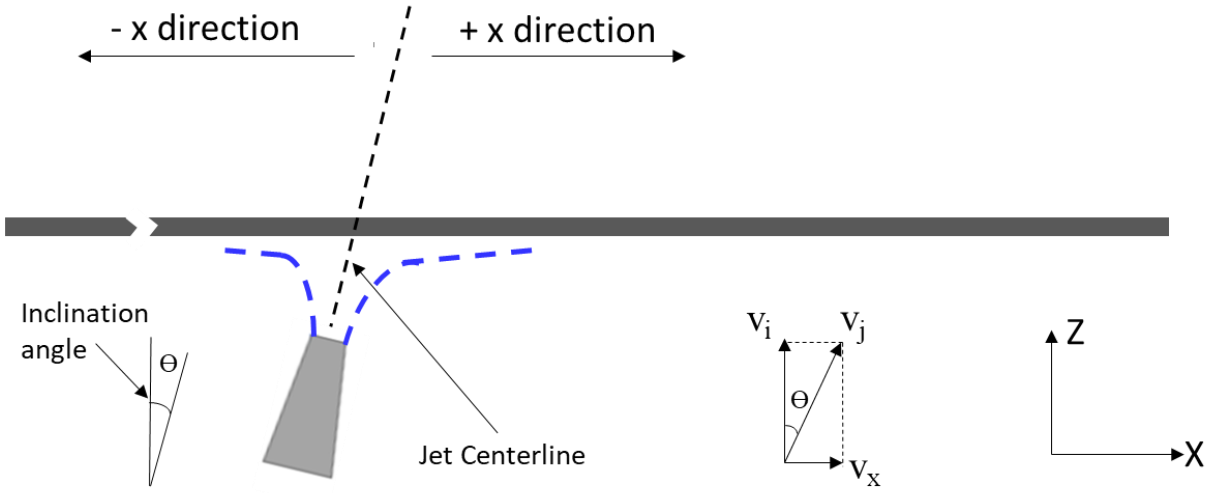

Figure 2.8 Schematic showing an impinging water jet inclined at an angle with respect to the vertical axis

In the experimental results obtained by Chester et al. [56], the effect of varying nozzle inclinations (0-30° with respect to vertical) was evident in the asymmetry of wetting front progression, and the wetting front travelled faster in the direction of jet inclination (+x direction), the effect of which increased with increasing nozzle inclination. The cumulative heat extracted with time and overall wetted zone was found to decrease with increasing nozzle inclinations (0-30°). For lower flow rates, the effect was seen to be more prominent and the ability of the jet to

reach the bottom surface was compromised. This can be explained as the influence of the projectile path followed by the water jet, which would be more pronounced for greater distances between the nozzle and the surface. However, it was not explicitly mentioned if the same nozzle to plate distance was maintained for all orientations. Simply tilting the nozzle with respect to the vertical at the set height would lower the nozzle tip and effectively increase the stand-off distance, which has an influence in the heat extraction rates [25].

2.5 Modelling of Run-out Table Cooling

Different approaches have been taken for modelling the temperature history on a run-out table. Timm et al. [58] used a statistical optimization approach to develop a model for predicting coiling temperatures up to 550 °C. Optimization of the model was based on data obtained from thousands of strips to minimize error in the predictions. A constant thickness of vapor film was assumed in a defined parallel flow zone. Constant values of maximum heat flux were assumed for jet impingement cooling on top and bottom surfaces in the defined impingement zone, and a corrective term dependent on water temperature was used for fitting. The model predicted coiling temperatures with an accuracy of ± 14 °C. Sikdar et al. [59] used a Finite Difference Method to develop a model for coiling temperatures of ~ 550 °C. The heat transfer coefficient was correlated as a simple third-order polynomial of instantaneous strip surface temperature during jet impingement cooling and fitting constants specific to the mill conditions were proposed. Guo et al. [60] developed a mathematical optimization technique using a feed forward and feed backward self-learning model designed to obtain the target coiling temperature for coiling temperatures of 594-743 °C. Sun et al. [61] developed an integrated model for phase transformation assuming steady state heat transfer in the run-out table and a lower heat transfer coefficient for bottom

cooling compared to top cooling, assuming higher contact of water with top surface. Chen et al. [62] developed an integrated model for heat transfer and phase transformation for a coiling temperature of 650 °C using a Finite Element method. Constant heat transfer coefficients were assumed for the impingement zone and parallel flow zones, respectively, and stable film boiling was assumed in the parallel flow zone. The heat transfer coefficient for water cooling was proposed in a multiplication form of corrective factors for different process parameters such as jet velocity, water temperature, strip speed and different nozzle types. An integrated hot strip mill model (HSMM) incorporating heat transfer, deformation behaviour and microstructure evolution was developed by the Microstructure Research group at UBC under the auspices of the American Iron and Steel Institute (AISI). This model is commercially available as the Integ-HSMM software package and is used worldwide by numerous steel companies [63]. Two different model modes are considered to track the temperature history and microstructure evolution along the length of the steel strip in a simulated hot strip mill: (a) single node mode which considers the steel strip as an average through thickness node, (b) multiple node mode which considers the steel strip as 100 nodes through thickness using a Finite Difference Method. The primary modes of heat transfer were considered to be transition boiling (given by equation 2.7) for the impingement zone (assumed to be 2.6 times the jet diameter/width) and film boiling outside the impingement zone. For bottom jets, an air cooling zone was considered outside the impingement zone, assuming water to fall off the strip surface due to gravity. A constant thermal conductivity of water was considered during run-out table cooling and the cooling rates and coiling temperatures depended on the volume of water used by different combinations of jet arrays (as per mill specification). The software was reported to have the ability to predict coiling temperatures with an accuracy of ±20 °C [64, 65]. Park [66–68] simulated the temperature evolution during plate cooling by multiple

circular jets using a Computational Fluid Dynamics (CFD) model. The dominant heat transfer mechanism was considered to be film boiling, and an iterative method was proposed to estimate the vapor layer thickness on the heated surface during film boiling.

Most of the above-mentioned models are mill specific and may not be applicable for different cooling conditions. Also, the local heat transfer coefficients are not well defined and approximations are made regarding the existence of different boiling regimes. Moreover, most of the models lay emphasis on conventional coiling or cooling stop temperatures of ~600 °C. However, advanced TMCP steels require lower coiling temperatures. For temperatures below 600 °C, heat transfer mechanisms change to transition and nucleate boiling domains and emphasis during modelling should be put on these boiling regimes. Nobari et al. [19] developed a mechanistic model based on experimental data to map the boiling curves for temperatures from 720 °C down to the saturation temperature of water. Local boiling curves were modelled for transient top cooling by a planar/circular nozzle considering the different boiling mechanisms i.e. film boiling, transition boiling, nucleate boiling. The influence of water temperature and jet velocity were incorporated in the heat flux values with respect to different surface temperatures and varying distances from the stagnation point.

2.6 Summary

The literature review shows that most of the jet impingement studies are focused on top cooling jets (Table 2.1). Moreover, correlations and models for different boiling regimes are also highly concentrated on the jet impingement mechanisms characteristic for top cooling [16, 19, 47, 49]. Studies on bottom cooling are limited and modelling of bottom jet impingement remains barely investigated. The model developed by Nobari et al. [19] is applicable to jet impingement

quenching on the top surface of a steel plate. Differences lie in the fundamentals of heat transfer in bottom cooling due to difference in jet hydrodynamics and flow patterns. Hence, it is worthwhile to thoroughly investigate the local boiling heat transfer characteristics during bottom jet impingement cooling.

Chapter 3: Objectives

The overall objective of this work is to develop a preliminary mathematical model for jet impingement cooling of the bottom surface of a steel plate by a planar nozzle. The model shall serve as a tool to predict the heat transfer during the cooling of a stationary steel plate. Emphasis is made to capture the cooling history from high temperatures of ~700°C to the saturation point of water at varying distances from the water jet. The considered temperature range takes into account coiling or cooling stop temperatures applicable to TMCP steel processing on an industrial run-out table. To achieve the overall objective of this work, the following goals need to be accomplished:

1) To quantify with systematic experiments the heat extraction during bottom cooling of stationary steel plates by a single planar nozzle
2) To develop correlations for the heat flux as a function of plate surface temperature (Boiling Curve) during transient cooling
3) To determine the effect of different process parameters, i.e. flow rate, water temperature and nozzle inclination on heat extraction rates
4) To propose a Boiling Curve model for transient bottom jet impingement cooling, integrating the effects of process parameters

The experimental results and model of this work shall form a database towards meeting the long-term goal of developing a physical predictive model for cooling of a moving steel strip/plate on an industrial run-out table.

Chapter 4: Methodology

4.1 UBC Pilot Scale Run-out Table Facility

Experiments were conducted on the pilot scale cooling test rig located in the Advanced Materials and Process Engineering Laboratory (AMPEL) at UBC. The facility houses a 15 m long pilot scale run-out table which simulates controlled industrial cooling conditions. It is designed to study heat transfer during cooling (top/bottom) of both stationary and moving plates. A schematic of the facility is depicted in Figure 4.1.

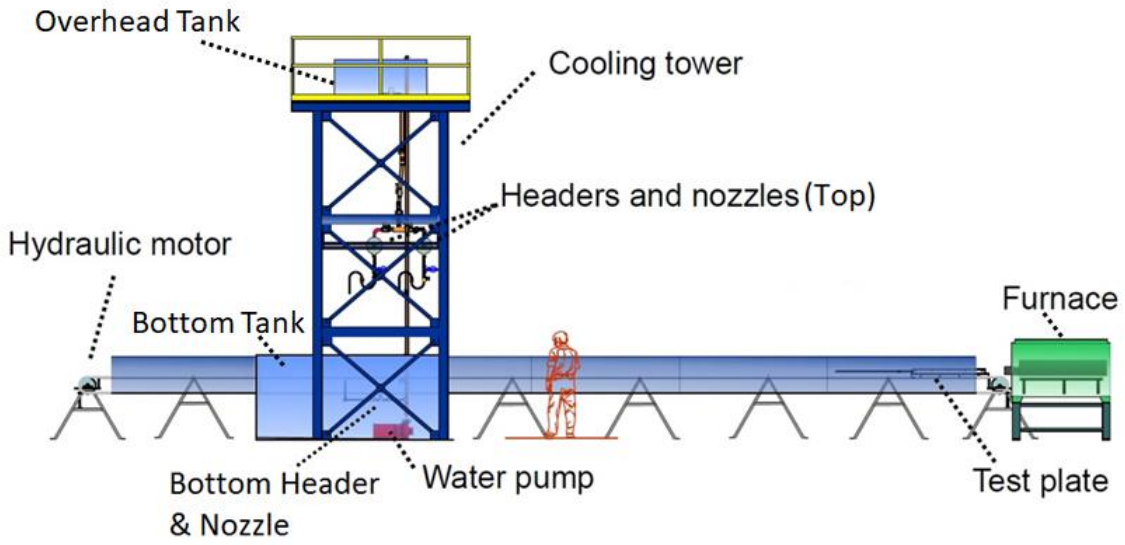

Figure 4.1 Schematic of pilot scale run-out table facility in the High Head Lab, AMPEL (modified from [6]).

The electrical furnace heats a test plate up to a maximum of 1000°C. A gas line is fitted in the furnace which supplies nitrogen gas, providing an inert environment to minimize the formation of scale on test samples. A chain pulley drive system powered by a hydraulic motor transports the test plate on a moving bed from the furnace to the cooling tower for stationary experiments. The

cooling tower consists of an overhead tank (upper tank), a containment tank (bottom tank) and headers and nozzles for both top and bottom cooling. A recirculation pump is used to circulate the water of the cooling tower in a closed loop. The overhead tank is fitted with an immersion heater which can heat water up to a temperature of 95 °C. The heated water from the overhead tank is mixed with tap water in the containment tank to obtain the desired experimental water temperature. The water temperature is measured using a thermometer (least count 1°C). Water can be pumped through the nozzles up to a flow rate of 500 l/min. A turbine flow meter measures the water flow rate and the values are displayed on a computer using a data acquisition software (discussed in Section 4.3.3). The experimental errors associated with the control of process parameters, i.e. water temperature and flow rate are estimated from experience in measurements of the values and are shown in Table 4.1. The bottom header consists of a replaceable nozzle arrangement, where a single planar nozzle or an array of multiple circular nozzles can be fitted. For the experiments of this study, a single planar nozzle of cross section 4 x 250 mm was used (Figure 4.2).

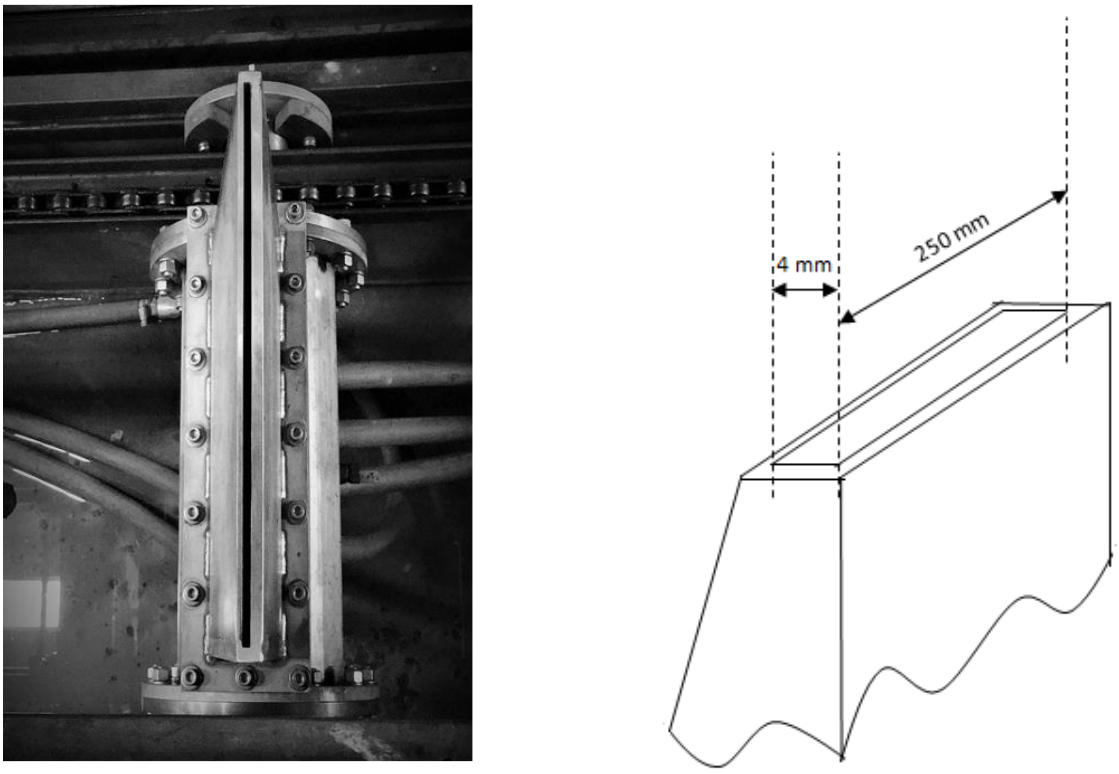

(a) **(b)**

Figure 4.2 (a) Planar nozzle installed in the bottom header of run-out table facility (top view) (b) schematic showing planar nozzle dimensions.

Table 4.1 Experimental errors

Quantity	**Error**
Flow rate	±0.5 l/min
Water temperature	±1 °C
Measured thermocouple temperature [69, 70]	±2 °C (T ≤ 277°C)
	±0.75% (T >277°C)
Thermocouple hole depth	±0.01 mm

4.2 Test Samples

4.2.1 Plate Dimensions and Chemistry

High Strength Low Alloy (HSLA) steel plates of 6.6 mm thickness, provided by ArcelorMittal Dofasco Inc. (Hamilton), were used for the cooling experiments. The detailed chemistry of the plates is given in Table 4.2. A new plate was used for each experiment to ensure plate flatness and uniform surface roughness. The surface roughness (ISO 1997) was measured prior to each test at different surface locations using Mitutoyo Surface Roughness Measurement Surftest (SJ-310) [6]. The arithmetic mean roughness (Ra) recorded within an evaluation length of 1 cm and measured with an accuracy of ± 0.01 μm was obtained to be 1.72 μm (average roughness of three samples).

Table 4.2 Chemistry of HSLA steel plates (provided by ArcelorMittal Dofasco Inc.)

Element	Fe	Mn	Nb	Si	Ti	V	C	N
Wt. %	98.515	1.1203	0.0399	0.2383	0.0148	0.0045	0.0614	0.0058
Element	P	S	Cu	Cr	Ni	Mo	Al	Sn
Wt. %	0.0111	0.0027	0.1567	0.0746	0.0509	0.0167	0.0286	0.0098

4.2.2 Instrumentation and Mounting

Steel plates of dimension 60 x 43 cm were used for all stationary experiments. 1.59 mm diameter flat bottom holes were drilled into the top surface of the test plate at different locations to accommodate thermocouples. Generally, the thermocouple wires are welded together at the tip to form of a bead or junction. However, in this experimental study an intrinsic type junction was employed in order to enhance transient responsiveness and minimize the thermal inertia of the

thermocouples [71, 72]. 14 intrinsic type-K thermocouples of 1.59 mm diameter were welded at approximately 1 mm above the bottom surface of the plate. The test plates and thermocouple holes were cleaned with denatured ethyl alcohol prior to instrumentation to get rid of any debris. Although the depth of all TC holes is approximately 1mm from the bottom surface, the exact hole depth at each location was measured before connecting thermocouples using a digital micrometer (Mitutoyo Digimatic Micrometer: least count 0.01 mm), within an estimated accuracy (considering least count) of ±0.01 mm (Table 4.1). No instrumentation was done on the bottom surface of the plate to ensure a uniform surface for cooling. A ceramic tube insulator was used to insulate the pair of thermocouple wires from each other as well as the cylindrical hole surface. The schematic of a spot-welded thermocouple is shown in Figure 4.3.

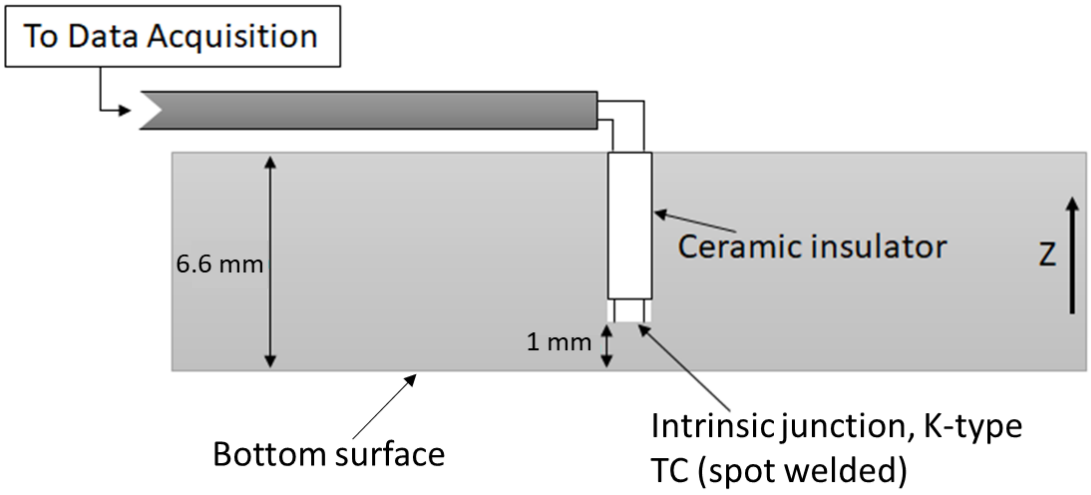

Figure 4.3 Schematic of a thermocouple spot-welded at a location on a test plate.

The thermocouples record the transient sub-surface temperature during jet impingement cooling at each location. The standard error associated with the measurement of temperature by type-K thermocouples is shown in Table 4.1.

Thermocouple locations were spatially arranged over the test plate to record the temperature history at different locations. A higher density of thermocouples was situated near the centerline of the plate (x-axis) expecting a significant gradient of heat fluxes in this area. For backup of data, multiple thermocouples were situated along the stagnation line (y-axis) and at symmetric locations along the length of the plate (x-axis). Figure 4.4 illustrates the locations of all thermocouples on the surface of the plate. The same TC configuration was used for all tests conducted. Figure 4.5 (a) shows a schematic of the TC locations with respect to an impinging bottom planar jet with no nozzle inclination. For experiments with nozzle inclination, the thermocouples on the side of the plate centerline along the direction of inclination recorded temperature histories in the 'positive x' direction (+x-axis) and the thermocouples against the inclination recorded temperature histories in the 'negative x' direction (-x-axis) (Figure 4.5 (b)).

The test plate was mounted on an upper carrier which rested on the lower carrier attached to the chain pulley drive system. The carrier design is an evolution of previous bottom cooling experiments conducted at UBC [10]. The rectangular frame of the carrier was built out of angle iron. Steel pipes were attached to one end of the carrier which facilitated handling of the test plate. The instrumented thermocouples on the top surface of the plate were clamped to the outside of the steel pipes. Figure 4.6 shows a schematic of the upper carrier with a mounted plate.

The stand-off distance between the bottom surface and the nozzle head was set at 88 mm for all orientations. The centerline of the test plate (y-axis) was aligned with the centerline of the planar nozzle by means of the lower carrier before each experiment (Figure 4.7). A static physical

barrier was placed to ensure that the centerline of the stationary test plate (y-axis) lined up with the jet centerline during the experiment. For tests with nozzle inclination, the centerline of the plate was aligned with the centerline of impinging jet manually using plexiglass by turning on the nozzle at the desired flow rate before the experiment.

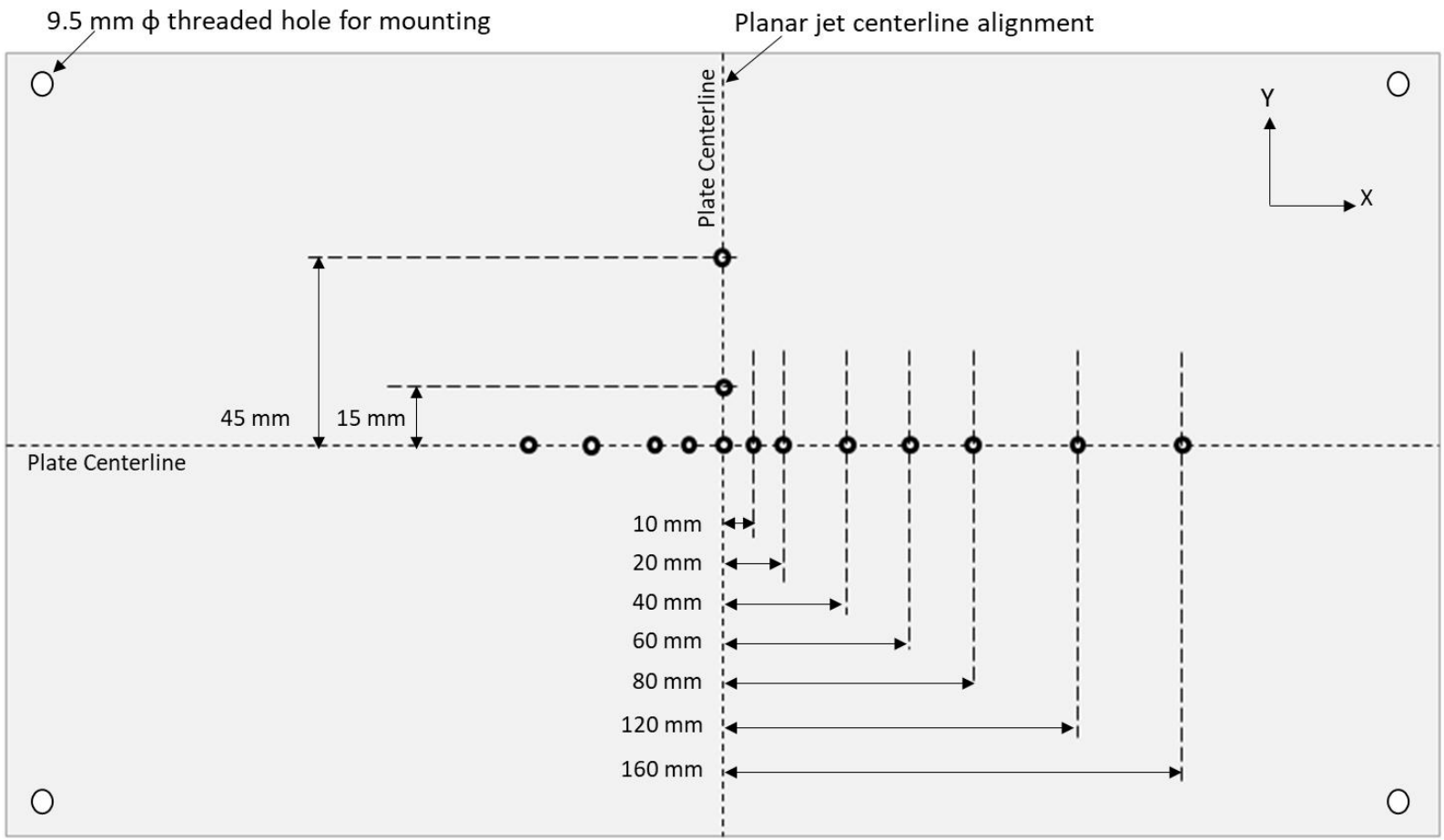

Figure 4.4 Schematic showing thermocouple locations on test plate.

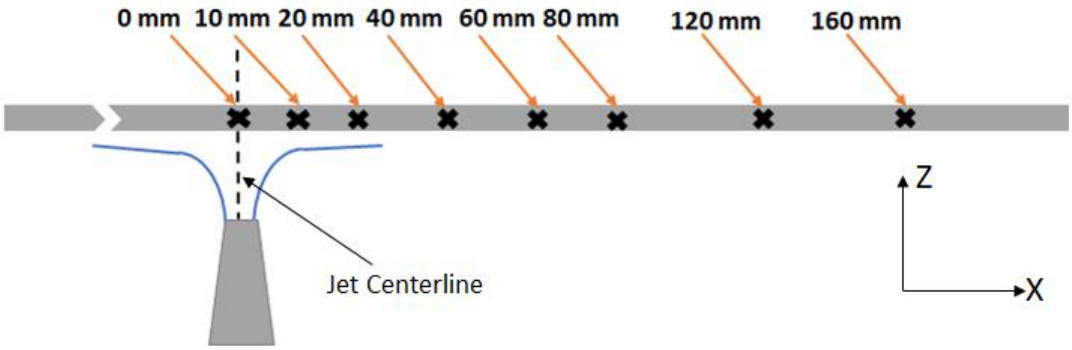

(a)

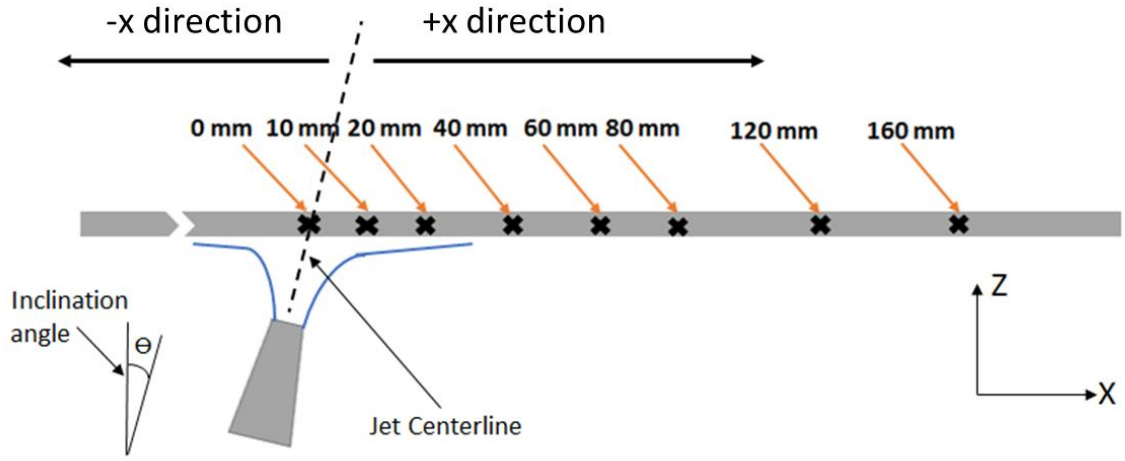

(b)

Figure 4.5 Schematic showing thermocouple locations with respect to jet centerline for (a) no nozzle inclination (b) with nozzle inclination.

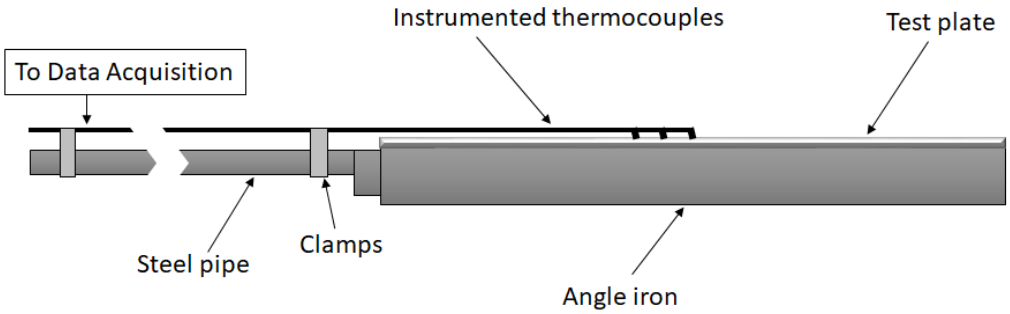

Figure 4.6 Schematic of test plate mounted on an upper carrier (side view).

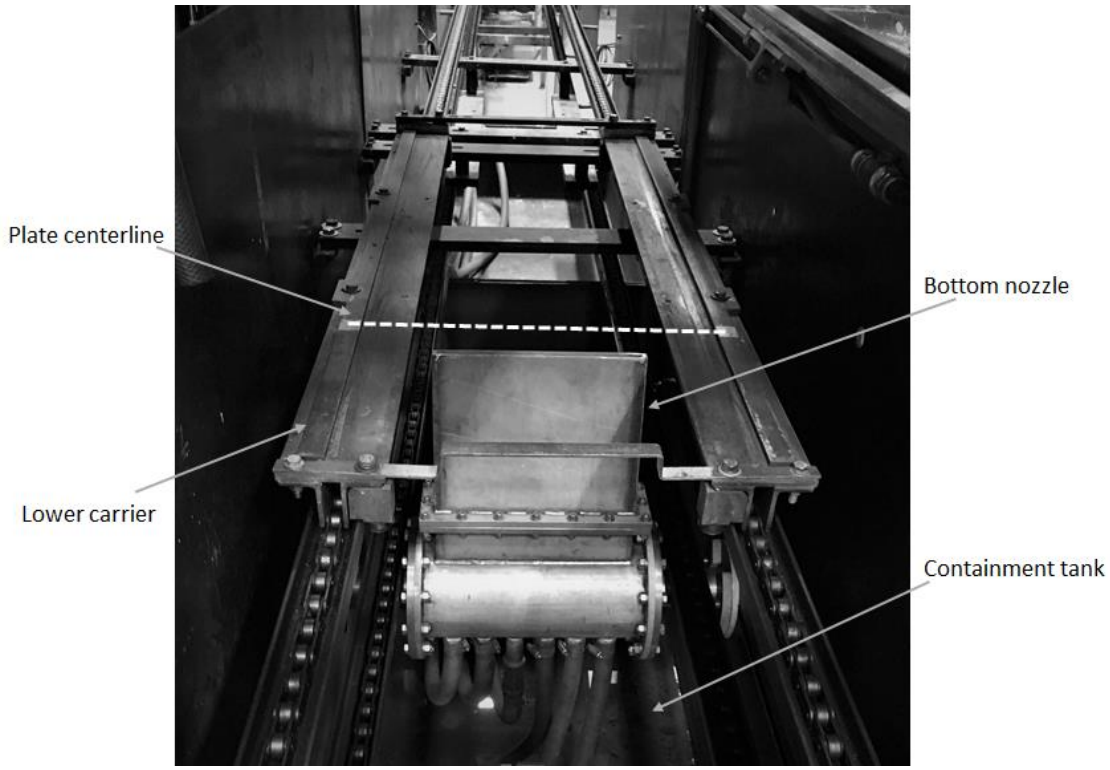

Figure 4.7 Lower carrier placed under the bottom planar nozzle.

4.3 Test Procedure

4.3.1 Test Matrix

A series of tests were conducted to study the effect of process parameters, i.e. flow rate, water temperature, and nozzle inclination, on heat extraction rates. Water flow rate and temperature were varied between 160-300 l/min and 10-40 °C, respectively. Further, the planar nozzle was inclined in steps of 10 degrees up to 20 degrees from vertical to study the effect of nozzle inclination on heat transfer. These numbers are relevant to industrial cooling applications. All the test conditions are listed in Table 4.3.

Table 4.3 Experimental matrix

Test setup	Flow rate (l/min)	Water temperature (°C)	Impingement velocity (m/s)	Nozzle inclination (degrees)
1	160	40	2.3	0
2	200	40	3.1	0
3	300	40	4.8	0
4	160	25	2.3	0
5	200	25	3.1	0
6	300	25	4.8	0
7	160	10	2.3	0
8	160	25	2.3	10
9	160	25	2.3	20

4.3.2 Experimental Procedure

The furnace was pre-heated to a set temperature of 800 °C. It takes about 8 hours for the furnace to reach this set temperature. The upper carrier with the instrumented plate mounted on it was inserted into the furnace to heat to the set temperature. Each plate took ~20 minutes to heat. During this time, the pump was started and water of the desired temperature was pumped through the bottom planar nozzle. After the water flow was stable, the flow rate was set to the desired value. Water was kept flowing through the nozzle continuously to ensure that the flow rate was within the limits of error (Table 4.1). As soon as the plate reached the set temperature (800 °C), it was taken out of the furnace and placed on the lower carrier. A diverter sheet made of stainless steel was placed under the plate to keep the plate from coming into direct contact with the water jet before reaching the quench start temperature. The plate was moved to the cooling tower by means of the hydraulic chain pulley drive system. During this entire period, the plate undergoes air cooling. When the temperature of the plate dropped to 700 °C, the diverter sheet was removed at once and the plate was quenched. The temperature history was recorded till the temperature of all thermocouples dropped below 100 °C. The estimated experimental errors associated with different parameters during plate instrumentation and test procedure have been summarized earlier in Table 4.1.

4.3.3 Data Acquisition

The thermocouple signals are transmitted to an iotech DaqBook 2005 processor unit, and the flow meter readings are collected by an instruNet (iNet-200) hardware unit. The collected data is transferred from the hardware to a computer by DASYLab 8.0 data acquisition software. The frequency of recording temperature data was set at the maximum capacity of 52 Hz.

4.4 Data Processing

The transient sub-surface temperature data collected from each thermocouple was post processed to quantify the surface temperatures and heat fluxes. An inverse heat conduction (IHC) model, which uses a 2D axisymmetric finite element method (FEM), established by Zhang [11] was used for the data analysis.

The calculation for surface temperatures and heat fluxes is done in two steps. First, an initial guess of heat flux is made to find the direct solution (using FEM) of the heat conduction differential equation given by:

$$\frac{1}{r}\frac{\partial}{\partial r}\left(rk\frac{\partial T}{\partial r}\right)+\frac{\partial}{\partial z}\left(k\frac{\partial T}{\partial z}\right)=\ \rho C_p\frac{dT}{dt} \tag{4.1}$$

where ρ is the density of the material (kg/m^3), k is the conductivity (W/m.°C) and C_p is the specific heat capacity (J/kg.°C).

A schematic of the 2D axisymmetric domain used in the FEM is shown in Figure 4.8. A finer mesh was used near the quenched surface expecting high heat flux gradients. The mesh density applied to the domain is given in Table 4.4 [7]. Nobari [6] increased the number of elements from 175 to 559 to study the effect of mesh sensitivity and observed that the calculated heat fluxes changed by less than 1%.

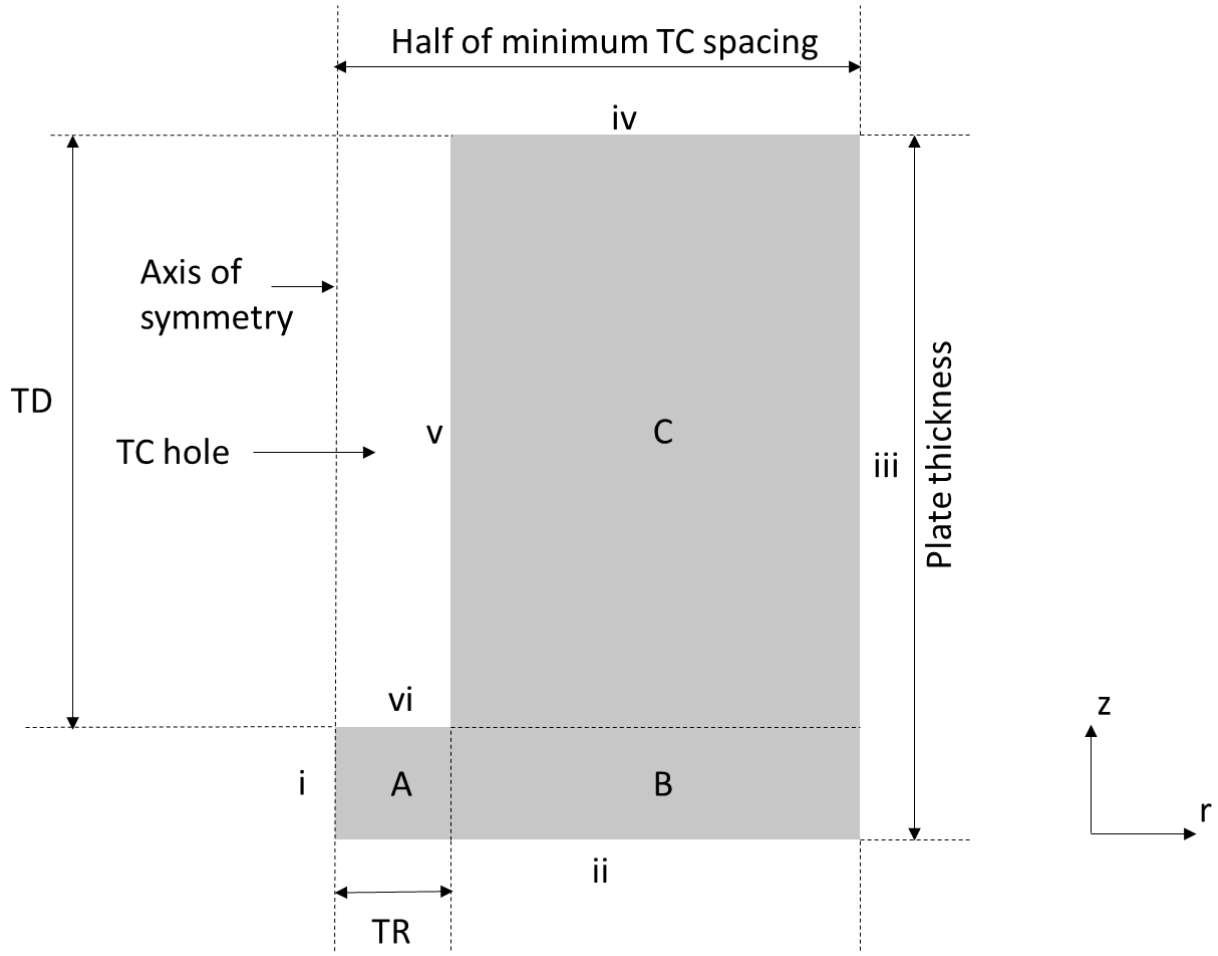

Figure 4.8 Schematic of FEM domain (axisymmetric).

Table 4.4 Meshing details of 2D domain [7]

Section	**Number of elements**	**Arrangement (r x z)**
A	25	5X5
B	50	10X5
C	100	10X10

The boundary conditions applied on the domain (Figure 4.8) are as follows:

Boundary i: Adiabatic boundary condition due to axis of symmetry, governed by:

$$-k\frac{\partial T}{\partial r}\Big|_{r=0} = 0 \tag{4.2}$$

Boundary ii: Heat flux (to be calculated) on the quenched (bottom) surface, governed by:

$$-k\frac{\partial T}{\partial z}\Big|_{z=0} = q \tag{4.3}$$

Boundary iii: Adiabatic boundary condition is assumed on the outer radius of the domain, assuming insignificant temperature gradient in the radial direction, governed by:

$$-k\frac{\partial T}{\partial r}\Big|_{r=5mm} = 0 \tag{4.4}$$

Boundary iv: Free convection and radiation (air cooling) occurs on the top surface of the plate. However, the heat transfer by radiation is relatively much greater than convection at high temperatures, and the contribution of convective heat transfer is assumed to be negligible in this model. The boundary condition on the top surface is governed by:

$$h_r = \sigma\epsilon(T^2 + T_\infty^2)(T + T_\infty) \tag{4.5}$$

where h_r is the heat transfer coefficient for radiation, σ is the Stefan-Boltzman constant, T_∞ is the ambient temperature (in K), and ϵ is the temperature dependent emissivity given by [7, 10]:

$$\epsilon = \frac{T}{1000}\left(0.125\frac{T}{1000} - 0.38\right) + 1.1 \tag{4.6}$$

Boundary v: Adiabatic boundary condition between the plate and ceramic insulator tube is assumed, governed by:

$$-k\frac{\partial T}{\partial r}\Big|_{r=TR,z>6.6mm-TD} = 0 \tag{4.7}$$

Boundary vi: Adiabatic boundary condition is assumed between thermocouple and plate at point of contact, governed by:

$$-k\frac{\partial T}{\partial z}\Big|_{0<r<TR,z=6.6mm-TD} = 0 \tag{4.8}$$

The initial condition of the model is the measured initial thermocouple temperature. A uniform temperature distribution is assumed in the beginning and the initial condition is governed by:

$$T_{r,z}\big|_{t=0} = T_{initial} \tag{4.9}$$

Subsequently, the IHC algorithm compares the measured sub-surface temperature values with the values calculated by the direct solution. The difference between the measured and calculated temperature values is used to update the pre-assumed heat flux. The process is continued till a set of pre-determined convergence criteria are met [6, 7, 11]. Further details of the IHC algorithm are provided in Appendix A.

Li et al. [26] used a 2D axisymmetric IHC model very similar to the one used in this work to obtain the surface heat fluxes and surface temperatures of a hot steel plate cooled by a spray jet. They verified the IHC algorithm against a commercial FE code, ABAQUS. To do so, a known variation of surface heat fluxes as a function of surface temperatures (i.e. a hypothetical boiling curve) was applied as the boundary condition in ABAQUS, and the thermal history was calculated

at a sub-surface location (i.e. a hypothetical TC junction). The predicted thermal history was then input into the IHC model in order to back calculate the heat fluxes and surface temperatures (i.e. the calculated boiling curve). Comparison between the two boiling curves (known vs. back calculated) showed very good agreement [26].

To solve the heat conduction differential equation, the FEM model requires thermo-physical properties of the material as input parameters. The temperature dependent thermo-physical properties of the HSLA steel sample were provided by ArcelorMittal Dofasco Inc.(Hamilton) and are detailed in Table 4.5. The thermal conductivity (k) and specific heat capacity (C_p) values are interpolated as continuous functions of temperature using the following relations:

$$k = 49 - 0.024\,T \tag{4.10}$$

$$C_p = 447.5 + (0.16\,T) + (0.002\,T^2) - (4.5e-6\,T^3) + (4.6e-9\,T^4) \tag{4.11}$$

where conductivity k is in W/m.°C, specific heat capacity C_p is in J/kg.°C, and T is the average temperature of an element in °C.

Table 4.5 Properties of HSLA steel sample (provided by ArcelorMittal Dofasco Inc.)

Temperature (°C)	**Density, ρ (kg/m^3)**	**Thermal conductivity, k (W/m.°C)**	**Specific heat capacity, C_p (J/kg.°C)**
740	7800	31.0	1087
650	7800	33.7	875
550	7800	36.3	737
450	7800	39.1	653
350	7800	41.8	591
250	7800	44.1	541
150	7800	45.5	499
50	7800	45.8	459

As mentioned earlier, the temperature history was recorded at the maximum capacity of 52 Hz. However, as delineated by Franco [7], the optimum data frequency for the input in the IHC model is 100 Hz. Hence, a 'hermite spline interpolation' approach was used to obtain the input data at a frequency of 100 Hz [6]. The raw temperature data was filtered before inputting in the IHC model. The filtering method uses two filters: a moving median followed by a moving average [6, 73]. Analysis shows that the characteristic slopes of the cooling curves in the raw data were retained in the smoothed curves (Figure 4.9).

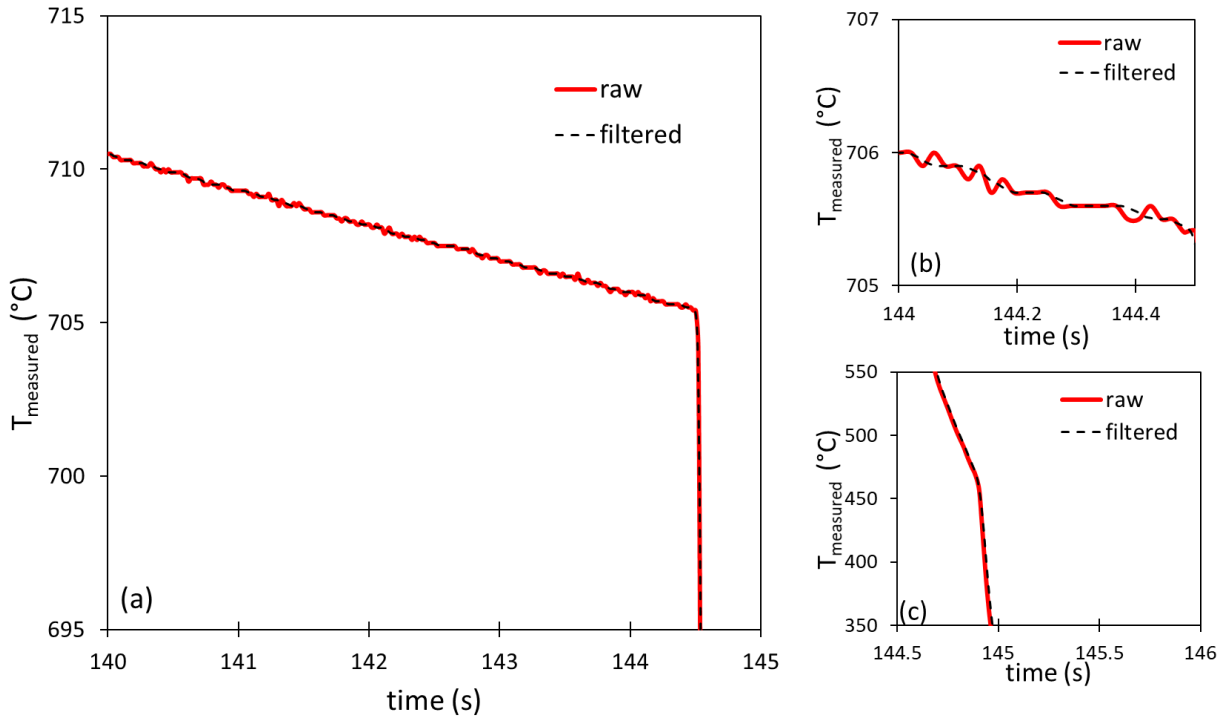

Figure 4.9 Effect of filtering approach on measured temperature data, (a) raw and filtered temperature data. Magnifications of temperature vs. time data are shown for (b) a not-wetted period and (c) a wetted period. The filter smoothens out fluctuations in the non-wetted period (figure b); however, the inherent cooling slope during wetting (figure c) is retained in the smoothed curve.

The input parameters used in the IHC program have a certain degree of error as described in Table 4.1 There is also some uncertainty in the calculated thermo-physical properties, i.e. thermal conductivity and heat capacity. These uncertainties cause a band of uncertainty in the output values of the IHC program. This uncertainty in the calculation of output values was determined by Vakili [74] using a numerical method called “computerized uncertainty analysis”. The uncertainty in the output values calculated by the IHC program was reported to be in the band of ±16% in the impingement zone and ±8% in the parallel flow zone. The experimental conditions of this previous study are comparable to those used in the present work. Hence, the above-

mentioned uncertainty values have been considered as the representative errors associated with the experimental heat flux values described in the present study.

Chapter 5: Results and Discussions

5.1 Cooling Curves and Heat Fluxes

The IHC analysis quantifies the transient surface temperatures (cooling curve) and heat fluxes at each thermocouple location as output. As a representative example of experimental results, Figure 5.1(a) shows the cooling curves obtained from the results of test 3 (Table 4.3) at 8 different locations with respect to the stagnation line. Figure 5.1(b) shows the heat fluxes at the corresponding locations on the test plate. The zero in the time axis is set at 1 second before the slope of the cooling curve at the stagnation line (x = 0 mm) transitions from air cooling to jet impingement. It can be observed that all cooling curves coincide prior to quenching (t < 1 s) showing homogeneous surface temperature across the length of the plate (Figure 5.1(a)). The surface is undergoing air cooling during this period.

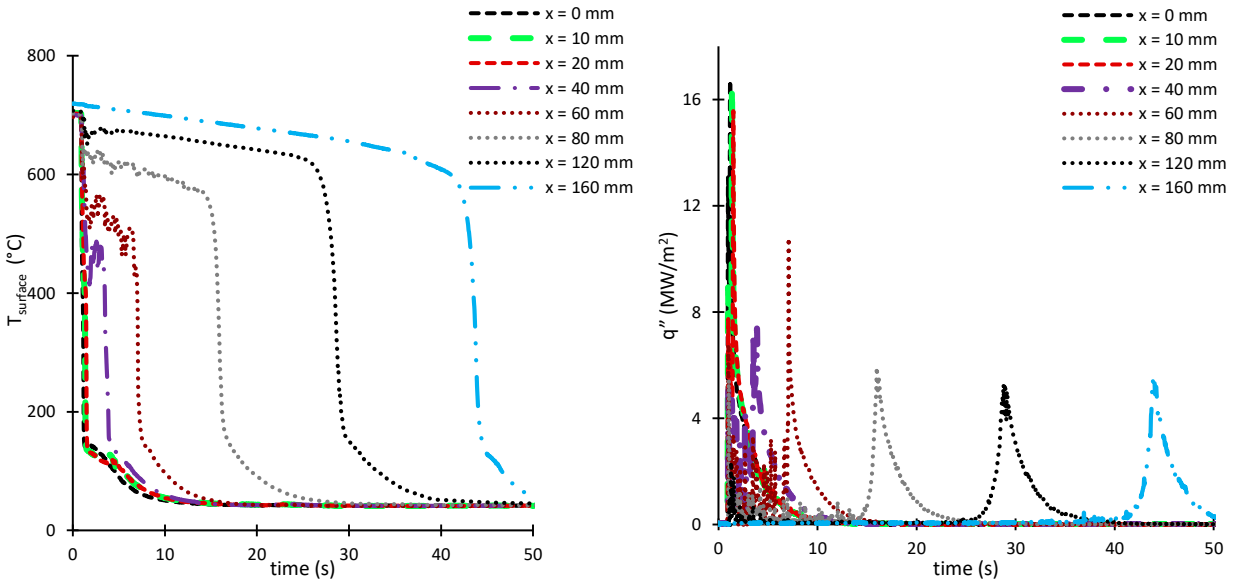

(a) **(b)**

Figure 5.1 (a) Surface temperatures vs time (b) heat fluxes vs time for all locations; flow rate = 300 l/min, water temperature = 40 °C.

As the water jet impinges the surface, a sharp drop in temperature to below 600°C happens in the cooling curve at the stagnation line (x = 0 mm) and locations in its vicinity (x = 10 mm, x = 20 mm) as shown in the magnified Figure 5.2 (a). This shows a jump in the heat flux to a first peak of around 8-12 MW/m^2 (in a decreasing order from x = 0 mm to x = 20 mm) as illustrated in Figure 5.2 (b) (magnified). Thereafter, there is an observable change in the slope of the cooling curves which shows a corresponding drop/fluctuation in the heat fluxes. Following this, a final sharp drop in the temperature from approximately 375°C to below 200°C occurs and the respective heat fluxes reach a maximum of 15.5-16.8 MW/m^2 (in a decreasing order from x = 0 mm to x = 20 mm). This region is associated with high heat extraction rates and can be characterized as the 'impingement zone'.

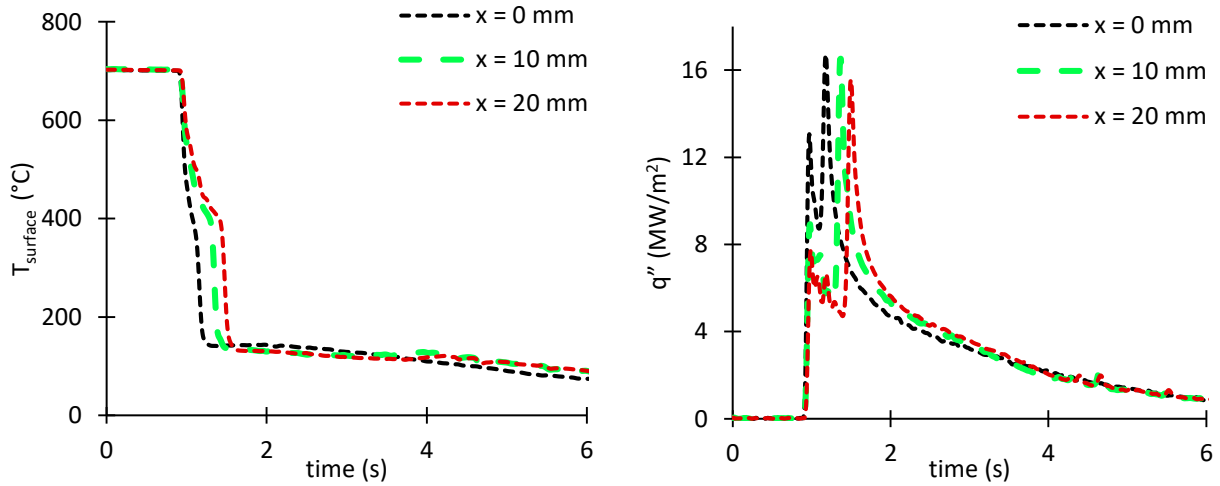

(a) **(b)**

Figure 5.2 Magnification of cooling curves and corresponding heat fluxes in the impingement zone. (a) cooling curves at x = 0 mm, x = 10 mm and x = 20 mm (b) transient heat fluxes at x = 0 mm, x = 10 mm and x = 20 mm; flow rate = 300 l/min, water temperature = 40 °C.

At distances far from the stagnation line (x = 80 mm, x = 120 mm, x = 160 mm), the cooling curves show a considerable period of air cooling (cooling rates <10 °C/s, i.e. free or forced air cooling of steel [75]), which increases with increasing distance from the stagnation line, before the temperature drops below 200°C (Figure 5.1 (a)), which is consistent with the progression of the wetting front. The slopes of the sharp drop in these cooling curves (x = 80 mm, x = 120 mm, x = 160 mm) show similar pattern, omitting some initial fluctuations, with a maximum heat flux of around 5 MW/m^2 (Figure 5.1 (b)). This region far away from the stagnation point is characterized as the 'parallel flow zone'.

The cooling curves at intermittent distances (x = 40 mm, x = 60 mm) show an initial drop of temperature to approximately 600°C followed by a period of modest cooling with some fluctuations before the sharp drop in the temperature below 200 °C occurs (Figure 5.3; magnified). The initial drop in temperature occurs when the hot surface comes in contact with the high velocity water jet. However, owing to quick vaporization of water associated with the rather high plate superheat, buildup of vapor pressure occurs which counters the impingement pressure of the water jet [36]. Due to the hydrodynamics of bottom jet cooling, it is fair enough to assume that the countering forces of liquid jet and vapor pressure (coupled with gravity) prevents uniform solid-liquid contact which may be the cause of fluctuations in heat fluxes. The eventual sharp drop in temperature to below 200°C can be attributed to increasing solid-liquid contact when the surface temperature is sufficiently low. This 'intermittent zone' of cooling between the impingement and parallel flow zones is characterized by significant fluctuations in heat flux values.

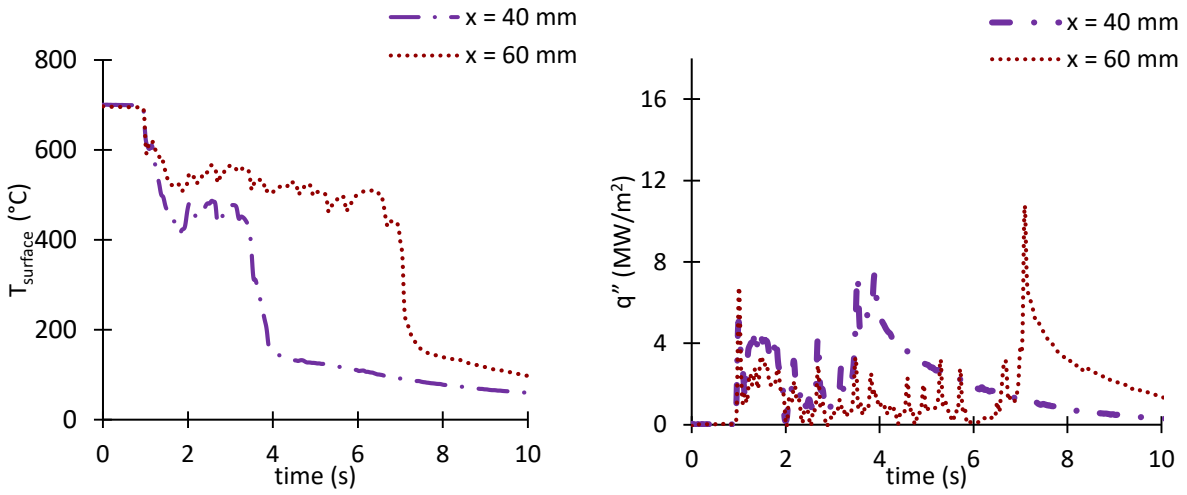

(a) **(b)**

Figure 5.3 Magnification of cooling curves and corresponding heat fluxes in the intermittent zone. (a) cooling curves at x = 40 mm and x = 60 mm (b) transient heat fluxes at x = 40 mm and x = 60 mm; flow rate = 300 l/min, water temperature = 40 °C.

5.2 Boiling Curves

5.2.1 Family of Boiling Curves

Plotting the transient heat fluxes with respect to the surface temperatures depicts the boiling curve at each thermocouple location. Figure 5.4 shows the family of boiling curves (at a select few locations) for the experimental results shown in Figure 5.1. The family of boiling curves illustrate the existence of different heat transfer mechanisms, i.e. nucleate boiling and transition boiling during jet impingement cooling.

For the boiling curves of different experimental setups, see Appendix B.

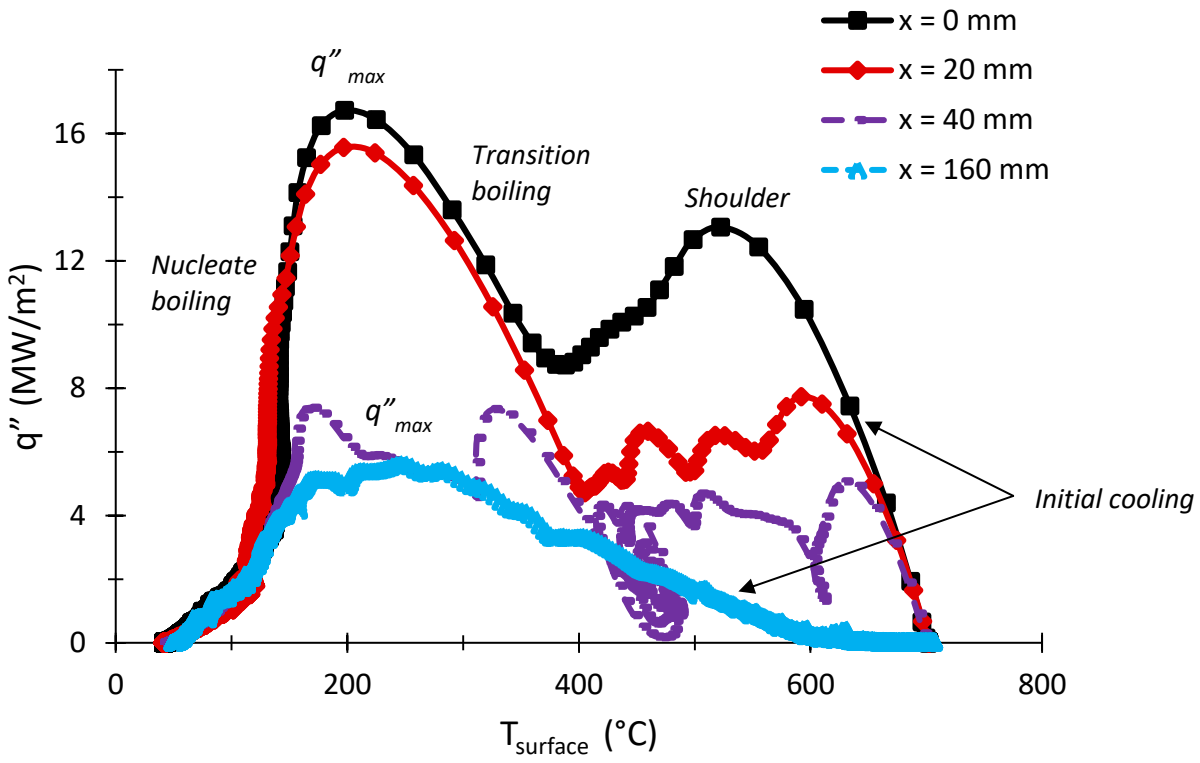

Figure 5.4 Family of boiling curves; flow rate = 300 l/min, water temperature = 40 °C. Uncertainties in values are ±16% in the impingement zone and ±8% in the parallel flow zone. Errors bars are omitted for clarity of data presentation.

The boiling curve at the stagnation line (x = 0 mm) shows an initial cooling region at high surface temperatures with a sharp increase in heat flux to ~12 MW/m^2, which coincides with the transition from air to jet impingement cooling. This initial cooling stage is characteristic for transient cooling experiments [26]. As the surface temperature drops below 600°C, the heat fluxes reach a 'shoulder', associated with a drop or fluctuations in the heat flux values. This 'shoulder' in the boiling curves of the impingement zone was consistently observed in the experimental results of all tests conducted (refer to Appendix B). The occurrence of a 'shoulder' in transition boiling at the stagnation line is consistent with top cooling planar nozzle experimental data of Robidou et al. [18] and Ishigai [31] (transient cooling). The extent of the shoulder region is seen

to be a function of water temperature in this study (discussed in Section 5.2.2.2). Following the termination of the shoulder, a transition boiling region is observed with further increase in heat fluxes till a maximum of ~16.8 MW/m^2 is reached as the surface temperature drops to ~210°C. With further drop of surface temperature below 200°C, this transition boiling region terminates and heat transfer changes to nucleate boiling. The boiling curve in the impingement zone close to the stagnation line (x = 20 mm) shows resemblance to the shape and characteristics of the boiling curve at the stagnation line. As evident from Figure 5.4, there is no influence of distance in the heat fluxes in the initial cooling stage and nucleate boiling region on the boiling curves in the impingement zone. The heat flux values in the 'shoulder' region drop to lower values with increasing distance from the stagnation line. In the transition boiling region following the shoulder, the heat fluxes are also somewhat lower than those for the stagnation line. However, the heat fluxes increase at the same rate with lowering the temperature for all locations in the impingement zone. As a result, the maximum value of heat flux drops from 16.8 MW/m^2 at the stagnation line (x = 0 mm) to 15.5 MW/m^2 at x = 20 mm. The boiling curves in the impingement zone shall henceforth be referred to as Type A (with shoulder).

The boiling curve in the parallel flow zone (x = 160 mm) shows characteristics very different from the boiling curves in the impingement zone. Following a period of air cooling, the transition from air to water cooling occurs at a lower temperature (consistent with the progression of the wetting front), and exhibits an initial water cooling stage where the heat flux increases with lowering the surface temperature much more gradually than for the impingement zone. Further, this cooling region extends to a surface temperature of ~300°C where a broad region of a maximum heat flux is reached, i.e. no evidence of a shoulder in the heat flux is observed. Instead it seems that initial cooling and transition boiling merge into a continuous heat flux regime for the parallel

flow zone, with characteristics predominantly indicating a transition boiling regime. The maximum heat fluxes in the parallel flow zone are with ~5 MW/m^2 about 1/3 of the values observed in the impingement zone. With further drop of surface temperature below 200°C, the heat fluxes merge into a single nucleate boiling curve, which is independent of distance from the stagnation point (Figure 5.4). The boiling curves in the parallel flow zone shall henceforth be referred to as Type B (without shoulder).

The boiling curve in the intermediate zone (x = 40 mm) shows mixed characteristics. We observe an initial cooling stage followed by the shoulder region as in the impingement zone. There are, however, substantial fluctuations in heat flux values for the shoulder region. Thereafter, the boiling curve reaches a maximum with a nature similar to Type B boiling curves, before merging into the nucleate boiling curve. This intermediate zone shows boiling curves with unpredictable and mixed characteristics and it is challenging to assign a set of characteristics to these curves. The boiling curves in this intermediate zone shall henceforth be referred to as Type C (mixed characteristics).

The boiling curves in Figure 5.4 show a clear dependence on distance from the stagnation point. Thus, the influence of distance needs to be taken into account while developing a predictive heat transfer model. A key observation to be noted is the absence of a fully developed film boiling region in the boiling curves, which is in contrast to the top cooling results of Nobari et al. [19] and Robidou et al. [18], where a clear film boiling region is observed away from the stagnation line. As a first step to investigate the effect of process parameters on boiling curves, a comparison of boiling curves with varying flow rates and water temperature are made in the impingement zone (x = 0 mm; ‘Type A’) and the parallel flow zone (x = 160 mm; ‘Type B’).

5.2.2 Effect of Flow Rate and Water Temperature

5.2.2.1 Flow Rate

The comparison of boiling curves for three different flow rates (160-300 l/min) at x = 0 mm and x = 160 mm are shown in Figures 5.5 (a) and (b), respectively. At the stagnation line (Figure 5.5 (a)), heat flux values increase with increasing flow rates, and the boiling curves are shifted to higher heat fluxes in the 'shoulder' and the following transition boiling regions. No appreciable effect of flow rate is observed in the initial cooling stage and the nucleate boiling domain. An increase in flow rate increases the jet impingement velocity and hence enhances heat extraction rates. Increasing the flow rate from 160 l/min to 300 l/min corresponds to an increase in jet impingement velocity from 2.3 m/s to 4.8 m/s, which results in an increase in the maximum heat flux from 14.5 MW/m^2 to 16.8 MW/m^2.

Likewise, the boiling curves in the parallel flow zone (Figure 5.5 (b)) show a similar trend with varying flow rates. The maximum heat flux increases from ~ 4 MW/m^2 to ~5 MW/m^2 with an increase in the flow rate from 160 l/min to 300 l/min. Similarly, a steady increasing trend is seen in the heat flux values and the corresponding slope of the initial cooling stage with increasing flow rates. Thus, the influence of flow rate is prominent in the impingement zone as well as the parallel flow zone.

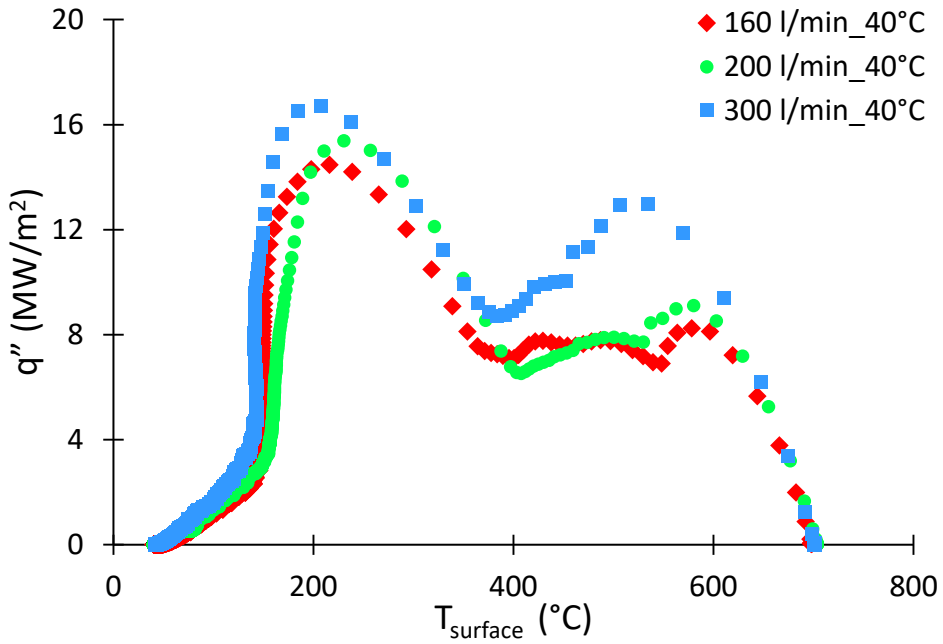

(a)

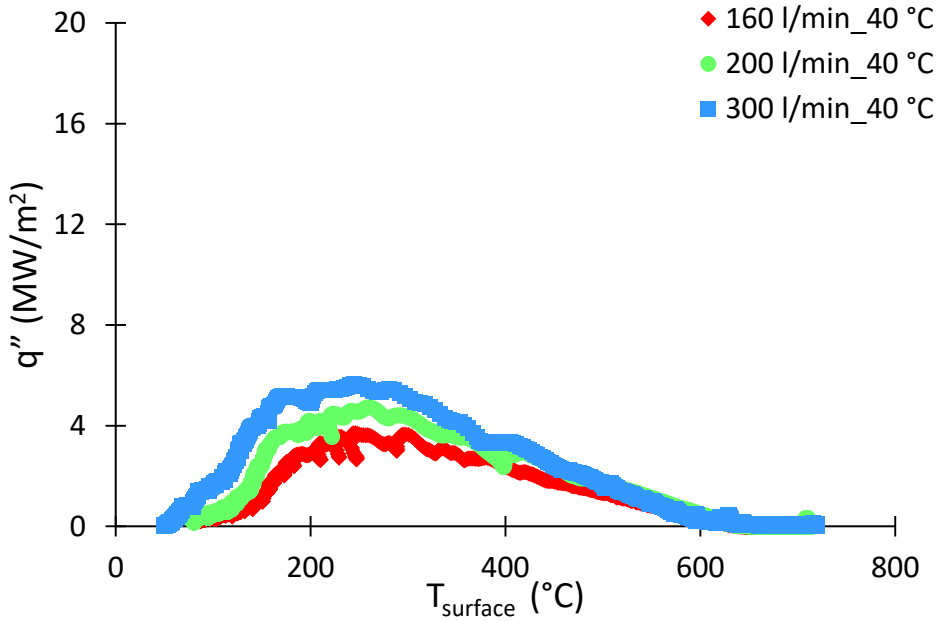

(b)

Figure 5.5 Comparison of boiling curves for different flow rates at (a) x = 0 mm (b) x = 160 mm; (water temperature: 40 °C). Uncertainties in values are ±16% in the impingement zone and ±8% in the parallel flow zone. Errors bars are omitted for clarity of data presentation.

5.2.2.2 Water Temperature

Figures 5.6 (a) and (b) show the comparison of boiling curves for three different water temperatures (10-40 °C) at x = 0 mm and x = 160 mm, respectively. It is observed that heat flux values increase with decreasing water temperatures in the 'shoulder' and following transition boiling regions at the stagnation line (Figure 5.6 (a)). Lowering the water temperature enhances the heat extraction capacity of the flowing medium and hence pushes the boiling curves to higher heat fluxes. A decrease in the water temperature from 40°C to 10°C increases the maximum heat flux from 14.5 MW/m^2 to 18.8 MW/m^2 at the stagnation line. Similar to the observations of varying flow rates, water temperature does not have any pronounced effect on the nucleate boiling and initial cooling stages. A notable influence of water temperature on the boiling curves is the expanse of the 'shoulder' in transition boiling. The shoulder terminates below 400°C (average ~ 375°C) for higher water temperature (40°C), whereas for lower water temperatures (25°C and 10°C) the shoulder consistently terminates at a surface temperature above 400°C (average ~ 425°C). This trend of the effect of water temperature on the extent of the 'shoulder' is in contrast with the observations of Ishigai [31] where the width of the shoulder region increased with decreasing water temperatures in the range of 45 to 95 °C.

In the parallel flow zone (Figure 5.6 (b)), the maximum heat flux increases from ~ 4 MW/m^2 to ~ 8 MW/m^2 with a decrease in water temperature from 40 to10 °C. The initial cooling stage shows a relatively higher degree of fluctuations for lower water temperatures (25°C and 10 °C), and transition from air to water cooling occurs at slightly higher temperatures (coincident with the rate of wetting front progression). Also, the characteristic slope of heat flux increase shows an increase with decreasing water temperature. Overall, water temperature appears to have a stronger influence on heat extraction rates when compared to the role of flow rate.

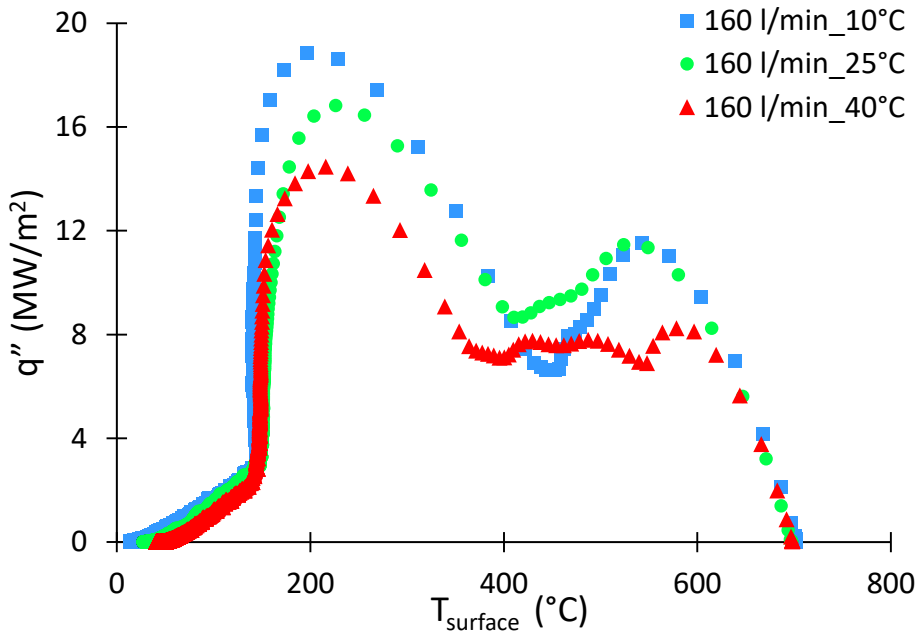

(a)

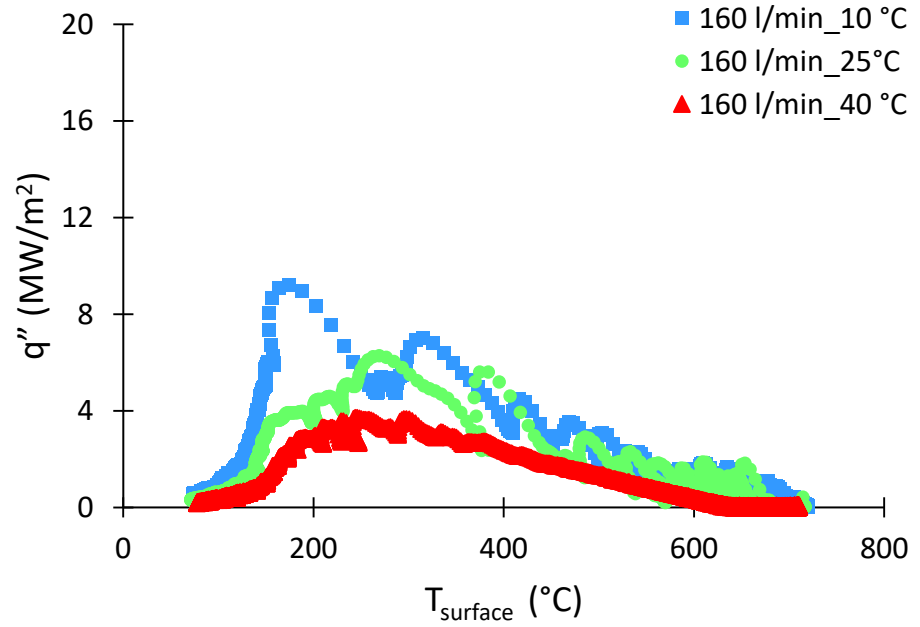

(b)

Figure 5.6 Comparison of boiling curves for different water temperatures at (a) x = 0 mm (b) x = 160 mm; (flow rate: 160 l/min). Uncertainties in values are ±16% in the impingement zone and ±8% in the parallel flow zone. Errors bars are omitted for clarity of data presentation.

5.3 Effect of Nozzle Inclination

5.3.1 Effect of Nozzle Inclination on Symmetry of Flow

During each test, the centerline of the plate was aligned with the centerline of the bottom planar jet (discussed in Section 4.2.2). A number of thermocouples were placed at equidistant locations (along the x-axis) up to a distance of ± 60 mm from the jet centerline (Figure 4.4). Figure 5.7 shows a comparison between the cooling curves at different equidistant locations (± x-axis) for a test with no nozzle inclination. The cooling curves in the different equidistant locations along the x-axis show a nearly symmetrical flow of water in the horizontal direction and the water reaches the corresponding equidistant locations at almost the same time intervals from the stagnation line.

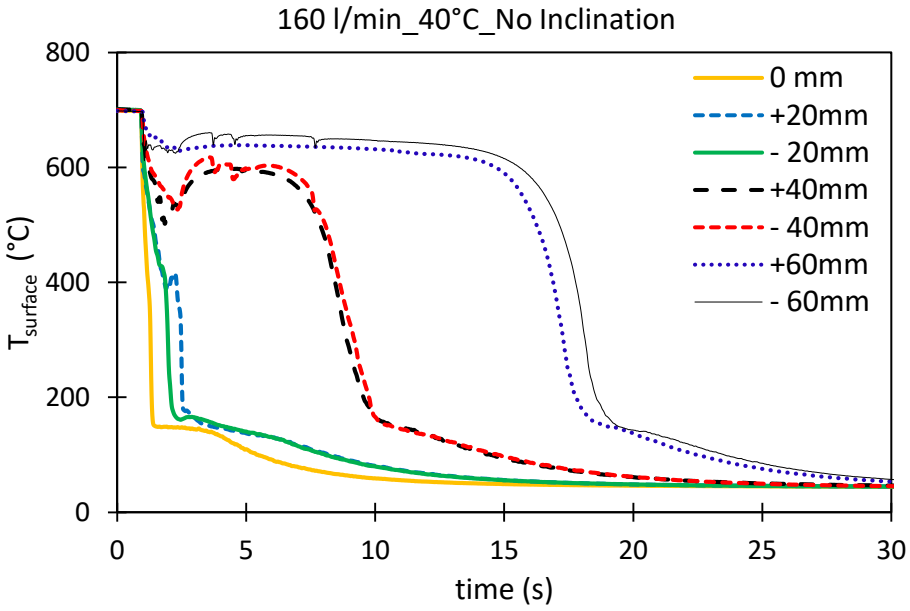

Figure 5.7 Cooling curves at different equidistant locations for no nozzle inclination; flow rate = 160 l/min, water temperature = 40°C.

Inclining the nozzle with respect to the horizontal causes asymmetry in the flow of water in the horizontal direction (discussed in Section 2.4.1.6). A +x direction (along the direction of nozzle inclination) and a -x direction (opposite to the direction of nozzle inclination) with respect to the stagnation line have been defined earlier in Section 4.2.2. Figures 5.8 (a) and (b) show comparisons of cooling curves at equidistant locations for tests with nozzle inclinations showing the asymmetry in the flow of water caused by the nozzle inclination. At locations in the impingement close to the stagnation line (±20 mm), the asymmetry due to nozzle inclination is not pronounced. At farther locations from the stagnation line, the wetting front reaches the TC locations in the +x direction (+60 mm) much earlier than the locations in the -x direction (-60 mm). The wetting front progresses at a faster rate in the +x direction due to the added component of horizontal velocity, and the asymmetry in the flow is seen to increase with increasing nozzle inclination, as the component of horizontal velocity increases (Section 2.4.1.6).

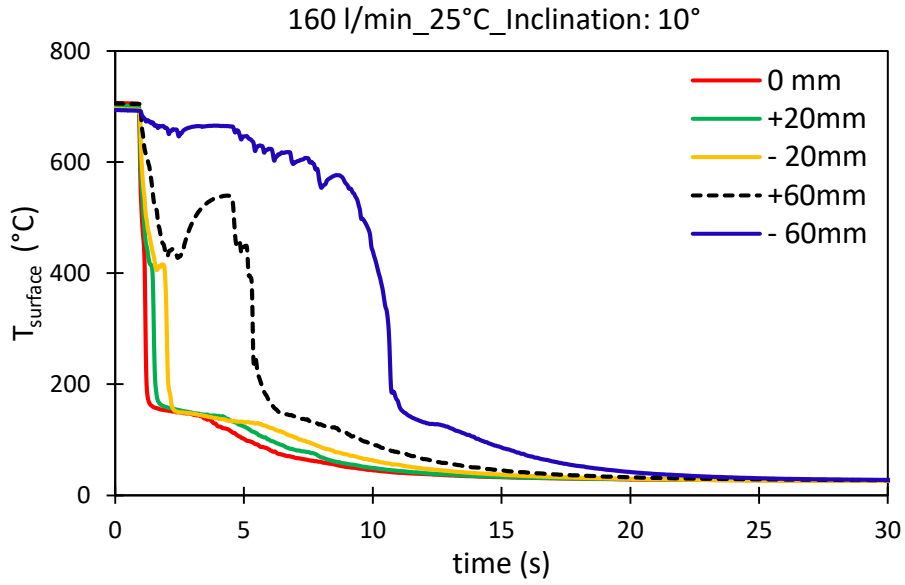

(a)

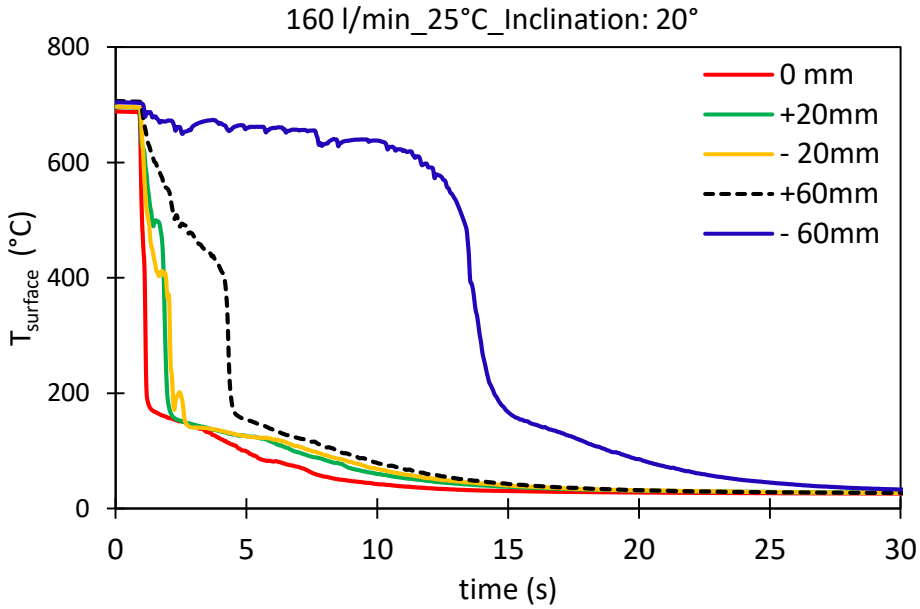

(b)

Figure 5.8 Cooling curves at different equidistant locations for tests with nozzle inclination (a) nozzle inclination: 10° (b) nozzle inclination: 20°; flow rate = 160 l/min, water temperature = 25°C.

5.3.2 Effect of Nozzle Inclination on Boiling Curves

Figures 5.9 (a) and (b) show the comparison of boiling curves for three different nozzle inclinations (0-20 degrees) in the impingement zone (at x = 0 mm) and in the parallel flow zone (at x = 160 mm; +x direction), respectively. In the jet impingement zone (Figure 5.9 (a)), changing the nozzle orientation does not show any net influence on heat fluxes and effectively reproduces the same boiling curve. Although there seems to be some variations in the heat flux values in the shoulder region, no trend with nozzle inclination is seen and all three boiling curves can be regarded as essentially the same, considering the uncertainties of experimental heat flux values. Similarly, the boiling curves in the parallel flow region (x = 160 mm; +x direction) do not show any apparent influence of nozzle orientation (Figure 5.9 (b)). Thus, changing the nozzle orientation does not seem to have any effect on the heat extraction rates.

Inclining the nozzle with respect to the horizontal creates asymmetry in the flow of water in the horizontal direction (x-axis) as is evident from the analysis of the cooling curves (Section 5.3.1). However, the changes in symmetry of flow does not seem to have any pronounced effect on the boiling curves in the impingement zone and the parallel flow zone. A study on the cumulative heat extracted from the surface of the plate with time is, however, suggested to determine the overall cooling efficiency as a function of nozzle inclination.

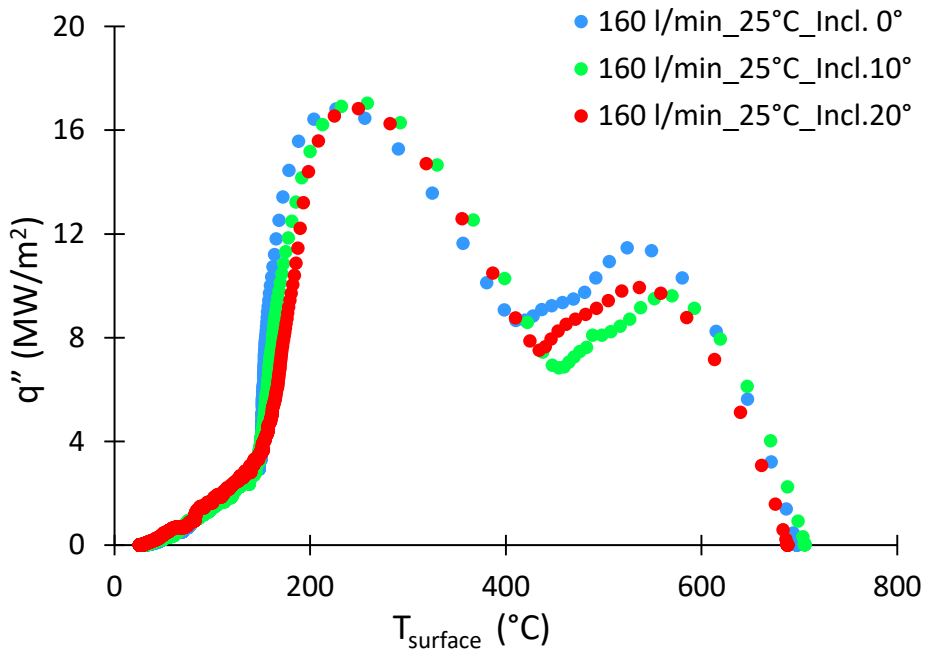

(a)

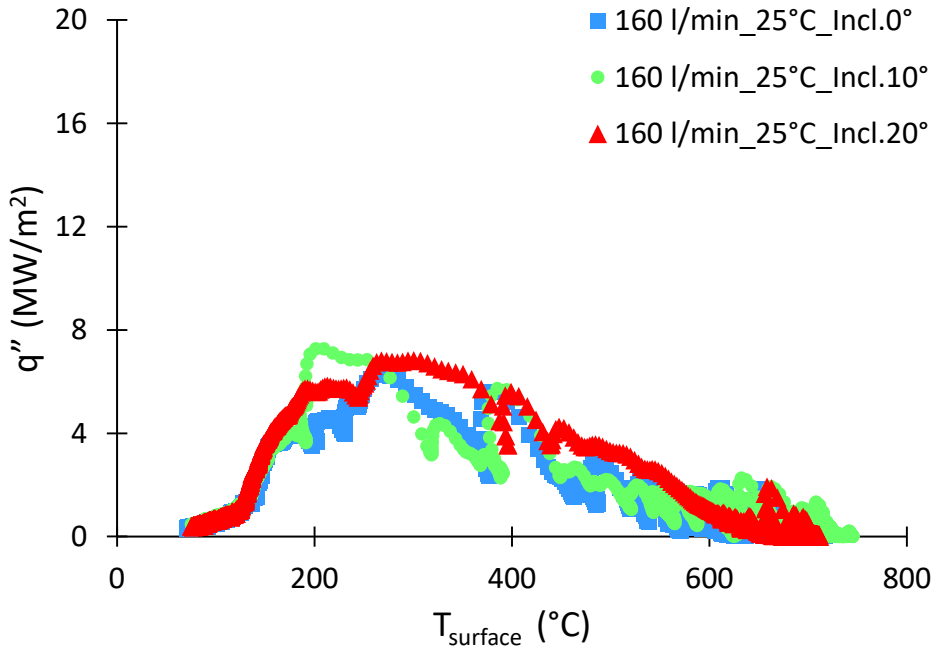

(b)

Figure 5.9 Comparison of boiling curves for different nozzle inclinations at (a) x = 0 mm (b) x = 160 mm; (flow rate: 160 l/min; water temperature: 40 °C). Uncertainties in values are ±16% in the impingement zone and ±8% in the parallel flow zone. Errors bars are omitted for clarity of data presentation.

5.4 Comprehensive Analysis

To do a comprehensive study on the influence of distance as well as process parameters, i.e. water flow rate and water temperature on the heat extraction rates, the maximum heat fluxes are plotted with respect to distance from the stagnation line (Figure 5.10). Also, the cumulative influence of distance and process parameters on the shape and characteristics of boiling curves is examined (Table 5.1). To determine the maximum value of heat fluxes (q''_{max}), two different scenarios are considered. For the characteristic boiling curves of 'Type A', the point of global maxima is selected as the experimental maximum heat flux (q''_{max}) for the corresponding boiling curve. The boiling curves of 'Type B' show a maximum heat flux region associated with fluctuations, the experimental maximum heat flux value (q''_{max}) is determined by the average of the heat fluxes in this region. For the curves of mixed characteristics (intermittent zone), the maximum heat flux region exhibits substantial fluctuations, and the experimental maximum (q''_{max}) is either selected as global maxima (Figure 5.11 (a)) or the average of fluctuations (Figure 5.11 (b)) in the maximum heat flux region, depending on the respective case. The experimental maximum heat flux vs. distance from jet centerline for different flow rates and water temperatures are illustrated in Figures 5.10 (a) and (b), respectively.

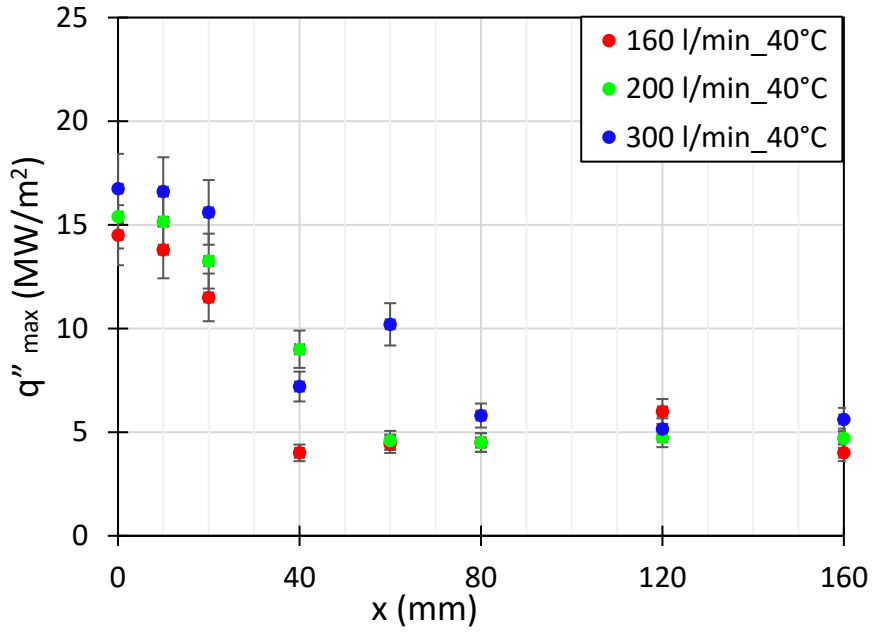

(a)

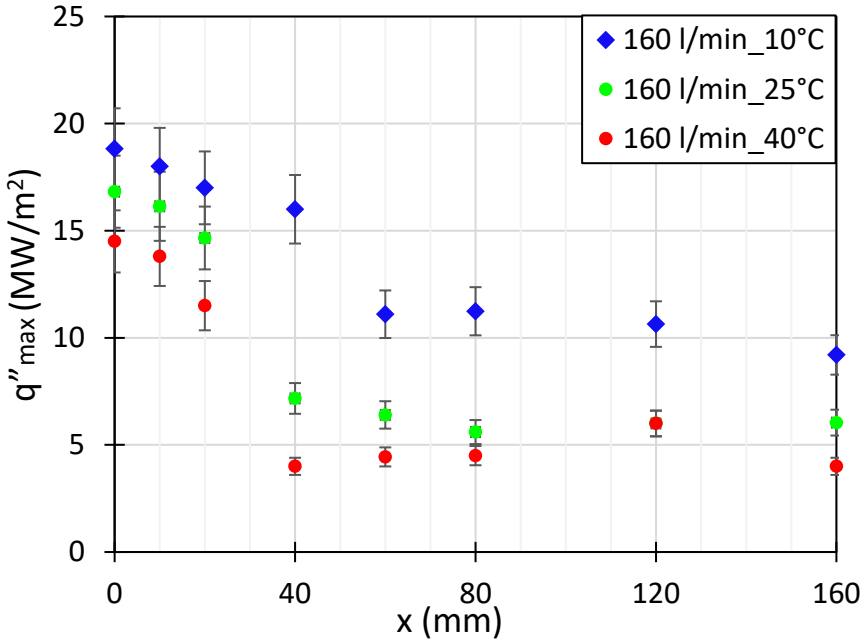

(b)

Figure 5.10 Experimental maximum heat flux with respect to distance from jet centerline, for (a) different flow rates (b) different water temperature. Uncertainties in values are ±16% in the impingement zone and ±8% in the parallel flow zone.

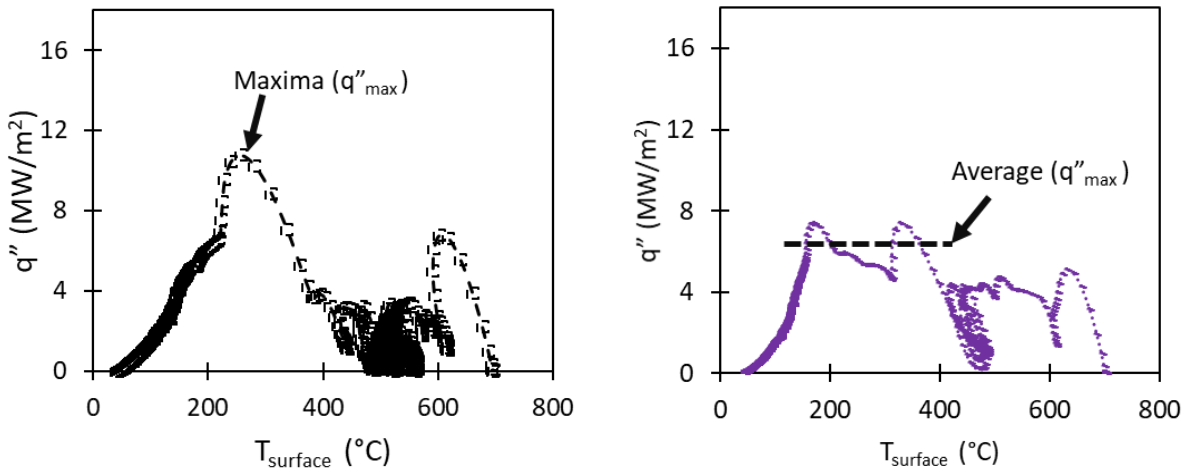

(a) **(b)**

Figure 5.11 Example of boiling curves in the intermittent zone. The maximum heat flux values are either selected as the global maxima (figure a) or the average of fluctuations (figure b).

The q''_{max} values show a slight decrease close to the jet centerline ($x \leq 20$ mm) for all three flow rates (Figure 5.10 (a)). With increasing distance, the maximum heat fluxes show a sharp drop, and the q''_{max} values drop to lower values in the parallel flow zone ($x \geq 80$ mm), where the heat fluxes become independent of distance. The sharp drop in maximum heat flux values from the impingement zone to the parallel flow region becomes less steep with decreasing water temperatures, indicating a broader effective impingement zone for lower water temperatures, and the influence on q''_{max} values is more pronounced at farther distances (Figure 5.10 (b)). Closer to the stagnation line the q''_{max} values are influenced by both flow rate and water temperature, whereas water temperature plays a predominant role at farther locations. This trend confirms earlier observations on the effect of process parameters, i.e. flow rate and water temperature (Section 5.2.2).

Table 5.1 Characteristics of boiling curves with distance from jet centerline, as a function of flow rate and water temperature

Setup No.	Water T (°C)	Flow rate (l/min) \ X (mm)	0	10	20	40	60	80	120	160
1	40	160	A	A	A	C	B	B	B	B
2	40	200	A	A	A	C	C	B	B	B
3	40	300	A	A	A	C	C	B	B	B
4	25	160	A	A	A	C	C	B	B	B
5	25	200	A	A	A	C	C	B	B	B
6	25	300	A	A	A	A	C	C	B	B
7	10	160	A	A	A	A	A	C	C	B

A	Impingement zone
B	Parallel flow zone
C	Intermittent zone (mixed characteristics)

Table 5.1 shows a comprehensive illustration on the integrated effect of flow rate and water temperature with distance from the water jet on the heat transfer rates. As indicated by earlier observations, the effective 'impingement zone' becomes wider with increasing flow rates and decreasing water temperatures and the 'parallel flow zone' is pushed to farther distances from the jet centerline. A confluence of lower water temperatures and higher jet velocities promotes higher heat extraction rates. The impingement zone increases from x = 20 mm ($^{x}/_{w_n} = 5$, where $'w_n'$ is nozzle width) in setup 1 (i.e. highest water temperature and lowest flow rate) to x = 60 mm ($^{x}/_{w_n} = 15$) in setup 7 (i.e. lowest water temperature and highest flow rate).

5.5 Reproducibility of Experimental Results

The computerized data analysis done by Vakili [74] estimated the uncertainties in experimental heat flux values in the band of ±16% in the impingement zone and ±8% in the parallel flow zone. The repeats of a few tests were conducted in order to verify the reproducibility of experimental results under the same experimental conditions. Figures 5.12 (a) and (b) show the local maximum heat fluxes with respect to distance for tests repeated under the same conditions [(a) water flow rate: 160 l/min, water temperature: 25°C; (b) water flow rate: 200 l/min, water temperature: 25°C]. The characteristic trend of heat fluxes vs. distance are identical for the repeated experiments. However, the data points show a higher degree of variation that the limits estimated by Vakili [74]. It can be seen in Figures 5.12 (a) and (b) that the data points are rather repeated with a relatively higher uncertainty of ± 20% (with one outlier in Figure 5.12 (b)). This shows that the reproducibility of experimental local heat fluxes may have a higher band of uncertainty than concluded by Vakili [74]. This suggests the need for further analysis on the estimated uncertainties in experimental heat flux values.

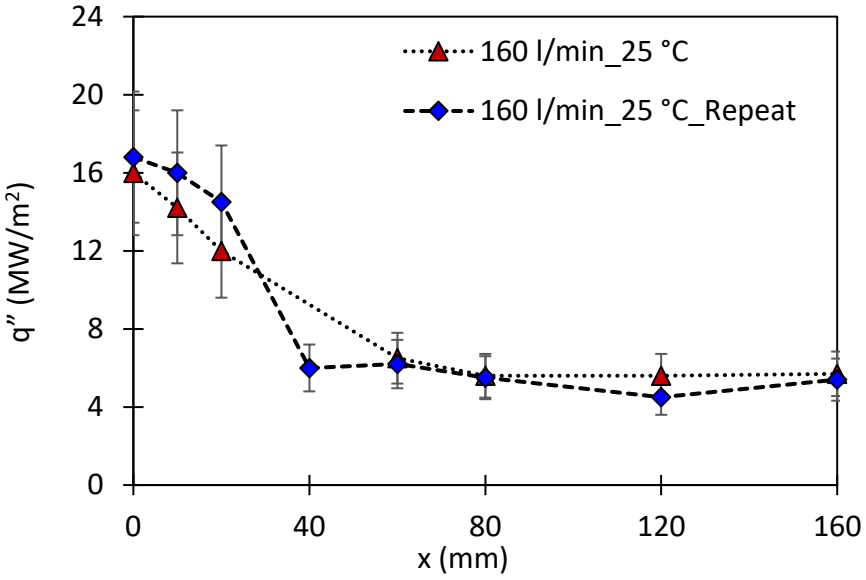

(a)

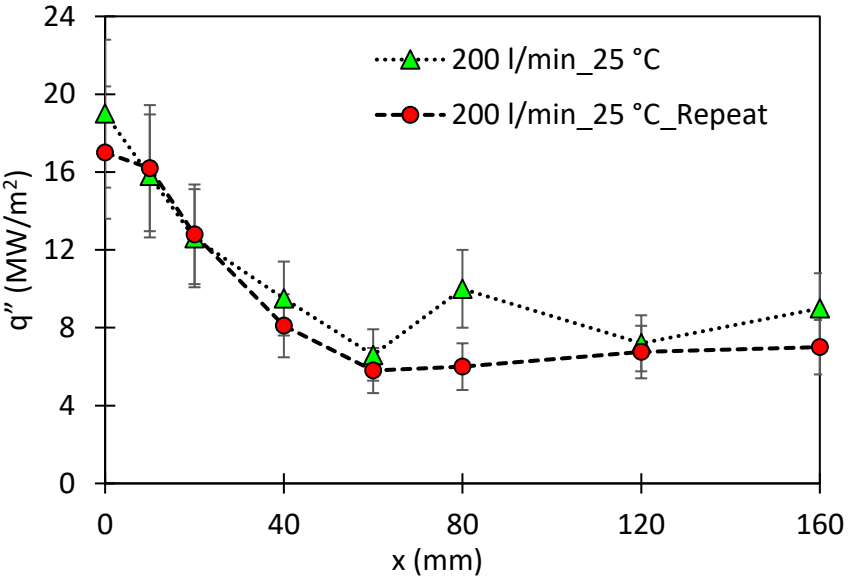

(b)

Figure 5.12 Maximum heat flux vs. distance from water jet for two tests repeated under same process conditions (a) flow rate: 160 l/min, water temperature: 25°C (b) flow rate: 200 l/min, water temperature: 25°C. Data points are repeated with an accuracy of ± 20% (with one outlier).

Chapter 6: Boiling Curve Model for Transient Cooling

6.1 Overview

Based on the experimental results discussed in Chapter 5, a preliminary model for calculating heat transfer on the bottom surface of stationary plates is proposed in this Chapter, taking a semi-empirical approach. Boiling curves in the impingement zone (Type A) as well as the parallel flow zone (Type B) have been determined with the model. To describe the boiling curves in the experimental temperature range of this work, simplified correlations are developed for the different stages in the boiling curves, i.e. nucleate boiling, shoulder heat flux, initial cooling, maximum heat flux. The influence of process parameters, i.e. water flow rate and water temperature are incorporated in the heat flux correlations.

6.2 Maximum Heat Flux

The local maximum heat flux values (q''_{max}) have been calculated in two steps. First, the q''_{max} values at the stagnation line (x = 0 mm) are correlated as a function of jet impingement velocity (2.3m/s < v_i < 4.8m/s) and sub-cooling (60°C < ΔT_{sub} < 90°C) by:

$$q''_{max}(x = 0) = \; c \; \Delta T_{sub}^{a} \{1 + (b \; v_i)\} \tag{6.1}$$

where v_i is the jet impingement velocity (m/s) and $\Delta T_{sub} = T_{sat} - T_{water}$ is the amount of sub-cooling (°C) defined as the difference between saturation point of water (T_{sat} = 100°C) and water jet temperature (T_{water}). The jet impingement velocities (Table 6.1) are calculated from the flow rates

using the energy conservation equation 2.2. The maximum heat flux values (q''_{max}) are in W/m^2. a, b and c are empirical fit parameters as follows:

$$a = 0.74 \tag{6.2}$$

$$b = 0.11\ (m/s)^{-1} \tag{6.3}$$

$$c = 5.45\ \text{X}\ 10^5\ (W\ m^{-2}\ ^{\circ}\text{C}^{-a}) \tag{6.4}$$

The calculated q''_{max} values at the stagnation line show reasonable agreement with the experimental local maximum values (Figure 6.1).

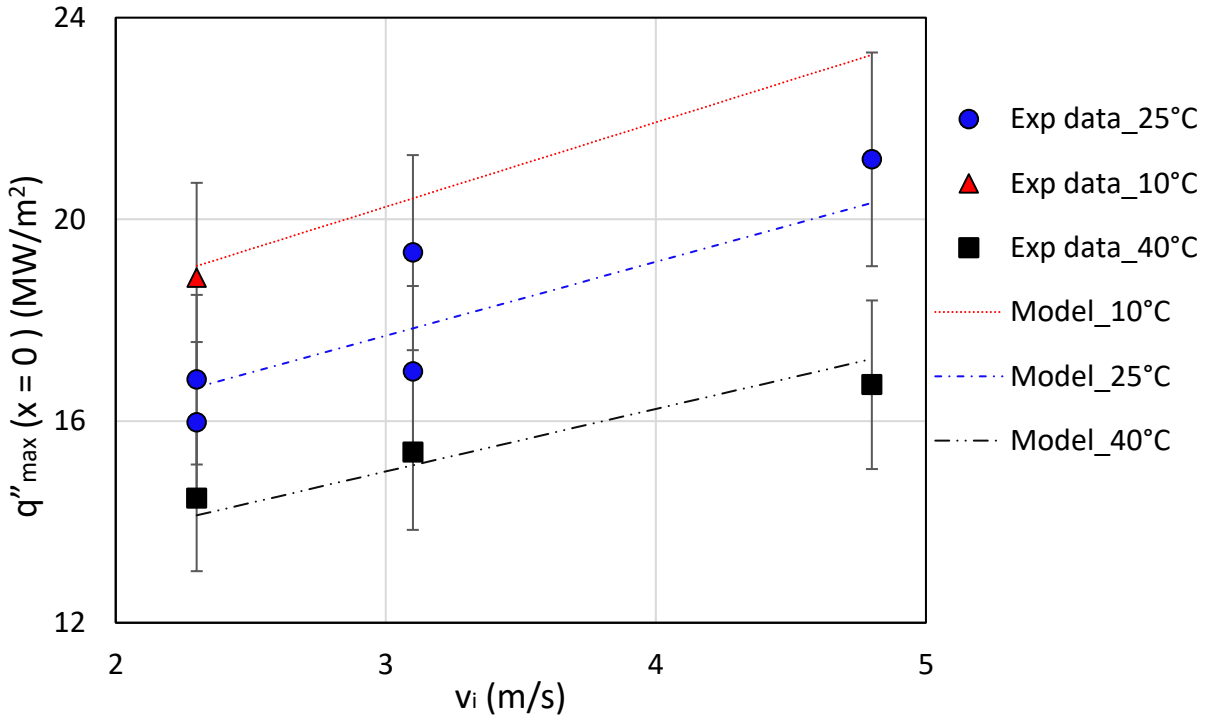

Figure 6.1 Experimental vs. calculated maximum local heat fluxes at the stagnation line (x = 0 mm).

Table 6.1 Jet impingement velocities for different flow rates

Flow rate, *FR* (l/min)	Impingement velocity, v_i (m/s)
160	2.3
200	3.1
300	4.8

To develop a model for the local maximum heat fluxes at different locations the following approach is taken. The local $q''_{max}(x)$ values are normalized with respect to the maximum heat fluxes at the stagnation line, and the distance (x) is normalized with respect to the nozzle width (w_n). The normalized maximum heat fluxes can then be described by

$$\frac{q''_{max}(x)}{q''_{max}(x=0)} = A + \frac{(1-A)}{\left[1+exp\left\{B\left(\frac{x}{w_n}\right)-4.5\right\}\right]} \tag{6.5}$$

where,

$$A = 0.27\left(\frac{T_{water}}{T_{sat}}\right)^{-0.3} \tag{6.6}$$

$$B = 0.97\left(\frac{T_{water}}{T_{sat}}\right)^{0.4} \tag{6.7}$$

Equation 6.5, a modified version of the mathematical hyperbolic function y = cot h (x), represents the general trend of heat flux variation with respect to distance from the jet centerline. The dimensionless empirical parameters A and B are functions of water temperature (equations 6.6 and 6.7), and control the size of the effective impingement zone and the influence of process parameters on q''_{max} values at varying distances from the stagnation line. Figures 6.2 (a) and (b)

show comparisons of calculated and experimental maximum heat flux values for varying flow rates and water temperatures, respectively.

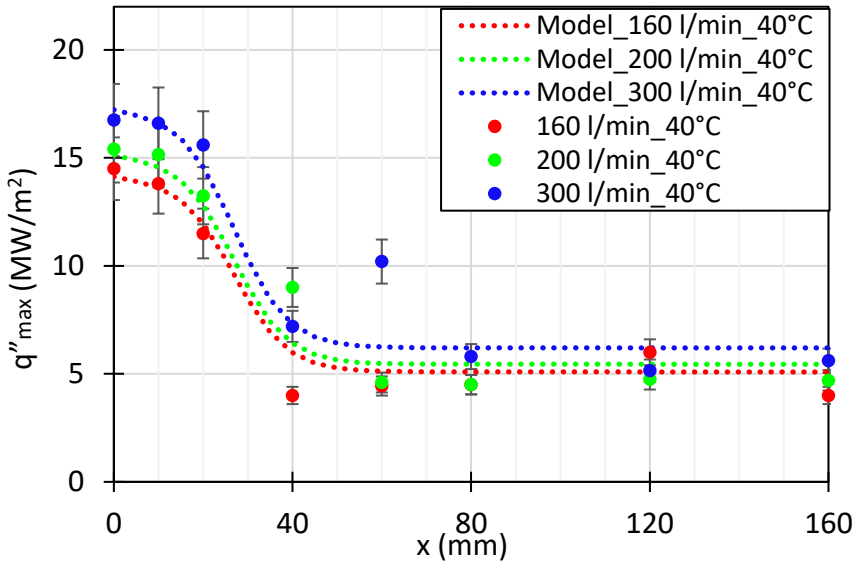

(a)

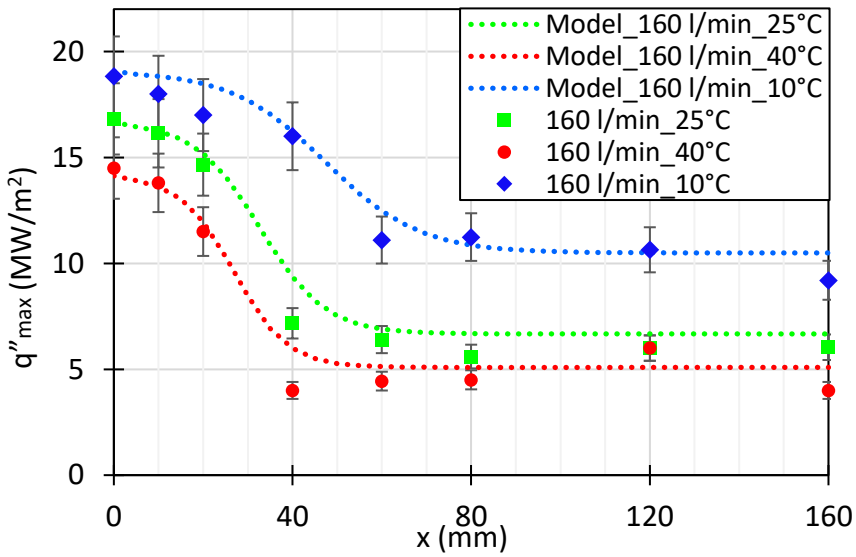

(b)

Figure 6.2 Calculated vs. experimental local maximum heat flux values (q''_{max}) for (a) different flow rates (b) different water temperatures.

Although both water temperature and flow rate play a role in the shape of boiling curves with distance, the influence of the former is more dominant on the effective size of the impingement zone as compared to the latter (Section 5.4). Hence, the adjustable parameters A and B (equations 6.6 and 6.7) can in a first approximation be taken as independent of flow rate.

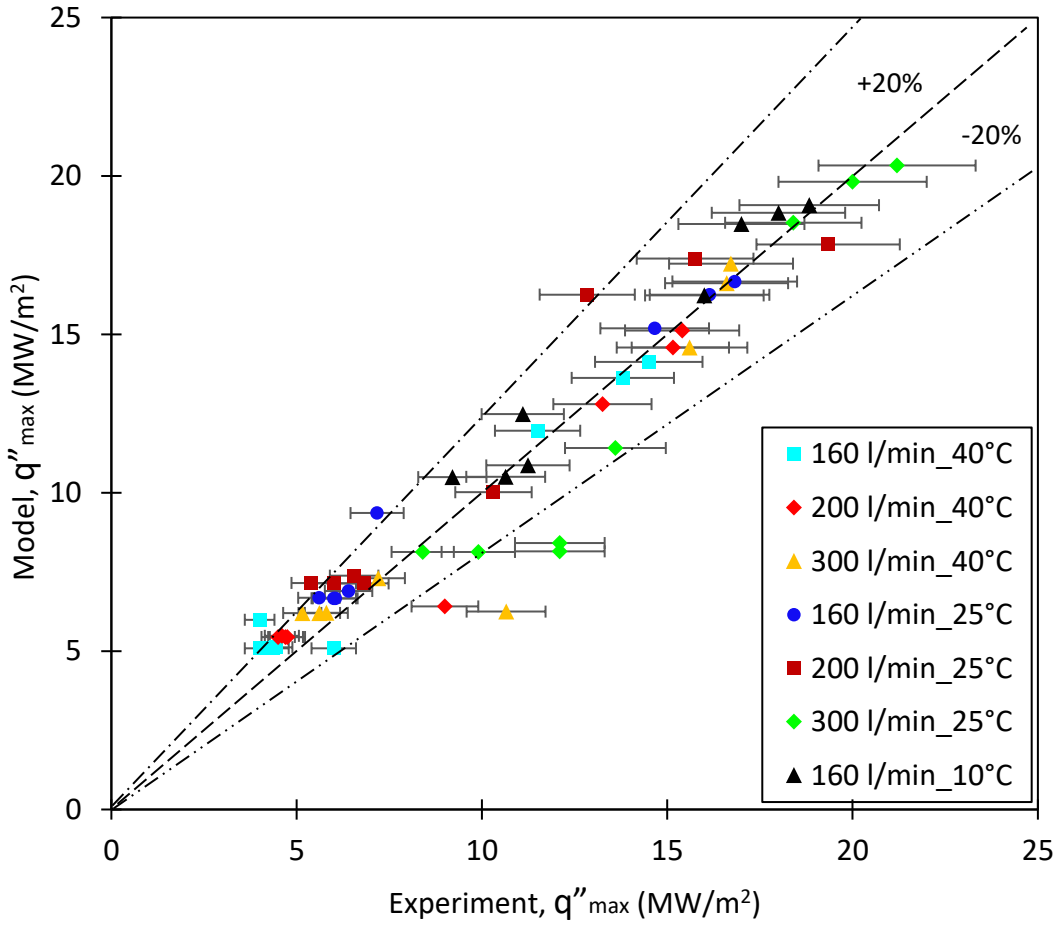

Figure 6.3 Calculated vs. experimental maximum heat flux values for all test conditions and TC locations.

The calculated local maximum heat fluxes using the proposed correlations are in reasonable agreement with experimental data (Figure 6.3), considering a model predictive capability of within ±20%. Some of the data points lie outside the limits of ±20%, belonging to the

described ‘intermediate zone’ of transitioning heat fluxes. Values in this ‘intermediate zone’ show significant scatter, owing to the substantial fluctuations and unpredictive nature of heat fluxes.

6.3 Shoulder Heat Flux

As witnessed in the experimental results, the heat fluxes in the ‘shoulder’ region of transition boiling exhibit fluctuations and the values decrease with increasing distance from the stagnation line (Figure 5.4). For simplicity of calculation, the average of the heat fluxes (q''_{sh}) is considered in the shoulder region of the Type A boiling curves. The averages of the heat flux (q''_{sh}) in the shoulder are correlated as a function of the local maximum heat flux values at the corresponding locations, i.e.

$$q''_{sh} = \frac{q''_{max}}{N} \; ; N = 2.07 \tag{6.8}$$

The local maximum (q''_{max}) and shoulder (q''_{sh}) heat flux values are in MW/m^2. Although there is some scatter in the experimental data (Figure 6.4), most data points are within ±25% of the mean.

The extent of the shoulder region is a function of water temperature (see Section 5.2.2.2) and can be described by

$$\frac{T_{sh\_end}}{T_{sat}} = a' \left(\frac{\Delta T_{sub}}{T_{sat}}\right)^{b'} + c' \tag{6.9}$$

where T_{sh_end} and T_{sat} are the shoulder termination temperature and saturation point of water respectively, $\Delta T_{sub} = T_{sat} - T_{water}$ is the amount of sub-cooling (°C) defined as the difference

between saturation point of water (T_{sat} = 100°C) and water jet temperature (T_{water}), and *a'*, *b'* and *c'* are empirical constants as follows:

$$a' = -0.01 \tag{6.10}$$

$$b' = -7.7 \tag{6.11}$$

$$c' = 4.3 \tag{6.12}$$

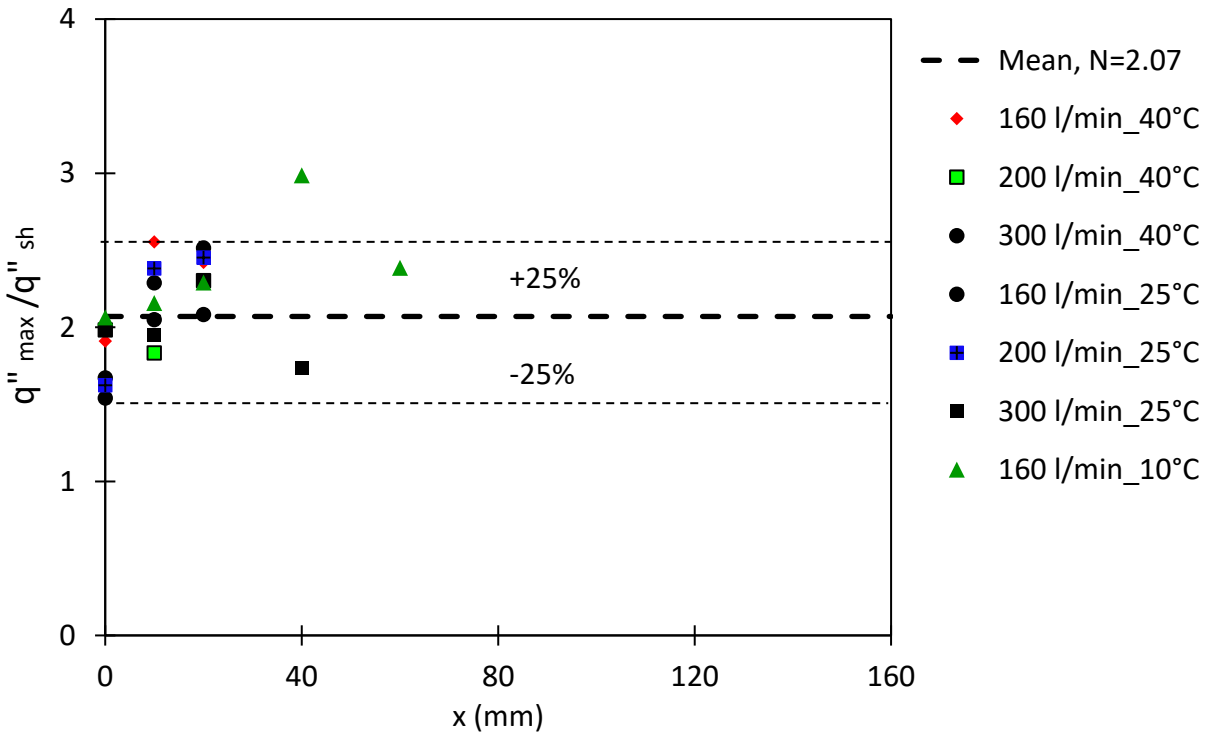

Figure 6.4 Shoulder heat fluxes as a fraction of maximum values for different distances in the impingement zone.

6.4 Nucleate Boiling

The experimental results do not show any appreciable effect of distance and process parameters, i.e. water flow rate and water temperature, in the nucleate boiling region (Figure 6.5). A fully developed nucleate boiling region was observed in all experiments above a plate surface temperature of ~150°C. The upper limit of nucleate boiling regime is reached when the local heat flux reaches its corresponding maximum value (q''_{max}). The following correlation for nucleate boiling is proposed as a function of plate surface temperature based on the experimental data of the impingement zone (Type A) of all tests:

$$q''_{NB} = C_1(T_{surface} - 150)^{n_1} \text{ …….. } [q'' \text{ in W/m}^2] \quad (6.13)$$

where,

$$C_1 = 1.50\ X\ 10^6\ \frac{W}{m^2}{}^{\circ}C^{-n_1} \quad (6.14)$$

$$n_1 = 0.667 \quad (6.15)$$

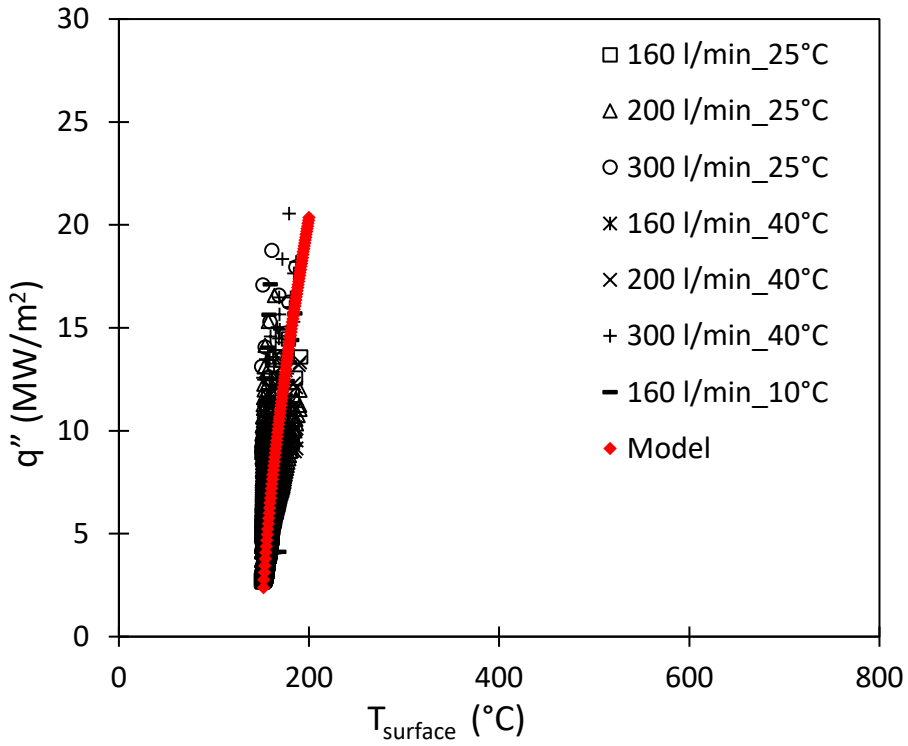

Figure 6.5 Nucleate boiling heat fluxes for all experiments in the impingement zone.

6.5 Initial Cooling

The transition from air cooling to jet impingement cooling (initial cooling stage of the boiling curve) in the impingement zone (Type A) is independent of distance and process parameters (Figure 6.6). The heat fluxes in the initial cooling stage as a function of plate surface temperature is correlated by

$$q''_{IC} = C_2(T_{initial} - T_{surface})^{n_2} \text{ ..... } [q'' \text{ in W/m}^2] \quad (6.16)$$

where,

$$C_2 = 2.80\ X\ 10^5\ \frac{W}{m^2}{}^{\circ}C^{-n_2} \quad (6.17)$$

$$n_2 = 0.760 \quad (6.18)$$

For the experiments of this work, $T_{initial} = 700°C$.

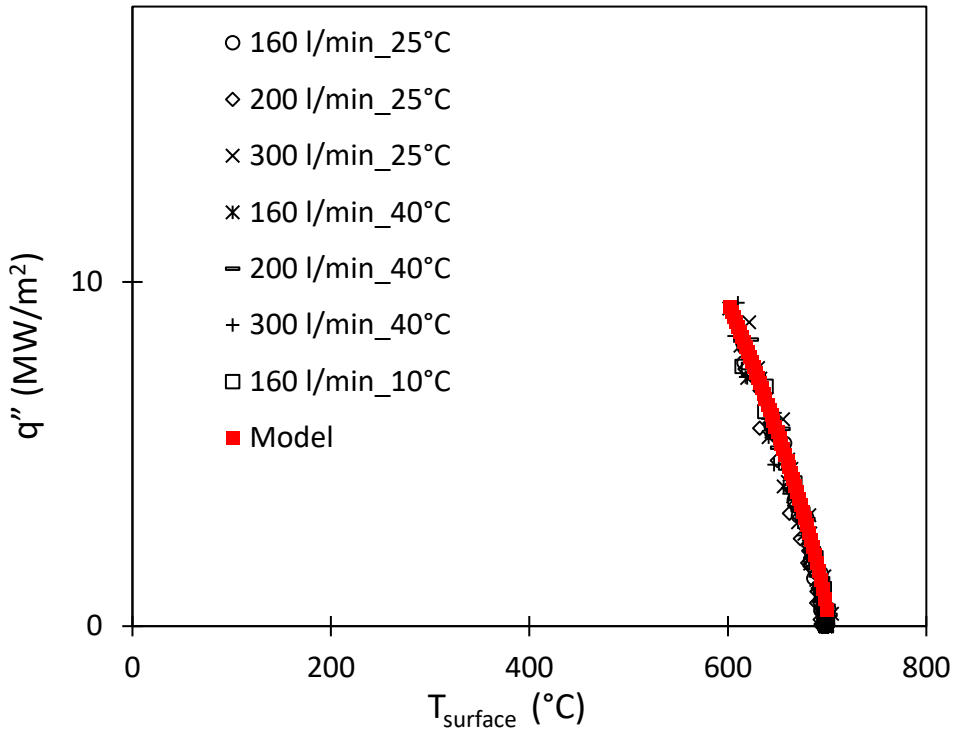

Figure 6.6 Heat fluxes of initial cooling stage in the impingement zone for all experiments.

In the boiling curves for the parallel flow region (Type B), the initial cooling (transition from air to water cooling) and transition boiling merge into a continuous heat flux regime (Figure 5.4), which appears to be predominantly characteristic of a transition boiling regime. Experimental results show an influence of flow rate and water temperature on the slope of this initial (transition boiling) region of boiling curves in parallel flow region (Section 5.2.2). The characteristic slope can be described as a function of flow rate and water temperature using the following correlation:

$$\frac{\Delta q^{"}}{\Delta T_{surface}} \left(MW/m^2\,°C\right) = -0.005\, v_i^{0.48} \left(\frac{T_{water}}{T_{sat.}}\right)^{-0.48} \tag{6.19}$$

where v_i is the jet impingement velocity in m/s correlated to the corresponding flow rate as given in Table 6.1. T_{water} and T_{sat} are the water temperature and saturation point of water, respectively.

6.6 Construction of Boiling Curves

In order to construct the boiling curves for transient cooling in the temperature range extending from the start of water cooling to the saturation point of water, the calculated heat fluxes for different regimes need to be combined. To combine the different heat flux regimes, an approach similar to the one taken by Nobari et al. [19] for transient top cooling has been adapted. Two different scenarios are considered independently for the construction of boiling curves. For the boiling curves of Type A (with 'shoulder'), the following steps are taken:

1) Starting from the cooling start temperature, heat fluxes are calculated by equation 6.16. The heat flux values continuously increase till the shoulder heat flux (q''_{sh}) for the corresponding location is intercepted. Depending on the process parameter i.e. water temperature, this shoulder extends up to the corresponding shoulder termination temperature, which is calculated by equation 6.9. The calculated heat flux in the shoulder regime (equation 6.8) remains constant till it terminates at the respective shoulder termination temperature.

2) The slope of the heat flux values with temperature in the transition boiling regime following the termination of the shoulder heat flux region is independent of distance from the water jet as well as process parameters i.e. flow rate and water temperature. For simplicity of calculation, the average of the transition boiling slopes is calculated for all tests. A similar approach was taken by Nobari et al. [19] and Li et al. [26] for determining heat fluxes in transition boiling. The mean value of the transition boiling slope derived from experimental results is 0.062 MW/m^2 °C. The

heat flux values continuously increase in the transition regime from the termination point of the shoulder till it intercepts the corresponding calculated local maximum heat flux value (q''_{max}).

3) The q''_{max} extends for a range of surface temperatures, the upper limit of which is given by the intersection of q''_{max} and the transition boiling heat fluxes calculated by the characteristic slope, and the lower limit is given by the intersection of q''_{max} and nucleate boiling heat fluxes calculated by equation 6.13. For temperatures below 150 °C, the heat transfer mechanism is partial nucleate boiling, and for temperatures lower than the saturation point of water (100 °C), the heat transfer mechanism is single phase convection. This temperature region is not of interest to run-out table cooling. For simplicity, the heat fluxes below 150 °C are calculated using the empirical correlation:

$$q''_{PNB/SPC}\left(\frac{W}{m^2}\right) = \left(1.91\,T_{surface} - 61.2\right) X\,10^4 \tag{6.20}$$

The characteristic boiling curves of Type B (without a shoulder) are observed starting at a distance from the stagnation line, which depends on the water flow rate and water temperature (Table 5.1). The dependence of this distance on the process parameters can be described by the following relation:

$$\frac{x}{w_n} = (1 + 1.8\,FR)\,T_{water}^{-0.87} \tag{6.21}$$

where, 'x' is the distance from the impingement line, 'w_n' is the width of planar nozzle, FR and T_{water} are the water flow rate (l/min) and water temperature (°C), respectively.

The boiling curves of Type B (without 'shoulder') are obtained in the following steps:

1) The transition from air to water cooling happens at relatively low temperatures in this region as compared to the impingement zone. This is coincident with the rate of progression of the wetting front as discussed earlier, with water cooling starting at slightly higher temperatures for lower water temperature, and can be described by the following relation:

$$T_{air-water} = 675 - T_{water} \tag{6.22}$$

where $T_{air-water}$ and T_{water} are the transition temperature from air to water cooling and water temperature in °C, respectively.

2) During the period of air cooling, the heat flux is negligible compared to water cooling (assumed to be ~ 0). As the mode of cooling changes from air cooling to quenching, the initial stage, predominantly characteristic of a transition boiling regime is modelled using the characteristic slope corresponding to the flow rate and water temperature given by equation 6.19.

3) The heat flux values increase with the characteristic slope from the respective cooling start temperature till it intercepts the corresponding calculated local maximum value (q''_{max}). Thereafter, with lowering surface temperatures the heat transfer modes change to nucleate boiling and partial nucleate boiling regimes calculated by equations 6.13 and 6.20, respectively.

A schematic of the boiling curves for both types constructed by combining the different regions is shown in Figure 6.7. One drawback of this model is that it does not provide any criteria to develop boiling curves in the intermittent zone (Type C). However, the variation of maximum heat flux values across all zones are mapped by the proposed correlations.

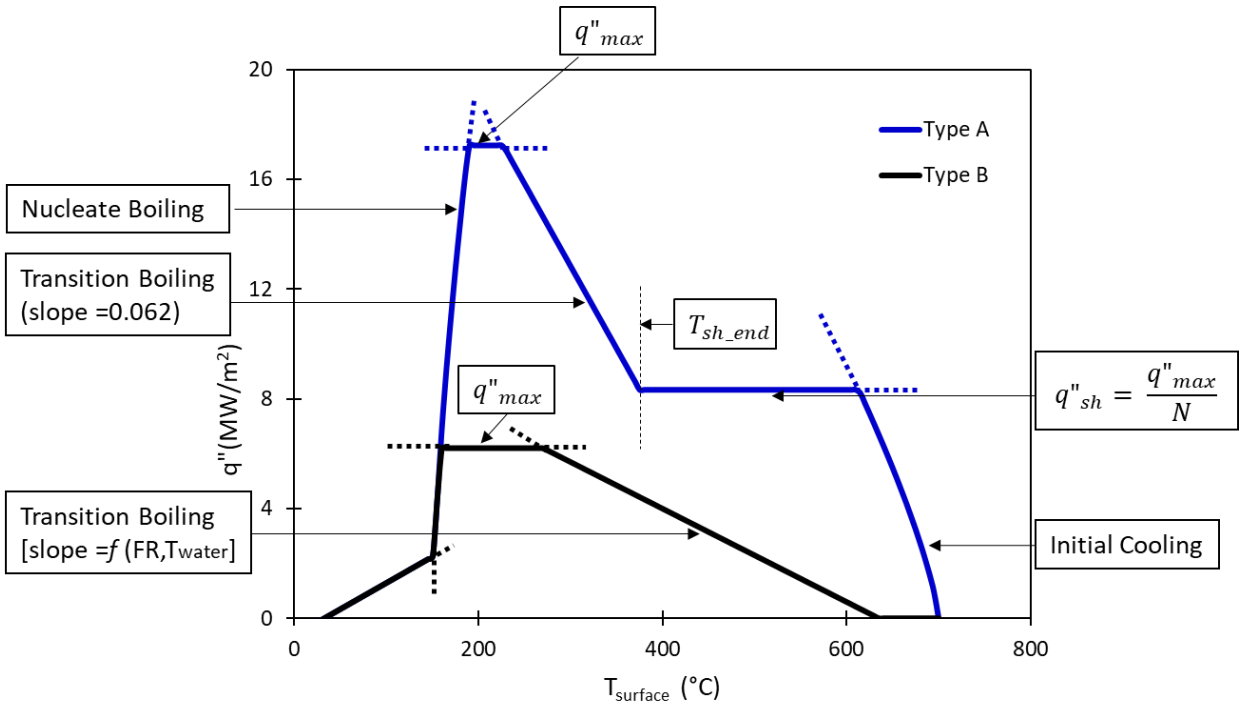

Figure 6.7 Schematic showing boiling curves combining different boiling regimes in the impingement zone and the parallel flow zone.

As an example, Figure 6.8 shows the comparison between calculated and experimental boiling curves in the impingement and parallel flow zones at different locations for test 1 (flow rate: 160 l/min, water temperature: 40°C). The heat fluxes in the calculated boiling curves show reasonable agreement with the experimental values. The comparisons between modelled and experimental boiling curves for all tests are shown in Appendix B. In general, the model is seen to describe heat flux values with acceptable accuracy, although in some cases discrepancies are observed in transition boiling, owing to the fluctuations in experimental heat flux values in the 'shoulder' of the boiling curves.

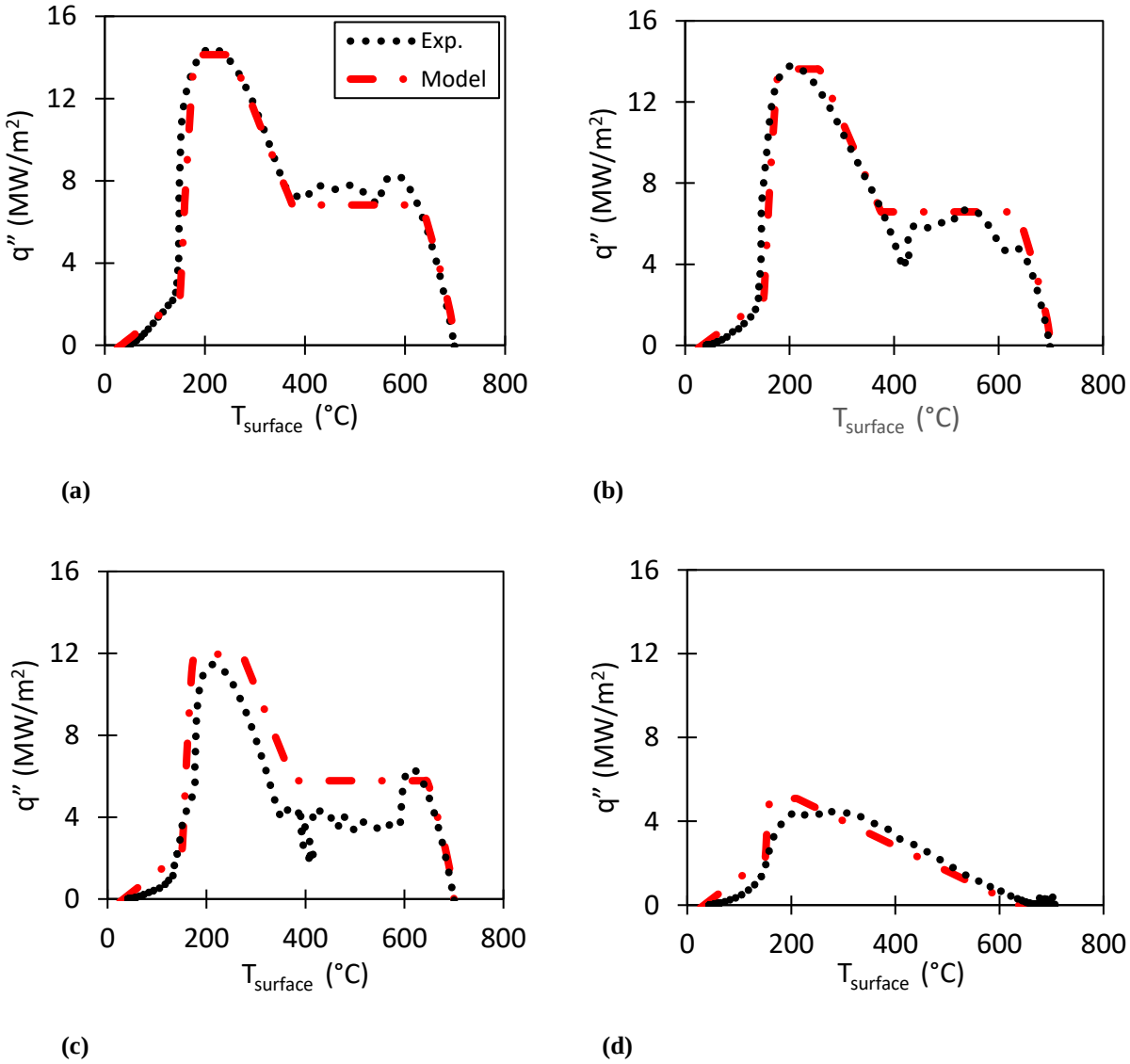

Figure 6.8 Calculated and experimental boiling curves at (a) x= 0 mm (b) x = 10 mm (c) x = 20 mm (d) x = 80 mm; flow rate = 160 l/min, water temperature = 40 °C.

Chapter 7: Conclusion

7.1 Summary and Contributions

A series of stationary cooling experiments have been conducted on hot steel plates on a pilot scale run-out table facility. A single planar nozzle is used for jet impingement cooling on the bottom surface of the test plate. The flow rate at the exit of the nozzle, temperature of water, and the inclination angle of the nozzle are varied systematically to investigate their effects on the cooling of a hot stationary steel plate. To quantify heat extraction rates during cooling, transient sub-surface temperature histories are measured at different distances from the water jet. Using an inverse heat conduction algorithm, the transient surface temperatures and heat fluxes are obtained to construct boiling curves at each location along the length of the plate.

The results show that distance from the water jet impingement significantly affects heat extraction rates and the shape of boiling curves. Two distinct zones are defined based on the nature of boiling curves and trend of heat transfer rates. A ‘shoulder’ in the transition boiling regime consistently appears in boiling curves of the impingement zone close to the water jet for all cooling conditions. This ‘shoulder’ is not observed in the characteristic boiling curves of the parallel flow zone sufficiently far away from the nozzle. A sharp drop in heat extraction rates is seen in the intermittent zone of transition from the impingement region to the parallel flow zone, and is characterized by boiling curves of mixed attributes.

Heat extraction rates increase with increasing flow rate. This is due to an increase in impinging velocity of water with increasing flow rates. A decrease in water temperature increases its heat absorption capacity, leading to increased cooling efficiency. Results show that the role of water temperature is stronger than that of flow rate. Further analysis of the results also brings into

light that a combined effect of flow rate and water temperature changes the nature of boiling curves with distance, and the resonant effect is more pronounced for lower water temperatures. Higher heat extraction rates are favored by a combination of decreased water temperatures and increased flow rates. Heat transfer is, however, not affected in the impingement zone as well as the parallel flow zone by variation of nozzle inclination.

Using the experimental results as database, simplified empirical correlations have been developed for different heat transfer regimes, i.e. nucleate boiling, shoulder heat flux, initial cooling, maximum heat flux. The role of distance, flow rate and water temperature is negligible on nucleate boiling and initial cooling regimes. Initial cooling and transition boiling merge into a single continuous heat flux regime, characteristic of transition boiling in the parallel flow zone. Influence of distance, flow rate and water temperature are incorporated in the correlations of maximum heat flux. The shoulder heat flux values are approximated as a ratio of maximum heat flux values at corresponding locations. The calculated heat fluxes in different regimes are combined to map the boiling curves for a range of temperatures that are relevant to industrial run-out table cooling. Boiling curves in the impingement zone as well as parallel flow zone are described. The calculated boiling curves show reasonable agreement with experimental results of this work.

Thus, the overall objective of developing a preliminary mathematical model for jet impingement cooling of the bottom surface of a steel plate by a planar nozzle has been accomplished.

7.2 Suggestions for Future Work

Considering the results and findings of this work, the following points are suggested for future work:

(1) Moving plate experiments should be conducted for bottom cooling to study the effect of plate velocity on heat transfer by a planar nozzle. The pilot scale facility has the capacity to conduct experiments with a plate velocity of up to ~ 1.6 m/s.

(2) A mechanistic model needs to be developed for bottom cooling, laying emphasis on the underlying physical phenomena of the shoulder region in the transition boiling regime.

(3) On an industrial run-out table, the steel strip/plate is moved forward by means of rollers acting on the bottom surface of the strip/plate. This may lead to accumulation of water and significantly change the water flow pattern. Systematic experiments need to be conducted simulating the presence of rolls under the bottom surface of the plate.

(4) The bottom cooling model needs to be combined with existing top cooling model [19] to develop a model for cooling on an industrial scale run-out table.

(5) The overall cooling model needs then to be calibrated and verified with an industrial database.

Bibliography

[1] C. Ouchi, “Development of steel plates by intensive use of TMCP and direct quenching processes,” *Isij*, vol. 41, no. 6, pp. 542–553, 2001.

[2] A. A. Gorni and J. H. Dolabela da Silveira, “Accelerated cooling of steel plates: the time has come,” *J. ASTM Int.*, vol. 5, no. 8, pp. 1–7, 2008.

[3] V. Schwinn, J. Bauer, P. Flüss, H.-J. Kirsch, and E. Amoris, “Recent developments and applications of TMCP steel plates,” *Rev. Métallurgie*, vol. 108, no. 5, pp. 283–294, 2011.

[4] K. Nishioka and K. Ichikawa, “Progress in thermomechanical control of steel plates and their commercialization,” *Sci. Technol. Adv. Mater.*, vol. 13, no. 2, pp. 1–20, 2012.

[5] Z. Liu, “Experiments and mathematical modelling of controlled runout table cooling in a hot rolling mill,” Ph.D. Thesis, University of British Columbia, 2001.

[6] A. H. Nobari, “Mechanistic jet impingement model for cooling of hot steel plates,” Ph.D. Thesis, University of British Columbia, 2014.

[7] G. Franco, “Boiling heat transfer during cooling of a hot moving steel,” M.A.Sc. Thesis, University of British Columbia, 2008.

[8] P. Chan, “Jet impingement boiling heat transfer at low coiling temperatures,” M.A.Sc. Thesis, University of British Columbia, 2007.

[9] K. V. Jondhale, “Heat transfer during multiple jet impingement on the top surface of hot rolled steel strip,” M.A.Sc. Thesis, University of British Columbia, 2007.

[10] N. L. Chester, “A study of boiling heat transfer on a hot steel plate cooled by an inclined circular bottom water jet,” The University of British Columbia, 2006.

[11] P. Zhang, “Study of boiling beat transfer on a stationary downward facing hot steel plate cooled by a circular water jet,” M.A.Sc. Thesis, University of British Columbia, 2004.

[12] B. Wang, X. Guo, Q. Xie, Z. Wang, and G. Wang, “Heat transfer characteristic research during jet impinging on top/bottom hot steel plate,” *Int. J. Heat Mass Transf.*, vol. 101, pp. 844–851, 2016.

[13] S. J. Slayzak, R. Viskanta, and F. P. Incropera, “Effects of interaction between adjacent free surface planar jets on local heat transfer from the impingement surface,” *Int. J. Heat Mass Transf.*, vol. 37, no. 2, pp. 269–282, 1994.

[14] S. Nukiyama, “The maximum and minimum values of the heat Q transmitted from metal to boiling water under atmospheric pressure,” *Int. J. Heat Mass Transf.*, vol. 9, no. 12, pp. 1419–1433, 1966.

[15] V. K. Dhir, “Boiling heat transfer,” *Annu. Rev. Fluid Mech.*, vol. 30, pp. 365–401, 1998.

[16] D. H. Wolf, F. P. Incropera, and R. Viskanta, “Jet impingement boiling,” *Adv. Heat Transf.*, vol. 23, pp. 1–131, 1993.

[17] D. A. Zumbrunnen, “Method and apparatus for measuring heat transfer distributions on moving and stationary plates cooled by a planar liquid jet,” *Exp. Therm. Fluid Sci.*, vol. 3, no. 2, pp. 202–213, 1990.

[18] H. Robidou, H. Auracher, P. Gardin, and M. Lebouché, “Controlled cooling of a hot plate with a water jet,” *Exp. Therm. Fluid Sci.*, vol. 26, no. 2–4, pp. 123–129, 2002.

[19] A. H. Nobari, V. Prodanovic, and M. Militzer, “Heat transfer of a stationary steel plate during water jet impingement cooling,” *Int. J. Heat Mass Transf.*, vol. 101, pp. 1138–1150, 2016.

[20] A. T. Hauksson, D. Fraser, V. Prodanovic, and I. Samarasekera, “Experimental study of boiling heat transfer during subcooled water jet impingement on flat steel surface,” *Ironmak. Steelmak.*, vol. 31, no. 1, pp. 51–56, 2004.

[21] Z. D. Liu, D. Fraser, and I. V. Samarasekera, “Experimental study and calculation of boiling heat transfer on steel plates during runout table operation,” *Can. Metall. Q.*, vol. 41, no. 1, pp. 63–74, 2002.

[22] H. Robidou, H. Auracher, P. Gardin, M. Lebouch, and L. Bogdanic, “Local heat transfer from a hot plate to a water jet,” *Heat Mass Transf.*, vol. 39, no. 10, pp. 861–867, 2003.

[23] J. Filipovic, F. P. Incropera, and R. Viskanta, “Quenching phenomena associated with a water wall jet: i. transient hydrodynamic and thermal conditions,” *Exp. Heat Transf.*, vol. 8, pp. 97–117, 1995.

[24] F. Xu and M. S. Gadala, “Heat transfer behavior in the impingement zone under circular water jet,” *Int. J. Heat Mass Transf.*, vol. 49, no. 21–22, pp. 3785–3799, 2006.

[25] D. Li and M. A. Wells, “Effect of Water Flow Rate, Water Temperature, Nozzle Size and Nozzle Stand-Off Distance on the Boiling Water Heat Transfer of Aisi 316 Stainless Steel Plate,” *Can. Metall. Q.*, vol. 44, no. 1, pp. 59–70, 2005.

[26] D. Li, M. A. Wells, S. L. Cockcroft, and E. Caron, “Effect of sample start temperature during transient boiling water heat transfer,” *Metall. Mater. Trans. B Process Metall. Mater. Process. Sci.*, vol. 38, no. 6, pp. 901–910, 2007.

[27] T. Ueda, S. Tsunenari, and M. Koyanagi, “An investigation of critical heat flux and surface rewet in flow boiling systems,” *Int. J. Heat Mass Transf.*, vol. 26, no. 8, pp. 1189–1198, 1983.

[28] M. A. Islam, M. Monde, P. L. Woodfield, and Y. Mitsutake, “Jet impingement quenching phenomena for hot surfaces well above the limiting temperature for solid-liquid contact,” *Int. J. Heat Mass Transf.*, vol. 51, no. 5–6, pp. 1226–1237, 2008.

[29] J. Filipovic, F. P. Incropera, and R. Viskanta, “Quenching phenomena associated with a

water wall jet: ii. comparison of experimental and theoretical results for the film boiling region," *Exp. Heat Transf.*, vol. 8, pp. 119–130, 1995.

[30] L. Bogdanic, H. Auracher, and F. Ziegler, "Two-phase structure above hot surfaces in jet impingement boiling," *Heat Mass Transf. und Stoffuebertragung*, vol. 45, no. 7, pp. 1019–1028, 2009.

[31] S. Ishigai, "Boiling heat transfer for a plane water jet impinging on a hot surface," in *6th International Heat Transfer Conference*, 1978, pp. 445–450.

[32] T. Ochi, "Cooling of a hot plate with an impinging circular water jet," *Multi-phase flow Heat Transf.*, vol. 3, pp. 671–680, 1984.

[33] H. Leocadio, J. C. Passos, and A. F. C. da Silva, "Heat transfer behavior of a high temperature steel plate cooled by a subcooled impinging circular water jet," in *7th ECI International Conference on Boiling Heat Transfer*, 2009, pp. 1–7.

[34] Z. H. Liu, "Prediction of minimum heat flux for water jet boiling on a hot plate," *J. of[1] Z. H. Liu, "Prediction Minim. heat flux water jet Boil. a hot plate," J. Thermophys. Heat Transf., vol. 17, no. 2, pp. 159–165, 2003. Thermophys. Heat Transf.*, vol. 17, no. 2, pp. 159–165, 2003.

[35] A. K. Mozumder, M. Monde, and P. L. Woodfield, "Delay of wetting propagation during jet impingement quenching for a high temperature surface," *Int. J. Heat Mass Transf.*, vol. 48, no. 25–26, pp. 5395–5407, 2005.

[36] A. K. Mozumder, M. Monde, P. L. Woodfield, and M. A. Islam, "Maximum heat flux in relation to quenching of a high temperature surface with liquid jet impingement," *Int. J. Heat Mass Transf.*, vol. 49, no. 17–18, pp. 2877–2888, 2006.

[37] A. K. Mozumder, P. L. Woodfield, M. Ashraful Islam, and M. Monde, "Maximum heat

flux propagation velocity during quenching by water jet impingement," *Int. J. Heat Mass Transf.*, vol. 50, no. 7–8, pp. 1559–1568, 2007.

[38] B. D. G. Piggott, E. P. White, and R. B. Duffey, "Wetting delay due to film and transition boiling on hot surfaces," *Nucl. Eng. Des.*, vol. 36, no. 2, pp. 169–181, 1976.

[39] N. Zuber, "Hydrodynamic aspects of boiling heat transfer," Ph.D. Thesis, University of California, Los Angelels, 1959.

[40] P. J. Berenson, "Experiments on pool-boiling heat transfer," *Int. J. Heat Mass Transf.*, vol. 5, no. 10, pp. 985–999, 1962.

[41] V. V. Kalinin, E.K., Berlin, I.I., Kostiouk, "Transition Boiling Heat Transfer," *Adv. Heat Transf.*, vol. 11, pp. 241–323, 1987.

[42] P. Chin, J. Y. Hwang, and T. L. Lin, "The mechanism of heat transfer in transition boiling," *Int. J. Heat Mass Transf.*, vol. 32, no. 7, pp. 1337–1349, 1989.

[43] C. Pan and K. T. Ma, "Modeling of transition boiling," in *Proc. Engineering Foundation Conference on Pool and External Flow Boiling, ASME, March, Santa Barbara, California*, 1992, pp. 263–270.

[44] S. Nishio and H. Auracher, "Film and transition boiling," in *S.G. Kandlikar, M. Shoji, V.K. Dhir (Eds.), Handbook of Phase Change— Boiling and Condensation, Taylor & Francis, London*, 1999, pp. 167–196.

[45] H. S. Ragheb and S. C. Cheng, "Surface wetted area during transition boiling in forced convective flow," *J. Heat Transfer*, vol. 101, pp. 381–383, 1979.

[46] M. Gradeck, A. Kouachi, M. Lebouché, F. Volle, D. Maillet, and J. L. Borean, "Boiling curves in relation to quenching of a high temperature moving surface with liquid jet impingement," *Int. J. Heat Mass Transf.*, vol. 52, no. 5–6, pp. 1094–1104, 2009.

[47] A. B. Ahmed and M. S. Hamed, “Modeling of transition boiling under an impinging water jet,” *Int. J. Heat Mass Transf.*, vol. 91, pp. 1273–1282, 2015.

[48] Y. Miyasaka, S. Inada, and Y. Owase, “Critical heat flux and subcooled nucleate boiling in transient region between a two-dimensional water jet and a heated surface,” *J. Chem. Eng. Japan*, vol. 13, no. 1, pp. 29–35, 1980.

[49] N. Seiler-Marie, J. M. Seiler, and O. Simonin, “Transition boiling at jet impingement,” *Int. J. Heat Mass Transf.*, vol. 47, no. 23, pp. 5059–5070, 2004.

[50] S. Ishigai and M. Mizuno, “Boiling heat transfer with an impinging water jet (about the critical heat flux),” *Prepr. JSME*, vol. 740, no. 16, pp. 139–142, 1974.

[51] D. E. Hall, F. P. Incropera, and R. Viskanta, “Jet Impingement Boiling From a Circular Free-Surface Jet During Quenching: Part 2—Two-Phase Jet,” *J. Heat Transfer*, vol. 123, no. 5, p. 911, 2001.

[52] K. Nishikawa, S. Uchida, H. Ohta, and Y. Fujita, “Effect of heating surface orientation on nucleate boiling heat transfer,” in *ASME/JSME Thermal Engineering Conference*, 1983, pp. 129–136.

[53] P. Patel and S. Roy, “Study of jet impingement heat transfer for varying fluid flow characteristics,” in *Proceedings of the ASME Fluids Enginerring Division Summer Meeting*, 2003, pp. 197–204.

[54] A. Y. Tong, “Hydrodynamics and heat transfer of an oblique plane jet impinging onto a substrate,” in *ASME International Mechanical Engineering Congress and Exposition*, 2002, pp. 23–30.

[55] A. H. Beitelmal, M. A. Saad, and C. D. Patel, “Effect of inclination on the heat transfer between a flat surface and an impinging two-dimensional air jet,” *Int. J. Heat Fluid Flow*,

vol. 21, pp. 156–163, 2000.

[56] N. L. Chester, M. A. Wells, and V. Prodanovic, “Effect of inclination angle and flow rate on the heat transfer during bottom jet cooling of a steel plate,” *J. Heat Transfer*, vol. 134, no. 12, p. 122201, 2012.

[57] D. Halliday, R. Resnick, and J. Walker, *Fundamentals of Physics*, 10th ed. John Wiley and Sons, 2013.

[58] W. Timm, K. Weinzierl, A. Leipertz, H. Zieger, and G. Zouhar, “Modelling of heat transfer in hot strip mill runout table cooling,” *Steel Res.*, vol. 73, no. 3, pp. 97–104, 2002.

[59] S. Sikdar and A. Mukhopadhyay, “Numerical determination of heat transfer coefficient for boiling phenomenon at runout table of hot strip mill,” *Ironmak. Steelmak.*, vol. 31, no. 6, pp. 495–502, 2004.

[60] R. M. Guo, “Modeling and simulation of run-out table cooling control using feedforward-feedback and element tracking system,” *IEEE Trans. Ind. Appl.*, vol. 33, no. 2, pp. 304–311, 1997.

[61] C. G. Sun, H. N. Han, J. K. Lee, Y. S. Jin, and S. M. Hwang, “A finite element model for the prediction of thermal and metallurgical behavior of strip on run-out-table in hot rolling,” *ISIJ Int.*, vol. 42, pp. 392–400, 2002.

[62] S. Chen, J. ZOu, and X. Fu, “Coupled models of heat transfer and phase transformation for the run-out table in hot rolling,” *J. Zhejiang Univ. A*, vol. 9, no. 7, pp. 932–939, 2008.

[63] “Integ-HSMM Software Package.” [Online]. Available: http://www.integpg.com/about/hot-strip-mill-model/. [Accessed: 28-Feb-2018].

[64] J. K. Brimacombe *et al.*, “Microstructure engineering in hot trip mills, part 1: integrated mathematical model,” Report for American Iron and Steel Institute, Advanced Process

Control Program, 1998.

[65] R. Shulkosky, D. Rosberg, and J. Chapman, “Validation of the Hot Strip Mill Model,” Department of Commerce, National Technical Information Service, USA, 2005.

[66] I. S. Park, “Numerical analysis for film boiling heat transfer of a moving hot steel plate,” *ISIJ Int.*, vol. 51, pp. 743–747, 2011.

[67] I. S. Park, “Numerical study on effect of nozzle diameter on plate cooling in run out table of hot plate rolling process,” *ISIJ Int.*, vol. 52, pp. 1080–1085, 2012.

[68] I. S. Park, “Effects of cooling water supply nozzle array on cooling performance of run out table in hot rolling process,” *ISIJ Int.*, vol. 53, pp. 71–75, 2013.

[69] M. S. Loveday, M. F. Day, and B. F. Dyson, “Measurement of high temperature mechanical properties of materials,” *Natl. Phys. Lab.*, pp. 58–82, 1982.

[70] R. L. Anderson, R. K. Adams, and B. C. Duggins, “Limitations of Thermocouples in Temperature Measurements,” in *25th ISA Anaheim CA*, 1979, pp. 1–33.

[71] C. D. Henning and R. Parker, “Transient response of an intrinsic thermocouple,” *Trans. ASME*, pp. 146–154, 1967.

[72] A. T. Hauksson, “Experimental study of boiling heat transfer during water jet impingement on a hot steel plate,” M.A.Sc. Thesis, University of British Columbia, 2001.

[73] E. Caron, “Secondary cooling in the direct-chill casting of light metals,” Ph.D. Thesis, University of British Columbia, 2008.

[74] S. Vakili, “Analysis of water cooling process of steel strips on runout,” Ph.D. Thesis, University of British Columbia, 2011.

[75] A. Bakkalog, “Effect of processing parameters on the microstructure and properties of an Nb microalloyed steel,” vol. 56, no. October, pp. 200–209, 2002.

[76] J. V. Beck, B. Blackwell, and C. R. St. Clair, *Inverse Heat Conduction*. John Wiley and Sons, 1985.

Appendices

Appendix A : Inverse Heat Conduction (IHC) Analysis

Zhang [11] developed the IHC program using a function specification method. The function specification method assumes a prescribed function for the heat flux within a future time interval and solves the problem in a sequential manner [11, 76]. This was combined with a zeroth-order Tikhonov regularization method to solve the IHC problem with a sequential in-time concept in order to improve computational facility. To enhance the accuracy and consider time lag, the future information (future time steps) was used in the sequential-in-time method [11].The developed IHC program was used to calculate the surface temperature and heat flux at each thermocouple location independently in this study. The latent heat of austenite-ferrite phase transformation is not included in the program. However, this limitation is insignificant in the present study as the austenite-ferrite transformation occurs above the quench start temperature during experiments [6].

The IHC problem is solved by the solver in the following steps [11]:

1. Input initial data: measured temperature history, assumed surface heat flux (q^o)
2. Call direct FEM conduction problem solver to calculate sub-surface temperature
3. Solve sensitivity equation and solve sensitivity matrix. The sensitivity matrix determines the change of heat flux with respect to the difference of temperatures.
4. Calculate increment of change in the assumed heat flux (Δq) using sensitivity matrix and update original heat fluxes using $q = q^o + \Delta q$
5. Repeat steps 1-4 until the sum of square error between the computed and measured sub-surface temperatures is smaller than a critical number ($1x10^{-5}$).

Appendix B : Calculated vs Experimental Boiling Curves

Figures B.1-7 show the comparisons between calculated and experimental boiling curves for varying water temperatures and flow rates. Boiling curves in the impingement zone (Type A) and the parallel flow zone (Type B) are compared for each experimental setup. For the boiling curves of Type B, in some cases close to the intermittent zone, fluctuations in the experimental heat flux values may be seen prior to the initial cooling stage in the experimental boiling curves. These fluctuations generally occur due to some degree of fluctuations in the measured sub-surface temperature values prior to the transition from air to water cooling (see Figure 5.1(a)), and are omitted in the proposed model for boiling curves.

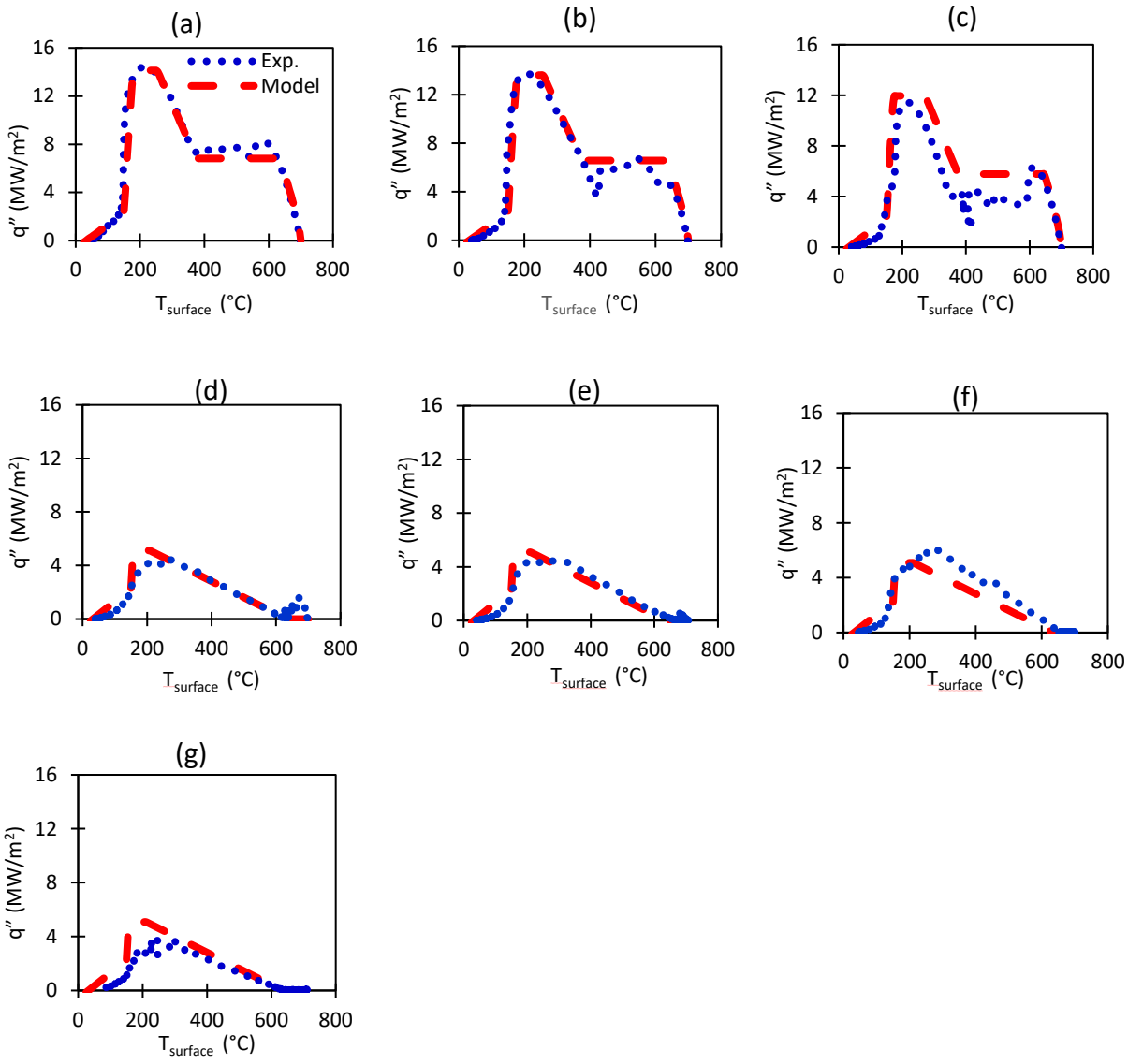

Figure B.1: Calculated vs. experimental boiling curves for test 1; flow rate = 160 l/min, water temperature = 40°C, x: (a) 0 mm, (b) 10 mm, (c) 20 mm, (d) 60 mm, (e) 80 mm, (f) 120 mm, and (g) 160 mm.

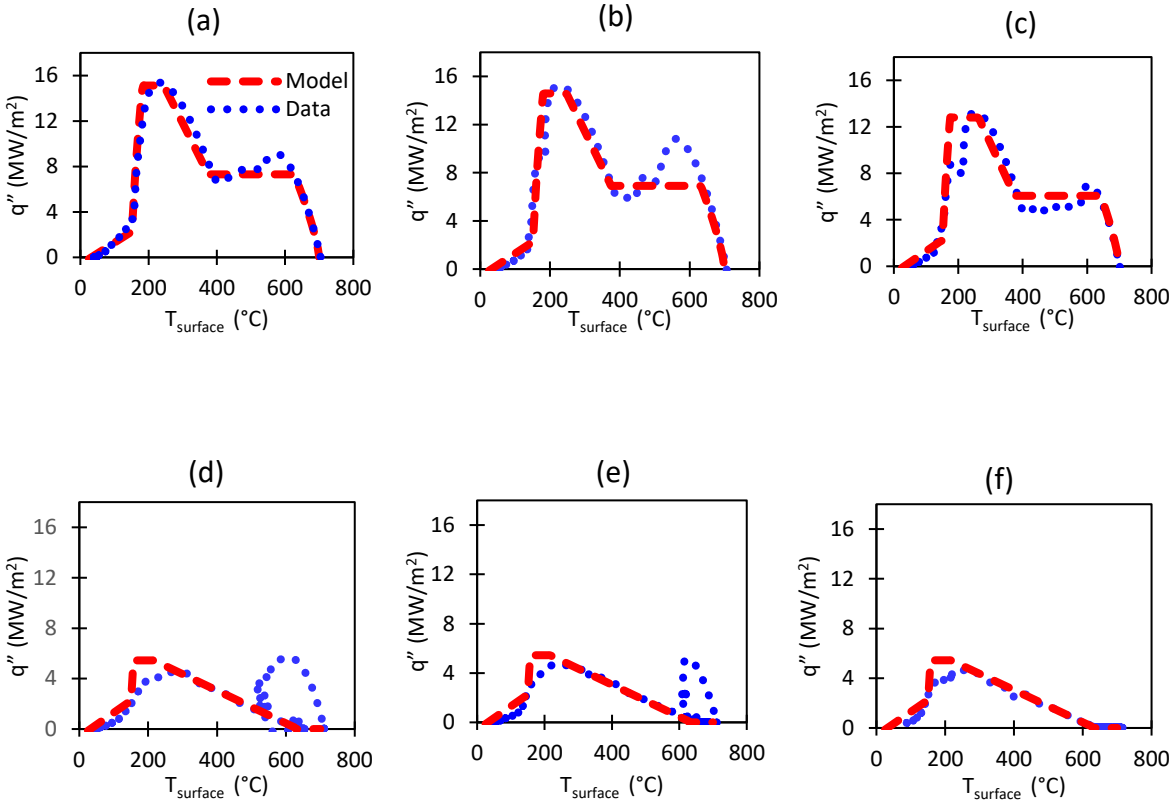

Figure B.2: Calculated vs. experimental boiling curves for test 2; flow rate = 200 l/min, water temperature = 40°C, x: (a) 0 mm, (b) 10 mm, (c) 20 mm, (d) 80 mm, (e) 120 mm, and (f) 160 mm.

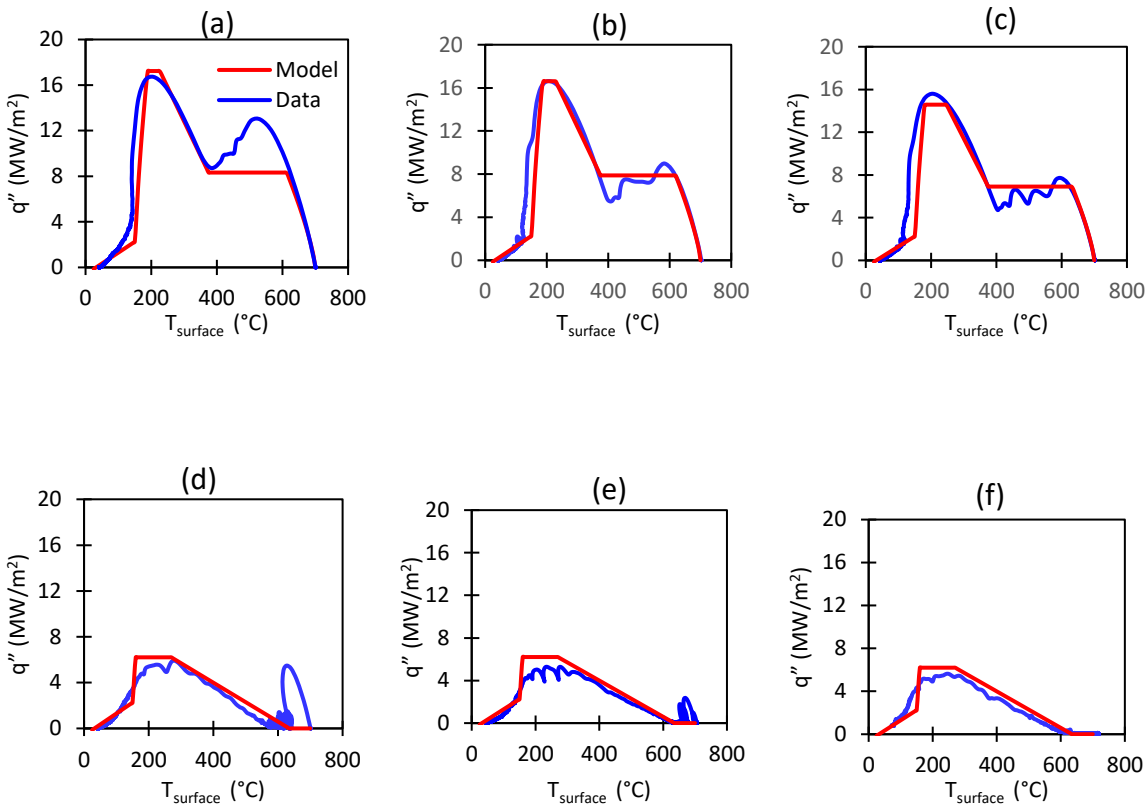

Figure B.3: Calculated vs. experimental boiling curves for test 3; flow rate = 300 l/min, water temperature = 40°C, x: (a) 0 mm, (b) 10 mm, (c) 20 mm, (d) 80 mm, (e) 120 mm, and (f) 160 mm.

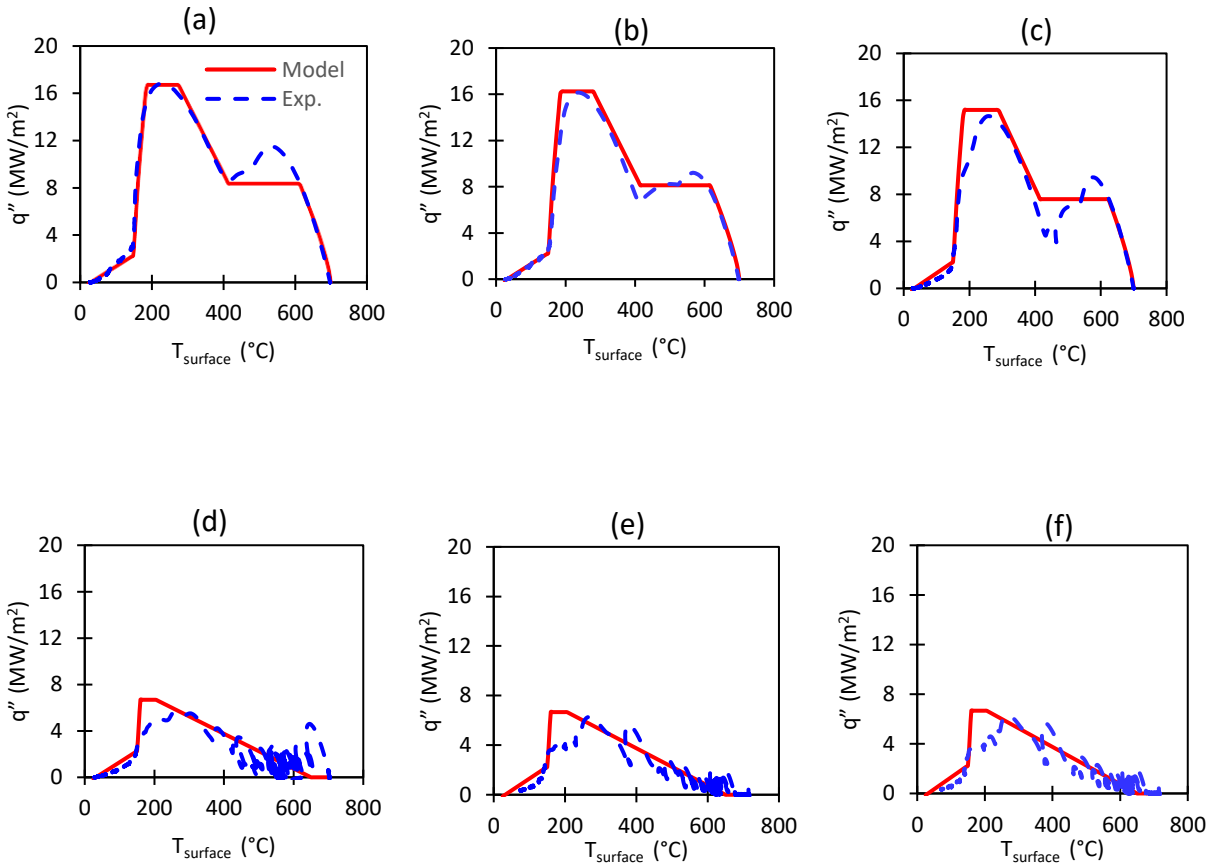

Figure B.4: Calculated vs. experimental boiling curves for test 4; flow rate = 160 l/min, water temperature = 25°C, x: (a) 0 mm, (b) 10 mm, (c) 20 mm, (d) 80 mm, (e) 120 mm, and (f) 160 mm.

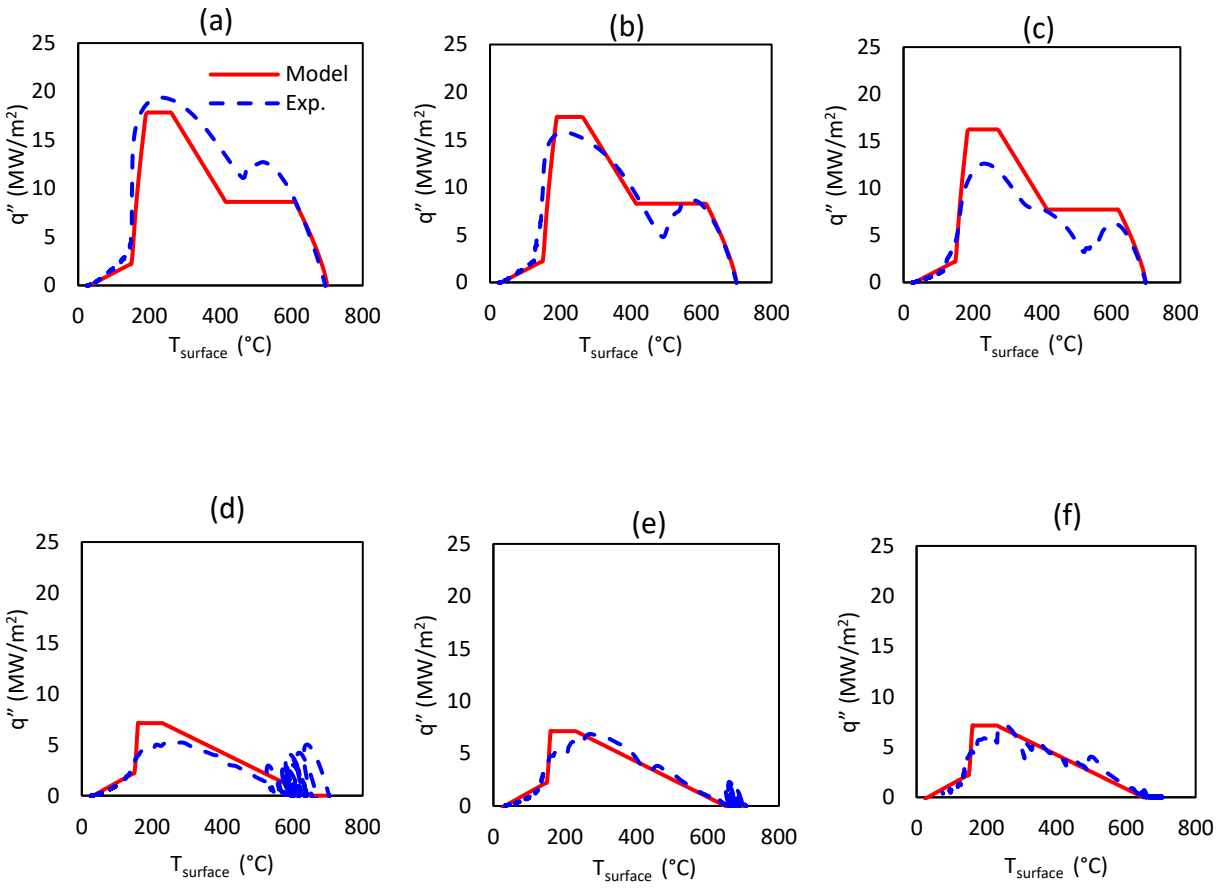

Figure B.5: Calculated vs. experimental boiling curves for test 5; flow rate = 200 l/min, water temperature = 25°C, x: (a) 0 mm, (b) 10 mm, (c) 20 mm, (d) 80 mm, (e) 120 mm, and (f) 160 mm.

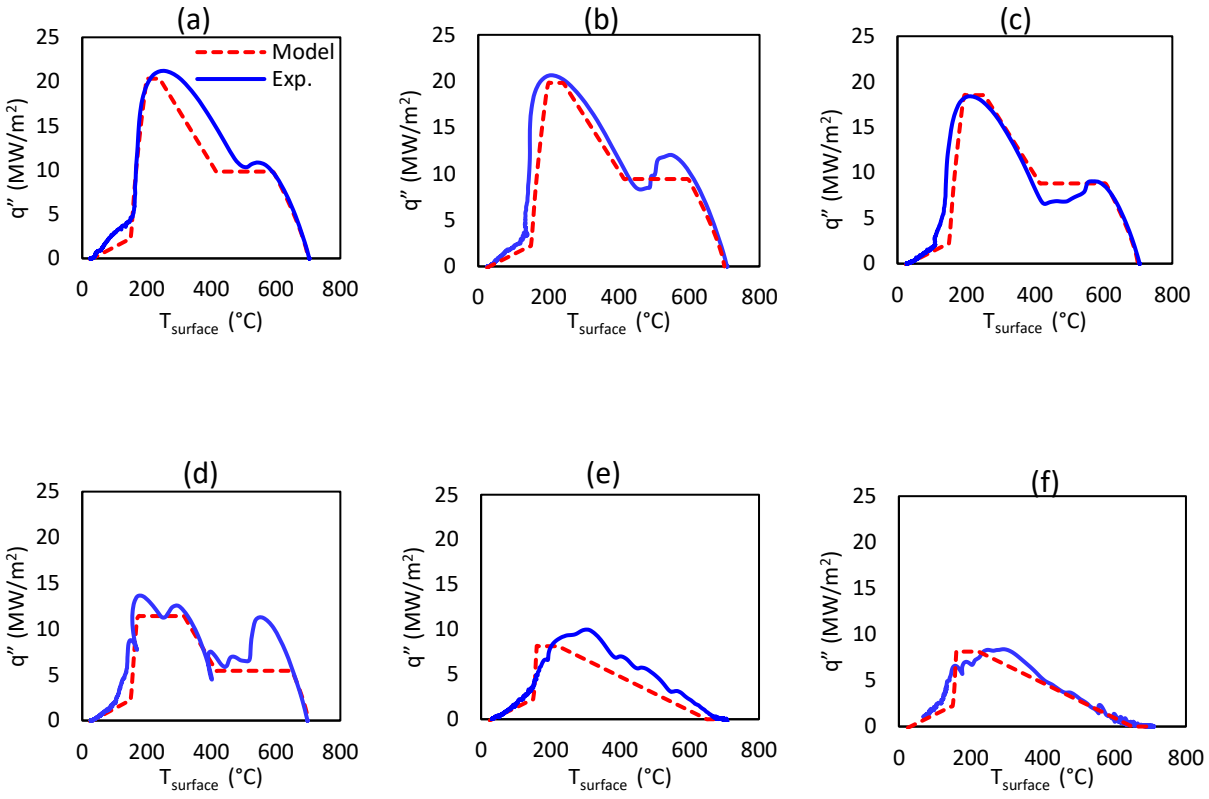

Figure B.6: Calculated vs. experimental boiling curves for test 6; flow rate = 300 l/min, water temperature = 25°C, x: (a) 0 mm, (b) 10 mm, (c) 20 mm, (d) 40 mm, (e) 120 mm, and (f) 160 mm.

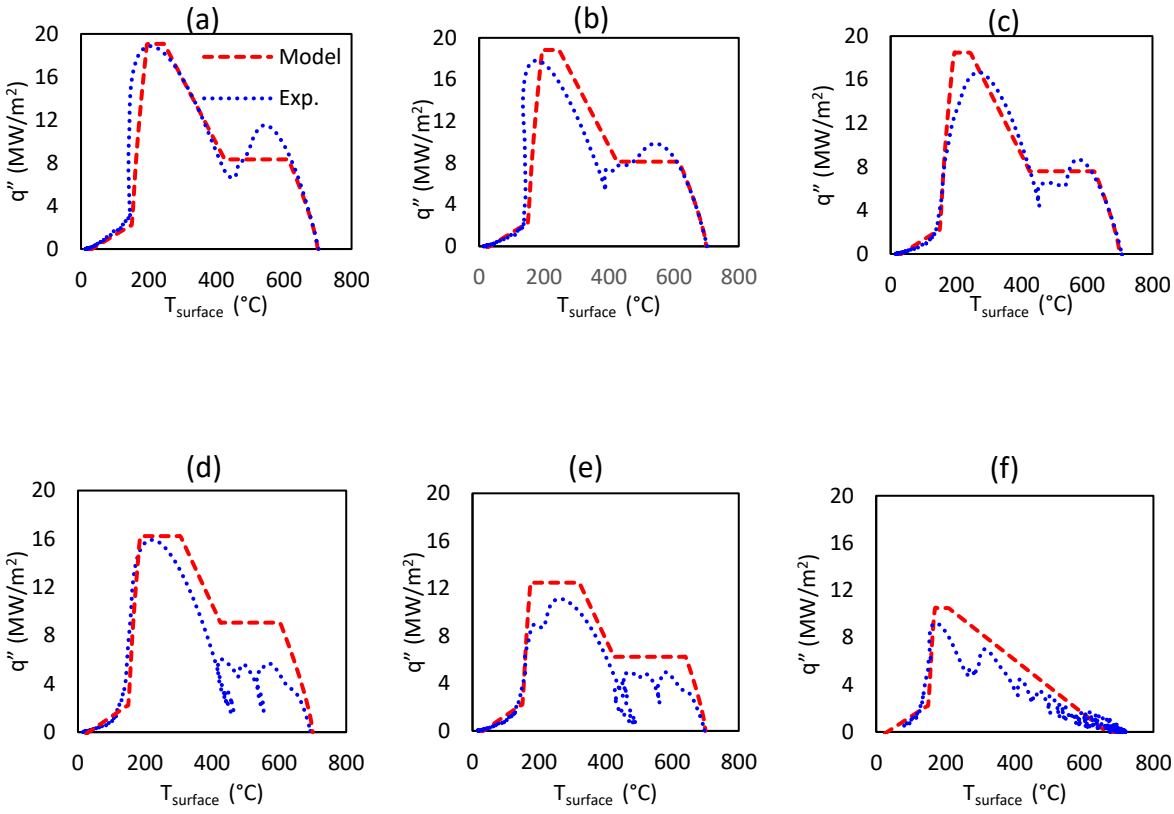

Figure B.7: Calculated vs. experimental boiling curves for test 7; flow rate = 160 l/min, water temperature = 10°C, x: (a) 0 mm, (b) 10 mm, (c) 20 mm, (d) 40 mm, (e) 60 mm, and (f) 160 mm.